

Model Reference Adaptive Sliding Mode Control of a Hexacopter Drones for Delivery Application



Senayt Setarge Lakew

A Thesis Submitted to
The Department of Electrical Power and Control Engineering
School of Electrical Engineering and Computing

Presented in Partial Fulfillment of the Requirement for the Degree of
Master's in Electrical Power and Control Engineering (Control Engineering)

Office of Graduate Studies
Adama Science and Technology University

September, 2024
Adama, Ethiopia

Model Reference Adaptive Sliding Mode Control of a Hexacopter
Drones for Delivery Application

Senayt Setarge Lakew

Advisor: Dr. Shimeles Demissie

Co-Advisor: Dr. Selewondim Eshetu

A Thesis Submitted to
The Department of Electrical Power and Control Engineering
School of Electrical Engineering and Computing

Presented in Partial Fulfillment of the Requirement for the Degree of
Master's in Electrical Power and Control Engineering (Control Engineering)

Office of Graduate Studies
Adama Science and Technology University

September, 2024
Adama, Ethiopia

DECLARATION

I hereby declare that this Master Thesis entitled “**Model Reference Adaptive Sliding Mode Control of a Hexacopter Drones for Delivery Application**” is my work. That is, it has not been submitted for the award of any academic degree, diploma or certificate in any other university. All sources of materials that are used for this thesis have been duly acknowledged through citation

Name of student

Signature

Date

RECOMMENDATION

We, the advisor of this thesis, hereby certify that I have read the revised version of the thesis entitled “**Model Reference Adaptive Sliding Mode Control of a Hexacopter Drones for Delivery Application**” prepared under my guidance by Senayt Setarge. submitted in partial fulfillment of the requirements for the degree of Mater’s of Science in Electrical Power and Control Engineering, postgraduate in control engineering. Therefore, we recommend the submission of the proposal to the department for further review and evaluation.

Major Advisor

Signature

Date

Co-Advisor

Signature

Date

APPROVAL PAGE

We, the advisors of the thesis entitled “**Model Reference Adaptive Sliding Mode Control of a Hexacopter Drones for Delivery Application**” and developed by Senayt Setarge, here by certify that the recommendation and suggestions made by the board of examiners are appropriately incorporated into the final version of the thesis.

| | | |
|---------------|-----------|-------|
| _____ | _____ | _____ |
| Major Advisor | Signature | Date |

| | | |
|------------|-----------|-------|
| _____ | _____ | _____ |
| Co-Advisor | Signature | Date |

We, the undersigned, members of the Board of Reviewers of the thesis by Senayt Setarge have read and evaluated the thesis proposal entitled “**Model Reference Adaptive Sliding Mode Control of a Hexacopter Drones for Delivery Application**” and examined the candidate during open defense. This is, therefore, to certify that the thesis is accepted for partial fulfillment of the requirement of the degree of Master of Science in Control Engineering.

| | | |
|-------------|-----------|-------|
| _____ | _____ | _____ |
| Chairperson | Signature | Date |

| | | |
|------------|-----------|-------|
| _____ | _____ | _____ |
| Reviewer 1 | Signature | Date |

| | | |
|------------|-----------|-------|
| _____ | _____ | _____ |
| Reviewer 2 | Signature | Date |

Final approval and acceptance of the thesis is contingent upon the submission of its final copy to the Office of Postgraduate Studies (OPGS) through the Department Graduate Council (DGC) and School Graduate Committee (SGC).

| | | |
|-----------------|-----------|-------|
| _____ | _____ | _____ |
| Department Head | Signature | Date |

| | | |
|-------------|-----------|-------|
| _____ | _____ | _____ |
| School Dean | Signature | Date |

| | | |
|--|-------|-------|
| _____ | _____ | _____ |
| Office of Postgraduate Studies, Dean Signature | | Date |

ACKNOWLEDGMENT

I would like to express my gratitude to God Almighty for granting me the strength and perseverance to navigate through this paper work. Next to this, I have a great thanks to Adama Science and Technology University, mainly the School of Electrical Engineering and Computing department of Electrical Power and Control Engineering Department, for giving me this chance to be a part of the Master's program. And also, my deepest gratitude is extended to my advisor, Dr. Shimeles Demissie, and co-advisor, Dr. Selewondim Eshetu, for their invaluable advice, invaluable help, and continuous support as I worked on my thesis. Additionally, I am grateful for their insightful comments and concepts that have helped me deepen my understanding.

Finally, but just as importantly, I'm grateful and blessed all of my family, friends, and other associates who helped me in any manner while I finished my thesis.

TABLE OF CONTENTS

| | |
|---|------|
| DECLARATION | i |
| RECOMMENDATION | ii |
| APPROVAL PAGE..... | iii |
| ACKNOWLEDGMENT | iv |
| LIST OF TABLES | viii |
| LIST OF FIGURES | ix |
| LIST OF ACRONYMS | xi |
| LIST OF SYMBOLS..... | xii |
| ABSTRACT | xiii |
| CHAPTER ONE..... | 1 |
| 1. INTRODUCTION..... | 1 |
| 1.1 Background..... | 1 |
| 1.2 Statement of Problem..... | 3 |
| 1.3 Objective of the Thesis | 4 |
| 1.3.1 General Objective | 4 |
| 1.3.2 Specific Objectives | 4 |
| 1.4 Scope of the Study | 4 |
| 1.5 Limitation of the Study | 4 |
| 1.6 Motivation of the Study | 5 |
| 1.7 Significance of the Study | 5 |
| 1.8 Thesis Organization | 5 |
| CHAPTER TWO..... | 6 |
| 2 LITERATURE REVIEW | 6 |
| 2.1 Chapter Overview | 6 |
| 2.2 Unmanned Aerial Vehicles (UAVs) | 6 |
| 2.3 Hexacopter UAVs | 7 |

| | | |
|--------------------|--|----|
| 2.3.1 | Hexacopters Configuration..... | 7 |
| 2.3.2 | Applications of Hexacopter Drone..... | 8 |
| 2.3.3 | Components of Hexacopter..... | 8 |
| 2.4 | Overview of Sliding Mode Controller..... | 9 |
| 2.5 | Model Reference Adaptive Controller..... | 11 |
| 2.6 | Proportional Integral Derivative Controller..... | 12 |
| 2.6.1 | Performance Index..... | 13 |
| 2.7 | Linear Quadratic Regulator..... | 14 |
| 2.8 | Related Works on Hexacopter Drone..... | 15 |
| CHAPTER THREE..... | | 18 |
| 3 | MODELING OF SYSTEM DYNAMICS..... | 18 |
| 3.1 | Introduction..... | 18 |
| 3.2 | Materials Used for the Study..... | 18 |
| 3.3 | Methods to Follow..... | 18 |
| 3.4 | Block Diagram of the System..... | 20 |
| 3.5 | Modeling of a Hexacopter..... | 20 |
| 3.5.1 | Rotation Matrix of Reference Frame (\mathfrak{R})..... | 21 |
| 3.5.2 | Hexacopter Kinematics..... | 22 |
| 3.5.3 | Hexacopter Applied Force..... | 24 |
| 3.5.4 | Hexacopter Applied Torque..... | 25 |
| 3.5.5 | Hexacopter Dynamic Model..... | 29 |
| 3.5.6 | Hexacopter Control Inputs and Rotor Speeds..... | 32 |
| 3.5.7 | State Space Equation for Hexacopter Dynamics..... | 33 |
| 3.6 | Open-Loop Analysis of the Hexacopter..... | 35 |
| CHAPTER FOUR..... | | 40 |
| 4. | CONTROLLER DESIGN..... | 40 |
| 4.1. | Controlling System Block Diagram..... | 40 |

| | | |
|---|--|----|
| 4.2. | Generation of Trajectories by Using Minimum Jerk Trajectory | 41 |
| 4.3. | Design of PID Sliding Surface Based SMC for Hexacopter..... | 44 |
| 4.4. | Model Reference Adaptive Sliding Mode Controller for Hexacopter | 51 |
| CHAPTER FIVE | | 57 |
| 5. | RESULTS AND DISCUSSIONS | 57 |
| 5.1. | Simulation Block Diagram for Tracking Problem..... | 57 |
| 5.2. | Parameters that are used in simulation purposes | 58 |
| 5.3. | Simulation Result of MRA-SMC for Tracking Performance | 59 |
| 5.3.1. | The ASMC System's Trajectory Tracking Performance..... | 60 |
| 5.3.2. | Control Signal of ASMC system for Tracking | 66 |
| 5.4. | Simulation Results when the Hexacopter is Subjected to Uncertain Parameters and External Disturbances..... | 67 |
| 5.4.1. | Trajectory Tracking Performance of ASMC for Mass Varies from 2.5kg-12kg 67 | |
| 5.4.2. | Trajectory Tracking Performance of ASMC for Mass Varies from 2.5kg-12kg with External Disturbances..... | 71 |
| 5.5. | Performance Index Analysis | 72 |
| CHAPTER SIX | | 73 |
| 6. | CONCLUSION AND RECOMMENDATION | 73 |
| 6.1. | Conclusion | 73 |
| 6.2. | Recommendation | 73 |
| REFERENCE | | 74 |
| REFERENCE LINKS | | 77 |
| APPENDICES | | 78 |
| APPENDIX A: Dynamic Modeling Block Diagram..... | | 78 |
| APPENDIX B: Proposed Controller Simulink diagram..... | | 78 |
| APPENDIX C: LQR Based Reference Model Simulink | | 79 |
| APPENDIX D: MATLAB Code for Reference Model of the System | | 79 |

LIST OF TABLES

| | |
|---|----|
| Table 3.1: The parameters value used in the simulation..... | 35 |
| Table 4.1: Initial and final boundaries of position, velocity and acceleration..... | 43 |
| Table 5.1: Initial parameters of controller | 58 |
| Table 5.2: Performance index values for MRA-SMC | 72 |

LIST OF FIGURES

| | |
|---|----|
| Figure 1.1: Hexacopter drones [L1] | 2 |
| Figure 2.1: Lawrence and Sperry [L2]..... | 6 |
| Figure 2.2: “X” configuration and “+” configuration of hexacopter [L2]. | 7 |
| Figure 2.3: The sliding mode control's trajectory of motion [L4]. | 10 |
| Figure 2.4: SMC block diagram for hexacopter | 11 |
| Figure 2.5: Direct Model Reference Adaptive control system (Yılmaz, 2019)..... | 12 |
| Figure 2.6: Controller algorithms of PID controller (Home et al., 2018)..... | 13 |
| Figure 2.7: The structure of the LQR control system (Choi, 2010). | 15 |
| Figure 3.1: Block diagram of the proposed study | 19 |
| Figure 3.2 Block diagram of the system..... | 20 |
| Figure 3.3: The structure and its frames of a hexacopter drone (Le & Nam, 2015)..... | 21 |
| Figure 3.4: Hexacopter rotor distances to center of gravity (L4) | 25 |
| Figure 3.5: Rolling motion | 26 |
| Figure 3.6: Pitching motion | 27 |
| Figure 3.7: Yawing motion | 28 |
| Figure 3.8: Open-loop block diagram for Simulink | 36 |
| Figure 3.9: Simulation result at $\omega_1 = \omega_2 = \omega_3 = \omega_4 = \omega_5 = \omega_6 = 101.5 \text{ rad} / \text{sec}$ | 37 |
| Figure 3.10: Simulation result at $\omega_1 = \omega_2 = \omega_3 = 101 \text{ rad} / \text{sec}$ and $\omega_4 = \omega_5 = \omega_6 = 102 \text{ rad} / \text{sec}$ | 38 |
| Figure 3.11: Simulation result at $\omega_2 = \omega_5 = 101.5 \text{ rad} / \text{sec}$, $\omega_3 = \omega_4 = 101 \text{ rad} / \text{sec}$ and $\omega_1 = \omega_6 = 102 \text{ rad} / \text{sec}$ | 38 |
| Figure 3.12: Simulation result at $\omega_1 = \omega_3 = \omega_5 = 101 \text{ rad} / \text{sec}$ and $\omega_2 = \omega_4 = \omega_6 = 102 \text{ rad} / \text{sec}$ | 39 |
| Figure 4.1: System block diagram..... | 40 |
| Figure 5.1: Simulink diagram of the proposed system..... | 57 |
| Figure 5.2: 3D minimum jerk trajectory reference..... | 59 |
| Figure 5.3: Altitude Z (a) tracking performance and (b) tracking error response | 60 |
| Figure 5.4: X position (a) tracking performance and (b) tracking error response..... | 61 |
| Figure 5.5: Y position (a) tracking performance and (b) tracking error response | 62 |
| Figure 5.6: Phi (a) tracking performance and (b) tracking error response | 63 |

| | |
|--|----|
| Figure 5.7: Theta (a) tracking performance and (b) tracking error response | 64 |
| Figure 5.8: Output of psi (a) tracking performance and (b) tracking error response | 65 |
| Figure 5.9: Performance of the 3D reference trajectory tracking controller using ASMC . | 65 |
| Figure 5.10: Control input U1 | 66 |
| Figure 5.11: Control input U2 | 66 |
| Figure 5.12: Control input U3 | 66 |
| Figure 5.13: Control input U4 | 67 |
| Figure 5.14: X position trajectory tracking controller for different mass | 68 |
| Figure 5.15: X position trajectory tracking error for different mass | 68 |
| Figure 5.16: Y position trajectory tracking controller for different mass..... | 69 |
| Figure 5.17: Y position trajectory tracking error for different mass..... | 69 |
| Figure 5.18: Z altitude trajectory tracking controller for different mass..... | 70 |
| Figure 5.19: Z altitude trajectory tracking error for different mass..... | 70 |
| Figure 5.20: X position trajectory tracking with external disturbance..... | 71 |
| Figure 5.21: Y position trajectory tracking with external disturbance | 71 |
| Figure 5.22: Z - altitude trajectory tracking with in external disturbance..... | 71 |

LIST OF ACRONYMS

| | |
|------|---|
| ASMC | Adaptive Sliding Mode Control |
| ASTU | Adama Science and Technology University |
| ATC | Local Traffic Control |
| BLDC | Brush Less Direct Motor |
| CW | Clock Wise |
| CCW | Counter Clock Wise |
| DOF | Degree Of freedom |
| FAA | Federal Aviation Administration |
| GCS | Ground Control Station |
| GPS | Global Positioning System |
| GWO | Gray Wolf Optimization |
| IMU | Inertial Measurement Unit Sensor |
| KV | Kilo Volte |
| LQG | Linear Quadratic Gaussian |
| LQR | Linear Quadratic Regulator |
| MIMO | Multiple Input Multiple output |
| MRAC | Model Reference Adaptive control |
| PID | Proportional Integral Derivative |
| SMC | Sliding Mode Control |
| STI | Space Technology Institute |
| STR | Self Tuning Regulator |
| USA | United States of America |
| UAV | Unmanned Aerial Vehicle |
| VTOL | Vertical Take Off and Landing |

LIST OF SYMBOLS

| | |
|--|--|
| F_D | Aerodynamics drag force |
| k_{fd} | Aerodynamics drag force constant |
| F_A | Air resistance force |
| ω_i | Angular velocity of i^{th} motor |
| ω_ξ | Angular velocity transformation from inertial frame to body frame |
| \mathfrak{R}_b | Body fixed frame |
| $\omega = [p \quad q \quad r]^T$ | Body frame angular velocity |
| $V_b = [V_{xb} \quad V_{yb} \quad V_{zb}]^T$ | Body frame linear velocity |
| \mathfrak{R}_i | Earth inertial frame |
| $(\phi \quad \theta \quad \psi) \in R^3$ | Euler angles |
| g | Gravitational acceleration |
| F_G | Gravitational force |
| $\dot{\xi} = [\dot{\phi} \quad \dot{\theta} \quad \dot{\psi}]^T$ | Inertial frame angular velocity |
| $\dot{\chi} = [\dot{x} \quad \dot{y} \quad \dot{z}]^T$ | Inertial frame linear velocity |
| l | Length of propeller |
| $\chi = [x \quad y \quad z]^T$ | Linear position vector |
| m | Mass of the body |
| J_{xx}, J_{yy}, J_{zz} | Moment of inertia in body frame |
| $\xi = [\phi \quad \theta \quad \psi]^T$ | Rotational position vector |
| $F_T, \tau_\phi, \tau_\theta, \tau_\psi$ | The four-control input |
| κ | Trust coefficient |
| F_T | Trust force |

ABSTRACT

Unmanned Aerial Vehicles (UAVs) are rapidly evolving due to technology improvement and low costs, with a wide range of applications. Its nonparametric uncertainty inputs, close coordination of subsystems, external disruptions, and unknown physical features make it a favourable location for control systems research as well. The hexacopter is a six-rotor UAV that is a nonlinear, underactuated, multivariable, and unstable system. To design a suitable controller, system modeling is required. In this regard, in this thesis the Newton-Euler-based mathematical modelling of hexacopter UAVs is developed. In order to enhance the altitude and attitude stabilization performance of hexacopter drones for delivery applications, a model reference adaptive sliding mode control (MRA-SMC) was implemented. To have a specific path of the drone, a minimum jerk trajectory generation was developed. The developed controller achieves asymptotic stability by applying the Lyapunov stability analysis. The PID controller generates sliding surfaces for the SMC controller, and also the reference model for the hexacopter is generated by using the LQR technique. The MRAC scheme adaptively adjusts the Sliding Mode Controller parameters to compensate for uncertainties and disturbances in the system dynamics. The developed controller's performance is tested for a given trajectory with varying loads and wind disturbances in a MATLAB/Simulink environment. The simulation results indicated that the proposed controller tracks the specified trajectory with a small tracking error of 0.01. Besides, the system was tested on different masses, considering from 2.5kg to 12kg efficiently with and without external disturbance. Accordingly, the proposed controller for a 12kg mass results in 0.15 error with 0.5 disturbance error. In general, due to the adaptation of the reference model, the result of the proposed SMC controller results in small errors under variable payloads and disturbances with minimum chattering effect.

Keywords: *Hexacopter, MRA-SMC, PID, and LQR.*

CHAPTER ONE

1. INTRODUCTION

1.1 Background

Unmanned aerial vehicles (UAV) are another name for drones, which have developed quickly in the last few years (Zhang et al., 2019). These aircraft have the ability of taking off and landing without a pilot, and an operator operating from a distance controls the aircraft's motion. (Rathod & Shinde, 2023). Initially, unmanned aerial vehicles (UAVs) were mostly used for military purposes. However, in trying to obtain the results of military applications, there has been a growing push to establish UAVs in non-military domains. One such application is delivery drones, which are used to transport foods, packages, and other goods. Even more, these drones are capable of collecting medical samples from inaccessible or remote areas and delivering vaccines and medical supplies. Under the "Let's Fly Wisely" program, the US Federal Aviation Administration (FAA) authorized the first drone delivery of medication to a rural Virginia medical clinic in July 2015 (Vinjavarapu et al., 2019).

A UAV's navigation system, flight control system, and communication link between the aircraft and ground station are some of its essential parts. While the navigation system employs GPS and other sensors to direct the aircraft to its destination, the flight control systems use sensors and software to maintain the stability and regulate the movement of the UAV. The pilot can operate the UAV and get real-time data and video from the aircraft over the communication link (ardiyansyah, M. 2023).

A hexacopter is a multirotor UAV, that has six-rotors, offering more lifting power and stability due to their extra motors as shown in Figure 1.1. It has gained significant traction because of their benefits in terms of low cost, high maneuverability, simple structure, and hovering ability. They have six motors, and even if one or two of them fail, they can still fly since they are mounted on six symmetrical frames that are spaced 120 degrees apart. Three sets of CCW (counter-clockwise) and CW (clockwise) propellers are on them. This kind of remote-controlled aircraft has a BLDC motor that runs independently and is connected to six propellers. They are positioned above the hexacopter's main body in a circle. Its two ski-like legs and camera-wielding body are common features. With the help of these skis, the

device can land steadily. Compared to a quadcopter, the hexacopter can fly more steadily and reach higher altitudes, have a longer flight time, carry a greater weight, and have better fault tolerance, because of its six propellers, which provide more lifting power (Vinjavarapu et al., 2019).



Figure 1.1: Hexacopter drones [L1]

The significant increase in online ordering usage has resulted in a multiplicity of demands for delivery personnel (Ali et al., 2022). But because of poor infrastructure, the product does not reach the customer in a timely manner (such as traffic); (Vinjavarapu et al., 2019). Drone-based technology is being used to address the drawback and meet this demand. A hexacopter can be used to transport cargo or gather data in a specific area by flying steadily and vertically. It reduces labor, reduces delivery times, and enhances system performance (Ali et al., 2022).

The modelling of hexacopter dynamics will be approached using either the Euler-Lagrange formulation, which is scalar-based to describe the motion, or the Newton-Euler formulation, which is vectoral in nature, to improve the controller algorithm's numerical efficiency and stability. Ideally, both methods should yield the same model. In this thesis, we used the Newton-Euler method. Currently, the ASTU Space Technology Institute (STI) center of excellence is conducting research on drones, and different flight controllers and sensors, including IMU sensors are used to develop hexacopter drones.

Designing an appropriate control system is the primary challenge and complicated system in every single UAV. Hexacopter position, attitude, and altitude controls have been carefully studied using both conventional and modern control techniques. Maintaining precise altitude and attitude control during delivery application can be challenging due to factors such as wind disturbance, uncertainty, highly nonlinear, payload variations, and complex flight maneuvers. Conventional control methods such as PID, Linear Quadratic Regulator/Gaussian (LQR/LQG), and backstepping, may struggle to achieve the desired

level of stability and accuracy under these conditions because of these traditional controllers. Advanced controllers like sliding mode controllers (SMC) are effective in cases of disturbance rejection capability and mitigating the nonlinearity effects. However, it has limitations due to the chattering effect.

So accordingly, the above problem and its solution in this research work on an Adaptive Sliding Mode Control (SMC) with integrated PID control to enhance the altitude and attitude stabilization performance of hexacopter drones for delivery applications. PID control is one of the most widely used and simple controllers. Engineers primarily use PID controllers for process industries, automatic control, etc. PIDs increase in value by robust and optimal controllers. In this thesis, integrating PID is used to generate sliding surfaces for the SMC controller, enhancing tracking accuracy and reducing control signal chattering. Modal Reference Adaptive Controller (MRAC) is one of the adaptive control methods that aims to solve control problems with limited parameters to compensate for changes in the system dynamics (Romdlony et al., 2022a). It adjusts the SMC controller parameters to compensate for uncertainties in the system dynamics. The Linear Quadratic Regulator (LQR) is a popular controller in flight control applications because of its inherent stability and durability (Sun et al., 2022). The LQR technique is used in the design of the hexacopter reference model because it yields an optimal control solution that minimizes a cost function, providing a stable and well-behaved target for the actual control system to track. The MATLAB software tool is used to implement the proposed system.

1.2 Statement of Problem

Drone modelling and control are complicated challenges. Hexacopters are one type of multicopter drone that uses six rotors for flight. Maintaining precise altitude and attitude control of the hexacopter during delivery application is challenged due to factors such as wind disturbance, presence of parameter uncertainty, highly nonlinear dynamics, payload variations, complex flight maneuvers, multivariable nature, underactuated, and instability.

Sliding mode control (SMC) has been commonly used in the development of the trajectory control systems for a hexacopter UAVs. What makes it so popular is that SMC exhibits good performance in the case of handling high dimensional control problems, uncertainty and disturbance rejection capabilities and against nonlinear dynamics. However, SMC suffers from certain drawbacks, such as the chattering effect, which results in varying voltage and

current distributions to the motors and reduced control precision. So, the torques in each rotor will be different and generate vibration on the hexacopter system. Additionally, the consideration of aerodynamic impacts was frequently neglected in previous studies. This research to address the above problems by considering aerodynamic effects in the modelling of the system and also, to overcome the effect of chattering, uncertainties, and disturbance by using model reference adaptive sliding mode control (MRA-SMC)

1.3 Objective of the Thesis

1.3.1 General Objective

The general objective of this study is to design the adaptive PID sliding surface SMC for a hexacopter drone to enhance the altitude and attitude stabilization performance.

1.3.2 Specific Objectives

- To minimize the tracking error (IAE) of the drone.
- To analyze the performance of the proposed controller at different payload.
- To analyze disturbance rejection performance of the proposed controller.
- To design MRA-SMC framework based on PID controller sliding surface.
- Evaluate simulation results with the proposed controller by using MATLAB/Simulink.

1.4 Scope of the Study

The scope of this research work is deriving a hexacopter systems mathematical model for delivery applications and to create an Adaptive PID-based Sliding Mode Controller (SMC) for stabilizing the drone in the presence of external disturbances and model uncertainties. The entire system and controller design process will be done by MATLAB/Simulink environment, allowing for comprehensive modelling, analysis, and validation of the proposed control approach to ensure stable and robust performance of the hexacopter drone under various operating conditions.

1.5 Limitation of the Study

The real hardware implementation requires the integration of numerous electronic devices, many of which are difficult to locate in Ethiopia. The research is limited to the theoretical design and simulation of the hexacopter system using MATLAB/Simulink without

evaluating the performance under real-world conditions, due to the time, complexity, and expense involved in creating the real prototype implementations.

1.6 Motivation of the Study

Due to their ability to make deliveries more quickly, effectively, and affordably, especially in urban areas delivery drone use is rapidly growing. Precise control over height and attitude is required for deliveries to be safe and trustworthy. Variations in cargo and wind disturbances can have a significant effect on altitude stability. The design of an advanced control algorithm plays an important role in overcoming the problems and increasing stability and efficiency for delivery drone applications in specific environmental conditions, ultimately enhancing the safety and reliability of these emerging technologies.

1.7 Significance of the Study

Controlling the position, attitude, and altitude of unmanned aerial vehicles (UAVs) is one of the most interesting topics in control system research. Such study is currently being carried out in numerous nations because to the benefits of multi rotor UAVs and their versatile application areas. These studies are useful in generating a technology-focused generation because Ethiopia is relatively new to this kind of innovation and technology. Furthermore, Adama Science and Technology University (ASTU) values the Space Technology Institute (STI) center of excellence especially because research and development teams are developing hexacopter drones especially for the Ethiopian market. It provides as an example of the technological advancements being made in the country's research.

1.8 Thesis Organization

There are six chapters in this thesis. The first chapter explains the background of UAV, scope, limitations, significance, statement of problems, and objectives of the research. A review of the literature on hexacopter drones, their controllers, and related works is covered in Chapter 2. The materials and methods utilized to complete this research project are covered in Chapter 3, as well as the Newton-Euler formalism-based dynamic and kinematic mathematical modelling of the hexacopter system. Chapter 4 deals with the control design (MRAC, PID, LQR, and SMC) for the hexacopter system's nonlinear dynamic model. Chapter 5 deals with the simulation results and discussions. Finally, a conclusion and suggestions for the next researcher are given in Chapter 6.

CHAPTER TWO

2 LITERATURE REVIEW

2.1 Chapter Overview

In this section, UAVs are described in detail, including their history and classifications. We then talk about the hexacopter UAVs' concept, history, applications, and components. Additionally, the concept and theoretical background of modal reference adaptive control (MRAC), sliding mode control (SMC), PID, and Linear Quadratic Regulator (LQR) are explained. Finally, related works are reviewed and discussed closely, along with their advantages and disadvantages.

2.2 Unmanned Aerial Vehicles (UAVs)

UAVs often known as pilot less aircraft are, aircraft that run without a human pilot present. They can be operated remotely by a human operator or independently using artificial intelligence algorithms or pre-programmed flight patterns. UAVs range in sizes and configurations from small portable devices to massive military-grade aircraft (Ahmed et al., 2022). In 1916, Lawrence and Sperry (USA) started manufacturing UAVs, also referred to as “aerial torpedoes.” However, due to problems with the control section and the workload of the pilot as shown in Figure 2.1, the UAV is now known as a helicopter. They were able to fly it thirty miles. Lawrence and Sperry reportedly use a gyroscope to balance the body. In the late 1920s, multicopter aerial vehicles were first referred to as "gyrocopters," or four-rotor helicopters. These early drones relied on mechanical gyroscopes to keep a straight flight path while they traveled till their fuel ran out. Later, a single-rotor aircraft with flawless structural integrity and stability took its place a helicopter(Poudel et al., 2015).



Figure 2.1: Lawrence and Sperry [L2]

Several UAV classes have been created based on a range of factors or attributes, including size, weight, speed, altitude, and endurance. UAVs used for commercial and recreational purposes are classed differently from those used for military purposes. No classification is more accurate than another, nor is there a single standard classification that applies to all applications. UAVs can be categorized into three groups depending on their flying style and body type. These are fixed-wing UAVs, which are airplanes, multirotor UAVs, and VTOL UAVs, which is a new class of UAVs that has emerged combining the capabilities of fixed-wing aircraft with multirotor UAVs (Alghamdi et al., 2021).

2.3 Hexacopter UAVs

The hexacopter is a six-rotor helicopter that is under-actuated, dynamic, and has six degrees of freedom (DOF), yet it has four control inputs. It is controlled by six propellers. By forcing the air downward, each of the six propellers creates an upward thrust force and simultaneously creates a vertical movement. On the other hand, all of the propellers' speeds must be reduced in order to generate a downward motion. In the late 2000s and early 2010s, hexacopter drones started to gain commercial traction and became more widely available for both professional and consumer applications.

2.3.1 Hexacopters Configuration

Hexacopters have six fixed-pitch blades, and their six motors are arranged in either an 'X' or a '+' shape, and they rotate in both clockwise and counterclockwise directions as shown in Figure 2.1. The 'X' and '+' modes have equal spacing between the rotors. The only difference between the two designs is that the two motors face forward in 'X' mode, while one of the motors faces forward in '+' mode. 'X' mode is typically used for aerial photography or recording purpose, whereas '+' mode is typically used for acrobatic flying (Tin et al., 2015); (Vinjavaram et al., 2019).

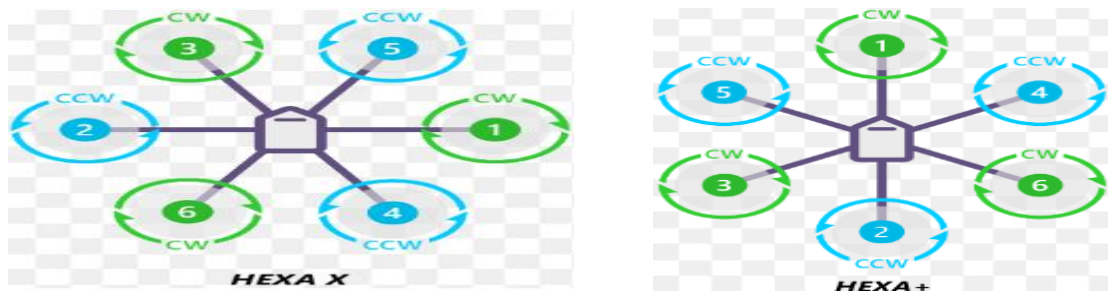


Figure 2.2: "X" configuration and "+" configuration of hexacopter [L2].

2.3.2 Applications of Hexacopter Drone

Hexacopters are used for different application areas. Its include but are not limited to (Dagher, 2018);(Ahmed et al., 2022):

Delivery applications: Hexacopters are being used by several companies as delivery kits or robots these days, which is used to deliver foods, medical supplies, masks, vaccines, and retrieve medical samples from remote or inaccessible regions.

Mapping and Surveying: Hexacopter drones are used in photogrammetry, mapping, and surveying applications to produce 3D models, topographic surveys, and high-resolution aerial maps. They have specialized cameras and sensors to record precise and detailed geospatial data.

Photography and cinema: Hexacopter drones are used in professional video shoots nowadays to capture specialized images on movie sets, TV shows, and commercials. It is utilized in direct product marketing as well as aerial photography for advertising tasks that include a city, beach, or building from a bird's eye perspective.

Agriculture development: In agriculture, hexacopters are utilized for tasks like crop spraying, fertilization, and plant damage detection applications.

2.3.3 Components of Hexacopter

The hexacopters are made up of different components; some of these are:

Circuit Board Frame: It serves as a hexacopter's base and provides the structure and form of the craft (SINGH, 2018). In order to provide an adequate amount of flight, the frame needs to be both light and strong enough to support a sufficient load. Several materials, including carbon fiber and aluminum, can be used to make it, depending on the efficiency, stiffness, and function that must be fulfilled.

Propellers: A hexacopter require six propellers, three CW and three CCW. The speed of flight and the ability to carry a load are controlled by the propellers(SINGH, 2018). A propeller with more blades produces more thrust and reduces vibration. However, they desire engines with greater power.

Motor: The motor is one of the most crucial components of a hexacopter. Each propeller has a single motor that must have the same size and be measured in KV.

Flight Controller: In order to control the vehicle's behavior while executing various maneuvers, it gathers data from sensors and computes the appropriate control strategy.

Battery and Battery Charger: The battery functions as the hexacopter's primary power source. The drone's weight, size, weight and size of its motors, and the tasks it performs all affect how long its batteries last.

Transmitter and Receiver: The signals to the hexacopter are sent and received by the transmitter and receiver, respectively. During a flight, the pilot can give instructions to the hexacopter to carry out specific tasks. The hexacopter receives the signals, and the flight controller takes appropriate action. Every hexacopter has a different transmitter and receiver combination that cannot be changed.

Electronic Speed Controller: It is an electronic device that controls the direction and speed of rotation of electric motors.

Telemetry: A hardware transmitter and receiver system called the telemetry kit allows an Android smartphone to establish a connection with the UAV and function as a ground control station.

2.4 Overview of Sliding Mode Controller

Sliding mode controller (SMC) is one kind of a nonlinear control system technique used to handle unexpected and large changes in system dynamics. It is a powerful and reliable control Method. This control method can handle modelling errors, parameter variations in the system, and nonlinear and time-varying systems. Its disadvantage is that it can create a high frequency oscillation known as the chattering effect (Walle, 2019). Sliding mode's primary goal is to move the trajectory of the system state to a specified surface and use a switching control to keep it there. The switching control law will bring the system state trajectory closer to the surface if it is currently outside of it. As seen in Figure 2.3, the sliding surface is the name given to this surface (Busarakum & Srichatrapimuk, 2014).

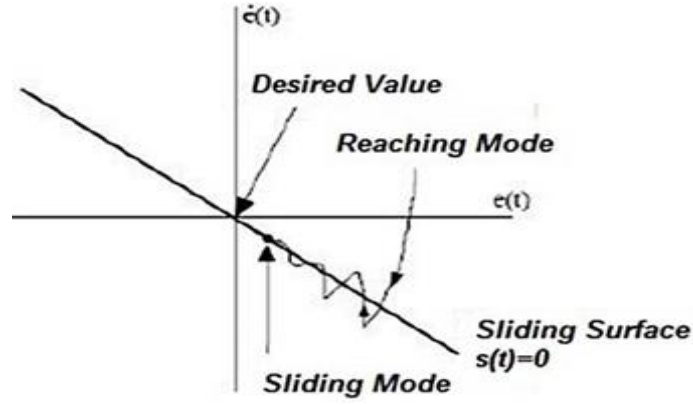


Figure 2.3: The sliding mode control's trajectory of motion [L4].

(Walle, 2019) There are two steps in the design of a sliding mode control: selecting the sliding surface and creating the control law. The design starts with the sliding surface selection, which is a boundary-containing geometrical locus and has to take tracking error into account. The sliding surface's general, typical form is expressed as

$$S(x) = \left(\lambda_x + \frac{d}{dt}\right)^{n-1} e(x) = \dot{e}(x) + \lambda_x e(x) \quad \text{where } e(x) = x_d - x \quad (2.1)$$

Where, $\lambda_x = s(x)$ performance tuning parameter, x = state vector, $e(x)$ = tracking error, and n = relative degree between input and output.

The sliding mode starts when the system trajectories reach the sliding surface, which is described by $S = 0$. The sliding surface has a finite duration. The next step is sliding control law design; it is composed of two parts as well: the linear component (U_{eq}) and the nonlinear component (U_{sw}) (Pati et al., 2014).

$$U(t) = U_{eq}(t) + U_{sw}(t) \quad (2.2)$$

When the system is on the surface, the linear portion protects its motion on the sliding surface. To maintain the sliding condition, this controller part needs to satisfy the following

condition. $\dot{S}(x)$. To reach the sliding surface, any variation in the state trajectories from it is compensated for by the nonlinear portion of the control law when $\dot{S}(x) \neq 0$. And is able to be stated as

$$U_M(t) = k \operatorname{sgn}(S) \quad \operatorname{sgn}(S) = \begin{cases} -1 & \text{if } s < 0 \\ 0 & \text{if } s = 0 \\ 1 & \text{if } s > 0 \end{cases} \quad (2.3)$$

Where, k is a positive constant of the design; In order to satisfy the stability of Lyapunov criterion $\dot{S} < 0$, it needs to be greater than zero. The stability analysis of the system was performed using the Lyapunov stability theory. Select the Lyapunov function as shown below, i.e., it must be positive-definite:

$$V = \frac{1}{2} S^2 \quad (2.4)$$

The Lyapunov theory states that the condition $\dot{V} = S \dot{S} < 0$, i.e., it must have to be negative, definite, and satisfied. Since the trajectories will stay on the surface, the system is stable (Busarakum & Srichatrapimuk, 2014). The block diagram that shows the sliding mode controller for hexacopter is shown in Figure 2.4.

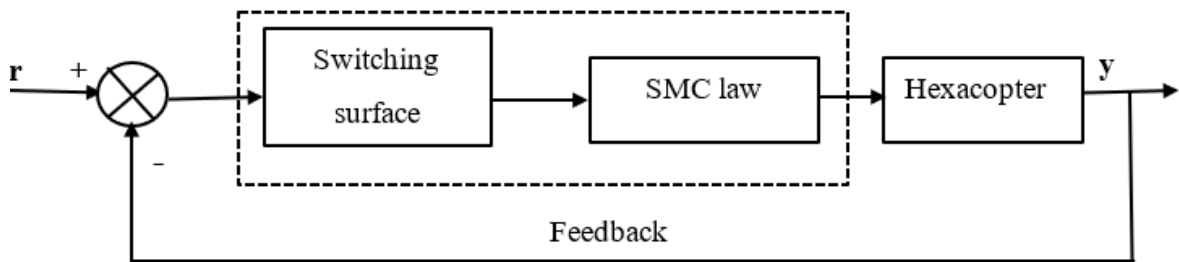


Figure 2.4: SMC block diagram for hexacopter

2.5 Model Reference Adaptive Controller

Model Reference Adaptive Control (MRAC) is a control technique which is used to regulate the behaviour of a dynamic system by adapting to changes in its parameters or operating conditions. MRAC is particularly effective when dealing with systems that have uncertain or time varying parameters (Romdlony et al., 2022a). The main objective of MRAC is to provide a reference model that accurately reflects the intended system behaviour. Usually, this reference model is presented as a collection of transfer functions or dynamic equations.

MRAC has two possible forms: direct and indirect. When using direct MRAC as shown in Figure 2.5, the controller adjusts its parameters directly in response to the differences

between the output of the system and the desired model. Systems with measurable or known states are suited for direct. When using indirect MRAC, the estimated system parameters are used to create the control law. The estimated system parameters are used to determine the controller parameters, which are not updated directly. Adaptive estimation algorithms, like least squares or Kalman filtering, are used to estimate system parameters. When direct state measurement is not possible or when system parameter estimation yields better results than direct state measurement, indirect MRAC can be helpful (Niit, 2017). In this research direct MRAC was used.

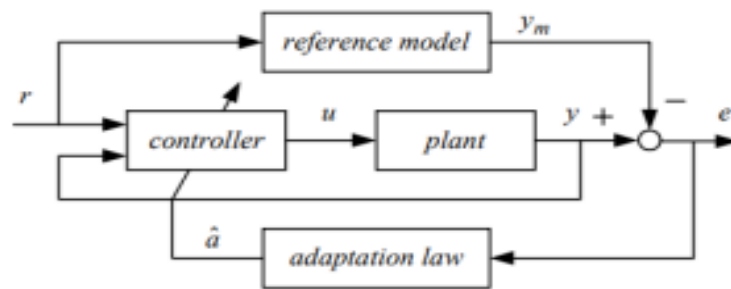


Figure 2.5: Direct Model Reference Adaptive control system (Yilmaz, 2019)

Two methods are taken into consideration for MRAC: the Lyapunov method and the MIT rule method. Because it is based on stability theory, the Lyapunov approach will be utilized in the final controller, while the MIT rule approach will be designed in parallel for comparative analysis.

2.6 Proportional Integral Derivative Controller

Industrial control systems frequently employ PID controllers as control loop feedback mechanisms. The first theoretical analysis of a PID controller was conducted in 1922 by Russian-American engineer Nicolas Minorsky, who created an automated ship steering system for the U.S. Navy based on observations of the steersmen's application of rate of change, past error, and current error to maintain the ship's course. Following World War II, electrical system controllers were developed (Ho, 2014). An error value is calculated by a PID controller as the difference between a process variable that is measured and a setpoint that is desired. Using a controlled variable, the controller modifies the process in an attempt to reduce error. As a result, the PID controller algorithm, also known as three-term control, involves three distinct constant parameters, represented by the letters P (proportional), I (integral), and D (derivative). In short, these variables may be understood in terms of time: D is a projection of future errors based on the present rate of change, P is based on the current

error, and I is based on the total of previous errors (Home et al., 2018). Figure 2.6 shows the PID control algorithms.

$$U(t) = \kappa_p e(t) + \kappa_i \int_0^t e(\tau) d\tau + \kappa_d \frac{d}{dt} e(t) \quad (2.5)$$

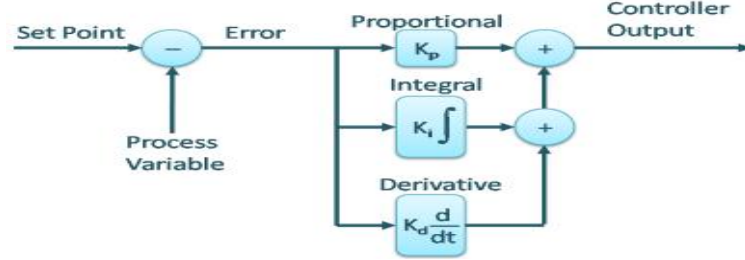


Figure 2.6: Controller algorithms of PID controller (Home et al., 2018).

In this study, the Proportional-Integral-Derivative (PID) controller is utilized to generate the sliding surfaces for the sliding mode controller, enhancing tracking accuracy and reducing control signal chattering.

2.6.1 Performance Index

The most performance index that used to evaluate the robustness of the system, specifically, for control engineering discipline prefers the Integral Square-Error (ISE), Integral Time Square-Error (ITSE), Integral Absolute-Error (IAE), and Integral Time Absolute Error (ITAE) of Equation (2.6) as fitness functions.

$$\begin{aligned} ISE &= \int_0^{\infty} e^2(t) dt \\ ITSE &= \int_0^{\infty} t e^2(t) dt \\ IAE &= \int_0^{\infty} |e(t)| dt \\ ITAE &= \int_0^{\infty} t |e(t)| dt \end{aligned} \quad (2.6)$$

Every fitness function specified in Equation (2.6) has a unique characteristic. Large errors are heavily penalized and small errors are lightly penalized using the ISE index. When a system is designed using this criterion, it usually exhibits a quick reduction in its large initial error, leading to a fast and oscillatory system response. While IAE penalizes control errors,

ITSE places a strong emphasis on initial errors and severely penalizes errors that happen late in the system's transient response. Small overshoots and minimal damped oscillations are characteristics of systems designed with iterative thermal analysis (ITAE). Large initial errors are penalized less severely than errors that occur later in the response, which results in long settling times and control errors. The study employed the IAE performance index.

2.7 Linear Quadratic Regulator

Linear Quadratic Regulator (LQR) is a control strategy that is based on state-space representation. It is the most preferred optimum controller due to its inherent stability, robustness, and optimality between response time and control input. Moreover, in order to develop a command tracking controller for a MIMO system, the LQR approach can be readily extended. LQR is a full state feedback controller. In LQR, first find the optimal K by choosing closed-loop characteristics.

Consider the linear system,

$$\dot{x} = Ax + bu \quad (2.6)$$

Using the state feedback control law,

$$u = -K_{LQR}x \quad (2.7)$$

By reducing the following cost function, the LQR controller attempts to strike a balance between the control input and reaction time.

$$J = \int_0^{\infty} [x^T(t)Qx(t) + u^T(t)Ru(t)] dt \quad (2.8)$$

The number of state variables and input variables, respectively, determines the elements of weighting matrices Q and R . The cost function is a weighted integral of the square of the inputs and states if the weighting matrices are selected as diagonal matrices. The following Lagrange multiplier-based optimization method can be used to find the optimal control gain K , which is the solution to the LQR problem.

$$K_{LQR} = R^{-1}B^T P \quad (2.9)$$

The following Algebraic Riccati Equation (ARE) is solved using the transformation matrix P .

$$A^T P + PA + Q - PBR^{-1}B^T P = 0 \quad (2.10)$$

The Block diagram representation of LQR structure is given in Figure 2.7

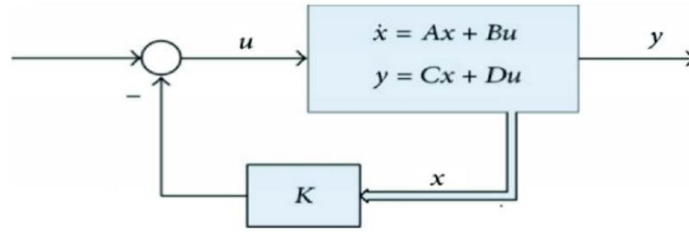


Figure 2.7: The structure of the LQR control system (Choi, 2010).

In this research, the LQR is used for to design the hexacopter reference model to get an optimal control solution that minimizes a cost function, providing a stable and well-behaved target for the actual control system to track.

2.8 Related Works on Hexacopter Drone

Several researchers studied how to model and control hexacopter UAVs for different applications. In this section, different related papers are reviewed based on stability, disturbance rejection, uncertainty parameter, chattering effect, controller performance, and so on.

Design of different controllers in quadcopter have was developed by Alias et al. (2018). The paper addresses the need to reduce quadcopter accidents caused by weather variations, air bumps, and other factors by designing, analyzing, and comparing the system's stability using several control methods: PID, Self-Tuning Regulator (STR), adaptive controller, Model Reference Adaptive Controller (MRAC), and Kalman filter-based controllers. The authors aimed to identify the most stable controller for quadcopters. To assess stability, they compared phase margin and gain margin values. Their findings show that the adaptive PID controller exhibits higher phase and gain margin values than the standard PID controller. Ultimately, the authors conclude that MRAC is the most effective choice for ensuring stable quadcopter operation. However, a significant drawback of this research is that it does not consider the unique control challenges and dynamics of hexacopters. Given that hexacopters have six rotors, they generally exhibit greater stability than quadcopters with four rotors, which could influence the applicability of the findings. (Alias et al., 2018).

A study on the modelling of a hexacopter have been developed by Le & Nam (2015). The paper presents a basic mathematical model for hexacopter control. This model can help

design methods to keep the hexacopter stable and follow a planned path. However, the way this model describes rotations (using Euler angles) can cause control and model failures at certain points. To avoid this problem, researchers changed to using quaternions to describe rotations. Quaternions are better because they are linear, stable, and efficient. The drawback of this research is that it doesn't consider the effects of aerodynamics to get better performance (Le & Nam, 2015).

The PID controller applied to hexacopter flight was developed by Alaimo et al. (2014). Their results demonstrate that the PID control scheme effectively stabilizes the hexacopter and achieves precise trajectory tracking. The authors suggest that the control strategy is robust against parameter uncertainties and external disturbances. They conclude that the proposed PID controller offers a promising approach to enhancing hexacopter flight performance. However, the research has notable drawbacks. It does not adequately address the impact of external disturbances, such as wind gusts or turbulence, which can significantly affect hexacopter stability and performance. Additionally, the study overlooks the issue of control signal chattering, which can result in vibrations and instability in hexacopter movement (Alaimo et al., 2014).

The dynamic modelling and control of a hexacopter using PID and back Stepping controllers were developed by Rao & Mathew (2018). Their study proposes two control schemes: PID and backstepping controllers; to regulate the hexacopter's altitude and attitude in space. The performance of these two control strategies was evaluated and compared in terms of stability. The findings indicate that hexacopter control poses challenges due to nonlinearities and modelling inaccuracies, which limit the performance of the PID controller. Effective design of the PID controller is essential for achieving the desired tracking of Euler angles. In contrast, the backstepping controller, which is specifically designed for nonlinear dynamical systems, demonstrates superior performance compared to the PID controller, even outside the linear region. However, a notable drawback of this research is that it does not address the issue of control signal chattering, which can lead to vibrations and instability in hexacopter movement (Rao & Mathew, 2018).

The robust and adaptive backstepping control for Hexacopter UAVs was developed by Zhang et al. (2019). Their study demonstrates that a hierarchically developed nonlinear robust and adaptive backstepping control scheme achieves robust trajectory tracking for the hexacopter UAV system. This proposed control scheme enables high-precision tracking,

improved anti-disturbance capability, and the generation of feasible control inputs for hexacopters. However, a notable drawback of this research is that it does not address the issue of control signal chattering, which can lead to vibrations and instability in hexacopter movement (Zhang et al., 2019).

The design and application of models reference adaptive control (MRAC) on balls and beams were developed by Romdlony et al. (2022b). This study demonstrates how an adaptive control method typically used for linear systems can be effectively applied to a nonlinear system like the ball and beam system. The objective is to achieve faster convergence and more consistent ball movement by fine-tuning the controller's initial conditions and gain limitations. Furthermore, the findings suggest that a similar MRAC controller could be applied to hexacopters, enabling it to manage the increased complexity of hexacopter dynamics and adapt in real-time to nonlinearities and uncertainties. MRAC has the potential to enhance overall controllability, robustness, and flight performance for hexacopters (Romdlony et al., 2022b).

Overall, this section discusses and reviews the research on the stability and modelling of hexacopters, as well as the performance of a hexacopter's altitude, position, and attitude controls using various controller techniques. A significant portion of the literature solely focused on stability performance, while some of the review examined trajectory tracking and the effects of external disturbances. These effects need to be considered in order to verify and examine the controllers' performance. When it comes to set point tracking issues and disturbance rejection capabilities, nonlinear control systems such as SMC perform very well. But the chattering effect of the traditional SMC can cause vibrations in the hexacopter system. Eliminating the chattering effect is another problem with the control mechanism of the hexacopter.

Therefore, this research study proposes an adaptive sliding mode control (SMC) with integrated proportional integral derivative (PID) control. This control system was designed to manage the altitude, position, and attitude of hexacopter drones. Additionally, the thesis developed more comprehensive models that incorporate aerodynamic effects for improved performance simulations.

CHAPTER THREE

3 MODELING OF SYSTEM DYNAMICS

3.1 Introduction

This chapter covers the materials and methods used in this research work, the dynamic and kinematic mathematical modeling of the hexacopter system based on Newton-Euler formalism.

3.2 Materials Used for the Study

MATLAB/Simulink, Microsoft Office 2019, and Math Type 7.7.0.237 equation are the software used in this research work. Simulink and technical toolboxes are components of MATLAB, while Microsoft Office is utilized to edit the thesis material and Math Type 7.7.0.237 equation is utilized to write mathematical formulas and equations in the Microsoft Office Word and PowerPoint presentation tools.

3.3 Methods to Follow

Figure 3.1 illustrates how the necessary task was completed for this research study. The literature and papers that are closely related are reviewed, and data are collected. In order to develop system modeling, the gathered data is mathematically and graphically analyzed. The hexacopter's dynamics modeling has been designed. Next, a minimum jerk trajectory is created. Then, a trajectory is generated that follows the minimum jerk principle. PID sliding surface Sliding mode controls is designed. The SMC is developed with an adaptive controller, and the system's suggested modelling and simulation results are then examined. As simulation tools, MATLAB and Simulink will be used to evaluate the system's performance.

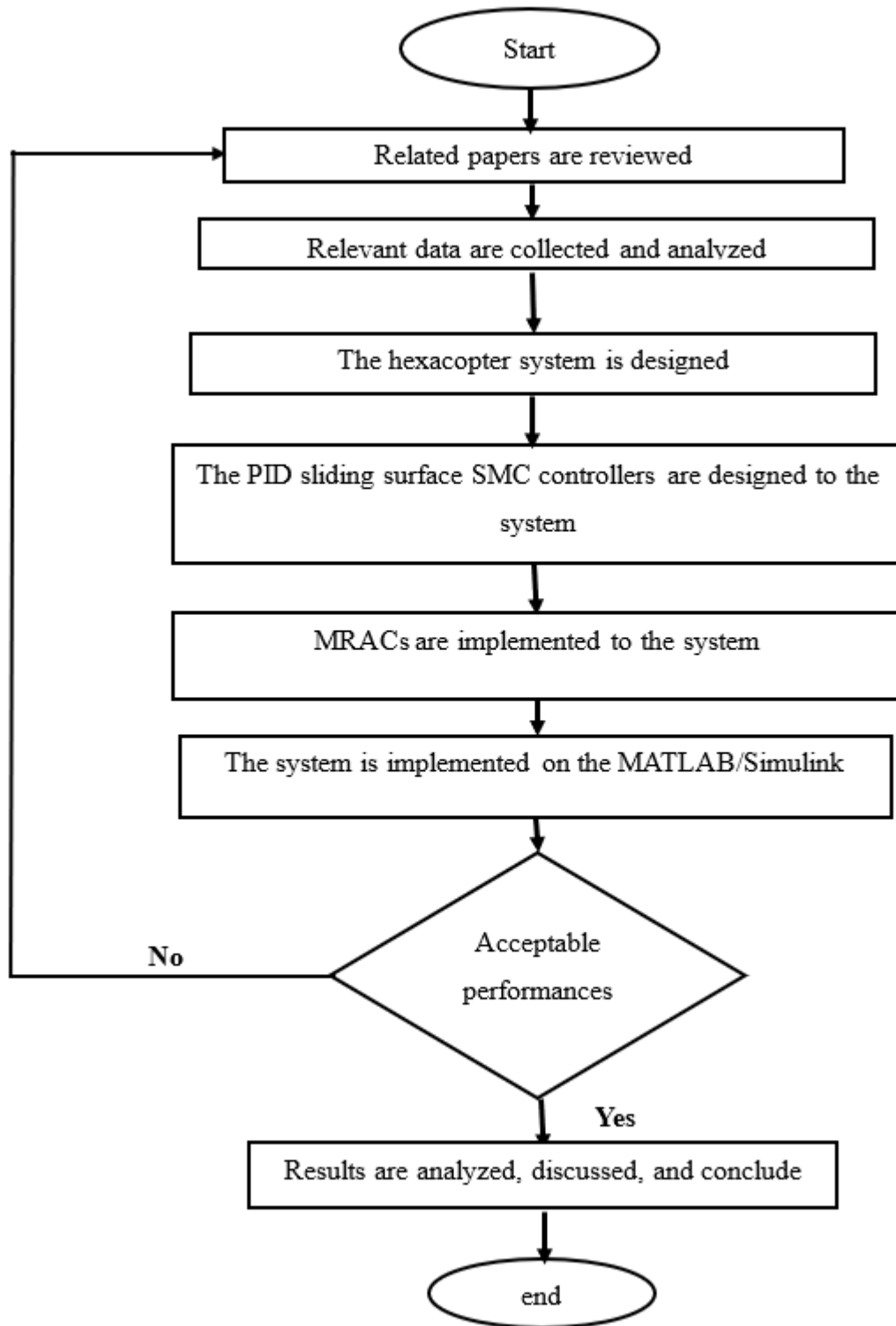


Figure 3.1: Block diagram of the proposed study

3.4 Block Diagram of the System

Figure 3.2 illustrates the block diagram of the suggested system designed to stabilize the altitude and attitude of hexacopter drones. The system is inherently complex, underactuated, extremely nonlinear, and unstable. Consequently, it requires an effective controller to maintain stability. To address this need and achieve optimal performance, an adaptive PID-based sliding mode control (SMC) controller is proposed and to get the best performance.

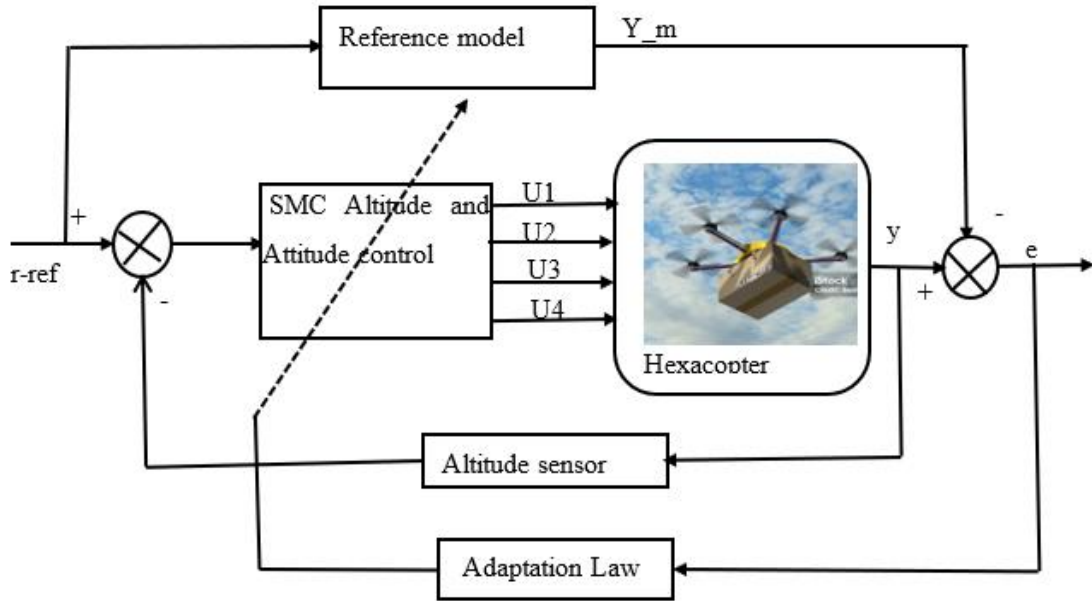


Figure 3.2 Block diagram of the system

3.5 Modeling of a Hexacopter

The mathematical model explains the attitude of a hexacopter, which features six propellers arranged orthogonally to its body frame. The attitude is characterized by three movements: Roll, which is rotation around the X-axis, occurs when the balance of rotors 1, 2, and 3 (or 6, 5, and 4) is altered by increasing or decreasing their speeds, resulting in lateral acceleration; pitch, rotation around the Y axis, is achieved by adjusting the speed of rotors 1 and 6 (or 3 and 4), leading to longitudinal acceleration; and yaw, the rotation about the Z axis, is obtained through a simultaneous change in the speed of the motors 1, 3, and 5, or 2, 4, and 6.

The dynamics and kinematics models of hexacopter are obtained by using a Newton-Euler formulation, and considered the following assumptions.

- The hexacopters structure is both rigid and symmetrical.
- The hexacopter's center of gravity aligns with the origin of the body fixed frame.

- It has rigid propellers.
- Drag and thrust forces acting on the hexacopter are related to the square of propeller's speed.

3.5.1 Rotation Matrix of Reference Frame (\mathfrak{R})

Figure 3.3 shows the hexacopter's schematic structure as well as the propellers' rotational directions. To describe the motion of a hexacopter, two reference systems are utilized: the earth inertial frame (\mathfrak{R}_I -frame) and the body fixed frame (\mathfrak{R}_b -frame). The flight of the hexacopter is controlled using Euler angles, which define the angular orientation of a fixed body relative to a reference frame. The three Euler angles for the aircraft are Pitch (θ), Yaw (ψ), and Roll (ϕ) (SINGH, 2018).

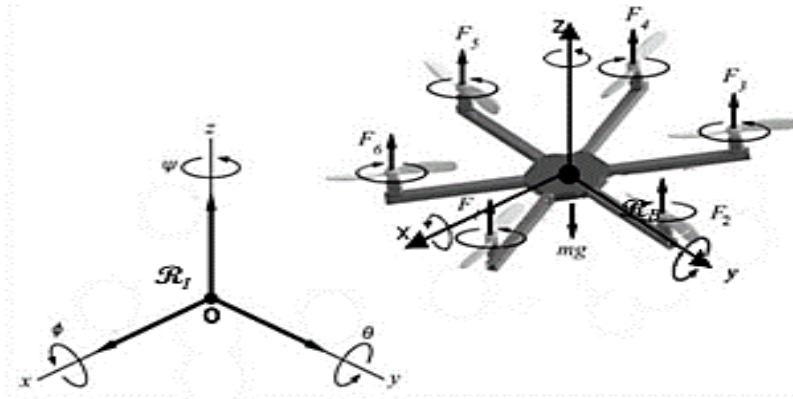


Figure 3.3: The structure and its frames of a hexacopter drone (Le & Nam, 2015)

To simplify the process, we represent the linear position vector and the attitude (Euler angle) vector in the inertial frame as $\chi = [x \ y \ z]^T$ and $\xi = [\phi \ \theta \ \psi]^T$, respectively. As a result, the linear and angular velocities in the inertial frame are denoted as $\dot{\chi} = [\dot{x} \ \dot{y} \ \dot{z}]^T$ and $\dot{\xi} = [\dot{\phi} \ \dot{\theta} \ \dot{\psi}]^T$. In the body frame, the angular velocities are represented by $\omega = [p \ q \ r]^T$ and the linear velocities by $V_b = [V_{x,b} \ V_{y,b} \ V_{z,b}]^T$. The orientation of the hexacopter has been expressed using a rotational matrix. Now, the thesis employs an orthogonal rotation matrix \mathfrak{R} to define the transformation from the body frame to the inertial frame. The matrix \mathfrak{R} can be described as the result of rotation along the x, y, and z axes combined:

The rotation along the x-axis, y-axis, and z-axis can be written as (Bathurst et al., 2022):

$$\mathfrak{R}_x = \begin{bmatrix} 1 & 0 & 0 \\ 0 & \cos \phi & -\sin \phi \\ 0 & \sin \phi & \cos \phi \end{bmatrix} \quad \mathfrak{R}_y = \begin{bmatrix} \cos \theta & 0 & \sin \theta \\ 0 & 1 & 0 \\ -\sin \theta & 0 & \cos \theta \end{bmatrix} \quad \mathfrak{R}_z = \begin{bmatrix} \cos \psi & -\sin \psi & 0 \\ \sin \psi & \cos \psi & 0 \\ 0 & 0 & 1 \end{bmatrix} \quad (3.1)$$

Assuming the center of gravity to be the origin, the hexacopter is expressed by the earth inertial frame. To achieve rotation from the body frame to the earth inertial frame, one must rotate in the ZYX- direction and depend on the three Euler angles as shown in Equation (3.2)

$$\text{Rotation matrix } \mathfrak{R} = \mathfrak{R}_z * \mathfrak{R}_y * \mathfrak{R}_x$$

The matrix of transformation from the body frame to the inertial frame is provided as:

$$\mathfrak{R}_{ib} = \begin{bmatrix} \cos \theta \cos \psi & \cos \psi \sin \theta \sin \phi - \cos \phi \sin \psi & \cos \phi \cos \psi \sin \theta + \sin \phi \sin \psi \\ \cos \theta \sin \psi & \cos \phi \cos \psi + \sin \theta \sin \phi \sin \psi & \cos \phi \sin \theta \sin \psi - \cos \psi \sin \phi \\ -\sin \theta & \cos \theta \sin \phi & \cos \theta \cos \phi \end{bmatrix} \quad (3.2)$$

The matrix of transformation from the inertial frame to the body frame will be

$$\mathfrak{R}_{bi} = \mathfrak{R}_{ib}^{-1} = \mathfrak{R}^T$$

$$\mathfrak{R}_{bi} = \begin{bmatrix} \cos \theta \cos \psi & \cos \theta \sin \psi & -\sin \theta \\ \cos \psi \sin \theta \sin \phi - \cos \phi \sin \psi & \cos \phi \cos \psi + \sin \theta \sin \phi \sin \psi & \cos \theta \sin \phi \\ \cos \phi \cos \psi \sin \theta + \sin \phi \sin \psi & \cos \phi \sin \theta \sin \psi - \cos \psi \sin \phi & \cos \theta \cos \phi \end{bmatrix} \quad (3.3)$$

3.5.2 Hexacopter Kinematics

The angular velocity addition theorem is used to calculate the hexacopter's kinematics (Niguse, 2020). The theorem states that for angular velocity vectors coordinated in a single frame, the resulting angular velocity of the cumulative rotations is equal to the simple sum of the individual contributing rotations. To ensure system continuity when transitioning from the body frame to the inertial frame, it is essential to derive the transformation matrix for angular velocities (SINGH, 2018). The rotation is done in the following order: first, rotation about the $\dot{\psi}$ must incorporate both \mathfrak{R}_x and \mathfrak{R}_y to achieve alignment with the body frame; second, rotation in the $\dot{\theta}$ must include \mathfrak{R}_x rotation to achieve alignment with the body frame; and third, rotation in the $\dot{\phi}$ that need not cover any rotations occurs. The two

transformation laws are $\omega = \omega_\xi \dot{\xi}$ and $\dot{\xi} = \omega_\xi^{-1} \omega$. ω_ξ^{-1} is only definable if $-\frac{\pi}{2} < \phi, \theta < \frac{\pi}{2}$ and $\psi \in (-\pi, \pi)$. Due to the fact that the given matrix's determinant approaches infinity and results in singularity. The specified range is used to prevent the singularity problem.

Therefore, the kinematic equation can be obtained:

$$\omega = \begin{bmatrix} p \\ q \\ r \end{bmatrix} = \begin{bmatrix} \dot{\phi} \\ 0 \\ 0 \end{bmatrix} + \mathfrak{R}_x \begin{bmatrix} 0 \\ \dot{\theta} \\ 0 \end{bmatrix} + \mathfrak{R}_x \mathfrak{R}_y \begin{bmatrix} 0 \\ 0 \\ \dot{\psi} \end{bmatrix} \quad (3.4)$$

$$\omega = \begin{bmatrix} \dot{\phi} \\ 0 \\ 0 \end{bmatrix} + \begin{bmatrix} 1 & 0 & 0 \\ 0 & \cos \phi & -\sin \phi \\ 0 & \sin \phi & \cos \phi \end{bmatrix} \begin{bmatrix} 0 \\ \dot{\theta} \\ 0 \end{bmatrix} + \begin{bmatrix} 1 & 0 & 0 \\ 0 & \cos \phi & -\sin \phi \\ 0 & \sin \phi & \cos \phi \end{bmatrix} \begin{bmatrix} \cos \theta & 0 & \sin \theta \\ 0 & 1 & 0 \\ -\sin \theta & 0 & \cos \theta \end{bmatrix} \begin{bmatrix} 0 \\ 0 \\ \dot{\psi} \end{bmatrix} \quad (3.5)$$

Then Equation (3.5) is further simplified as

$$\omega = \begin{bmatrix} p \\ q \\ r \end{bmatrix} = \begin{bmatrix} 1 & 0 & -\sin \theta \\ 0 & \cos \phi & \cos \theta \sin \phi \\ 0 & -\sin \phi & \cos \theta \cos \phi \end{bmatrix} \begin{bmatrix} \dot{\phi} \\ \dot{\theta} \\ \dot{\psi} \end{bmatrix} \quad (3.6)$$

Where the angular velocity transformation matrix from the inertial frame to the body frame is:

$$\omega_\xi = \begin{bmatrix} 1 & 0 & -\sin \theta \\ 0 & \cos \phi & \cos \theta \sin \phi \\ 0 & -\sin \phi & \cos \theta \cos \phi \end{bmatrix} \quad (3.7)$$

The angular velocities transformation matrix from the body frame to inertial frame will be:

$$\omega_\xi^{-1} = \begin{bmatrix} 1 & \sin \phi \tan \theta & \cos \phi \tan \theta \\ 0 & \cos \phi & -\sin \phi \\ 0 & \sec \theta \sin \phi & \cos \phi \sec \theta \end{bmatrix} \quad (3.8)$$

3.5.3 Hexacopter Applied Force

The hexacopter's motion is produced by both varying the speed and providing each propeller the same speed. There are three main force applied to the hexacopter: the thrust force (F_T), the aerodynamics drag force (F_D), and the gravitational force (F_G) (Bisgaard et al., 2010) .

Therefore,

$$\sum F = F_T + F_D + F_G \quad (3.9)$$

1. **Gravitational force (F_G):** In the body coordinate frame, the gravitational force vector operating on the hexacopter center of gravity is represented as

$$F_G = [0 \quad 0 \quad -mg]^T \quad (3.10)$$

Where: m = the body's mass, g = acceleration due to gravity.

2. **Thrust force (F_T):** Control design and simulation depend heavily on the thrust of the motors since it powers all hexacopter maneuvers. Each propeller/motor thrust force is provided by:

$$F_{Ti} = \kappa \omega_i^2 \quad (3.11)$$

Where: $F_T = U_1, U_1 = input 1$, κ = thrust coefficient;

ω_i = angular velocity of the i^{th} motor/propeller.

Thus, the total thrust will be as follows because there are six motors and each one produces a thrust

$$F_T = \sum_{i=1}^6 F_{Ti} = \kappa \begin{bmatrix} 0 \\ 0 \\ \sum \omega_i^2 \end{bmatrix} = \kappa \begin{bmatrix} 0 \\ 0 \\ \omega_1^2 + \omega_2^2 + \omega_3^2 + \omega_4^2 + \omega_5^2 + \omega_6^2 \end{bmatrix} \quad (3.12)$$

Then the further simplified form of thrust force is:

$$F_T = \kappa(\omega_1^2 + \omega_2^2 + \omega_3^2 + \omega_4^2 + \omega_5^2 + \omega_6^2) \quad (3.13)$$

3. **Aerodynamics drag force (F_D):** The impact of the aerodynamics drag force is mainly considered for translational dynamics, which can be represented mathematically by Equation (3.14).

$$F_D = \frac{1}{2} \rho_m \mu_v^2 C_D A \quad (3.14)$$

Where: ρ_m = density of mass, C_D = drag coefficient, A = area of propeller,

μ_v = velocity of propeller relative to the object.

$$F_D = \kappa_{fd} \dot{\chi} = I_{3 \times 3} \begin{bmatrix} \kappa_{fdx} & \kappa_{fdy} & \kappa_{fdz} \end{bmatrix}^T \begin{bmatrix} \dot{x} & \dot{y} & \dot{z} \end{bmatrix}^T \quad (3.15)$$

The vector of aerodynamics drag force constant is $\kappa_{fd} = \text{diag}(\kappa_{fdx}, \kappa_{fdy}, \kappa_{fdz})$.

3.5.4 Hexacopter Applied Torque

Theoretically, torques around the x, y, and z axes produced by the six rotors rotating at different speeds will result in roll, pitch, and yaw rotations. Depending on how far away from the center of gravity the rotors are, they will have varying effects on the overall rotation about that axis. Torque is defined as force multiplied by distance. The arms' lengths and angles are displayed in Figure 3.4 in relation to the rotor's distance from the rotational axis, or the distance in relation to the center of gravity.

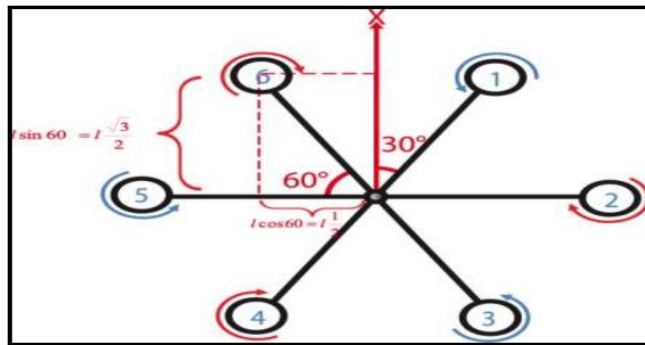


Figure 3.4: Hexacopter rotor distances to center of gravity (L4)

The torque vector τ :

$$\tau = \tau_A + \tau_G + \tau_D \quad (3.16)$$

Where: τ_A = propellers torque/actuator action, τ_G = gyroscopic torque τ_D = aerodynamic drag torque.

1. Actuator action/propellers torque (τ_A): The torque that the propeller of a hexacopter produces is: $\tau_A = \tau_\phi i + \tau_\theta j + \tau_\psi k$. τ_ϕ , τ_ψ , and τ_θ denote the roll, yaw, and pitch moments, respectively. The roll, yaw, and pitch of the hexacopter can be determined from its geometrical structure.

- **Roll torque**

Rotation on the x-axis is known as roll torque. Torque can be expressed as the propeller's force multiplied by the body's arm length, assuming that the arms are positioned at 60 and 30 degrees. In this case, the angular velocities that are active during rolling motion are ω_1 , ω_2 , ω_3 , ω_4 , ω_5 , and ω_6 , where rotor speed (ω_1 , ω_2 , and ω_3) act in one direction and the remaining three rotor speed (ω_4 , ω_5 , and ω_6) act in the opposite direction. Decrease or increase the speed of the rotors on the right side while maintaining the same speed on the rotors on the left side to produce rolling motion. Figure 3.5 below provides a description of rolling motion. In this case, the red arrow indicates a decreasing angular velocity, and the blue arrow indicates an increasing angular velocity. The generated roll torque is shown in Equation (3.17):

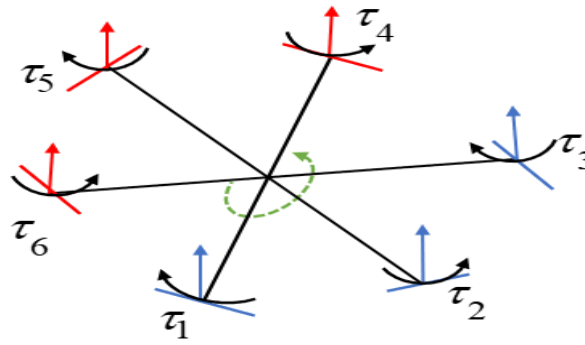


Figure 3.5: Rolling motion

$$\tau_\phi = -\sin 30^\circ lF_{T1} - lF_{T2} - \sin 30^\circ lF_{T3} + \sin 30^\circ lF_{T4} + lF_{T5} + \sin 30^\circ lF_{T6}$$

$$\tau_\phi = -\frac{1}{2}lF_{T1} - lF_{T2} - \frac{1}{2}lF_{T3} + \frac{1}{2}lF_{T4} + lF_{T5} + \frac{1}{2}lF_{T6}$$

$$\tau_\phi = \kappa l(-\omega_2^2 + \omega_5^2 + \frac{1}{2}(-\omega_1^2 - \omega_3^2 + \omega_4^2 + \omega_6^2)) \quad (3.17)$$

Where: $\tau_\phi = U_2, U_2 = \text{input } 2$

- **Pitch torque**

Rotation on the y-axis is known as pitch torque. In this case, the only angular velocities that are active during pitch motion are $\omega_1, \omega_3, \omega_4,$ and ω_6 , where ω_3 and ω_4 are increased or decreased in order to generate pitch torque, while ω_1 and ω_6 are also increased or decreased. Additionally, ω_2 and ω_5 do not form a moment since they are located at the moment reference axis.

Figure 3.6 below provides a description of pitch motion. In this case, the red arrow indicates a decreasing angular velocity, the black arrow indicates the angular velocity is not changing, and the blue arrow indicates an increasing angular velocity. The generated pitching torque is shown in Equation (3.18).

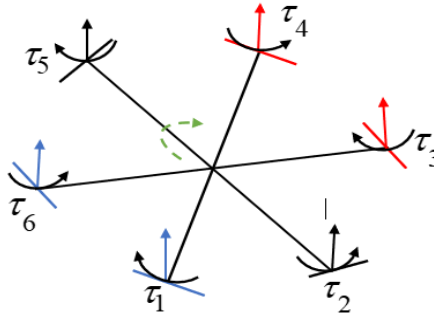


Figure 3.6: Pitching motion

$$\tau_\theta = \sin 60^\circ lF_{T1} - \sin 60^\circ lF_{T3} - \sin 60^\circ lF_{T4} + \sin 60^\circ lF_{T6}$$

$$\tau_\theta = \frac{\sqrt{3}}{2} lF_{T1} - \frac{\sqrt{3}}{2} lF_{T3} - \frac{\sqrt{3}}{2} lF_{T4} + \frac{\sqrt{3}}{2} lF_{T6}$$

$$\tau_\theta = \frac{\sqrt{3}}{2} \kappa l (\omega_1^2 - \omega_3^2 - \omega_4^2 + \omega_6^2) \quad (3.18)$$

Where: $\tau_\theta = U_3, U_3 = \text{input } 3$

- **Yaw torque**

Rotation on the z-axis is known as yaw torque. In this case, angular velocities $\omega_1, \omega_5,$ and ω_3 will act in one direction, while Conversely, the angular velocities $\omega_6, \omega_4,$ and ω_2 will

act opposite to one another. Thus, by raising or reducing the speed of rotors rotating clockwise and reducing or raising the speed of rotors rotating counter clockwise, the torque in the z-direction can be achieved. In Figure 3.7 below, the yawing motion is explained. The generated yawing torque is shown in Equation (3.19).

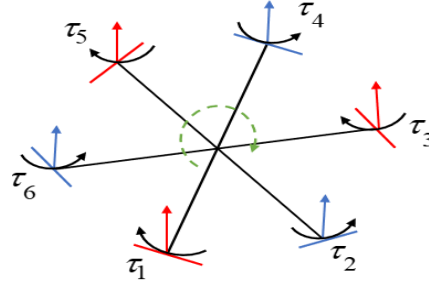


Figure 3.7: Yawing motion

$$\tau_{\psi} = d(-\omega_1^2 + \omega_2^2 - \omega_3^2 + \omega_4^2 - \omega_5^2 + \omega_6^2) \quad (3.19)$$

Where: $\tau_{\psi} = U_4$, $U_4 = \text{input } 4$, $d = \text{drag factor/torque coefficient motor}$

Consequently, the propeller's total torque can be expressed as:

$$\tau_A = \begin{bmatrix} \tau_{\phi} \\ \tau_{\theta} \\ \tau_{\psi} \end{bmatrix} = \begin{bmatrix} \kappa l(-\omega_2^2 + \omega_5^2 + \frac{1}{2}(-\omega_1^2 - \omega_3^2 + \omega_4^2 + \omega_6^2)) \\ \frac{\sqrt{3}}{2} \kappa l(\omega_1^2 - \omega_3^2 - \omega_4^2 + \omega_6^2) \\ d(-\omega_1^2 + \omega_2^2 - \omega_3^2 + \omega_4^2 - \omega_5^2 + \omega_6^2) \end{bmatrix} \quad (3.20)$$

2. Gyroscopic torque (τ_G): It is a physical phenomenon that occurs due to the rotation of the propellers on a hexacopter. As propellers 5, 3, and 1 rotate in a clockwise direction, while propellers 6, 4, and 2 rotate counterclockwise, resulting in an overall imbalance when the rotor speeds' algebraic sum does not equal zero. The result of this imbalance is a gyroscopic effect. The rotor's angular velocity, body attitude rate, and moment of inertia all contribute to the gyroscopic effect. It can be expressed by:

$$\tau_G = J_p \begin{bmatrix} \omega \times \begin{bmatrix} 0 \\ 0 \\ 1 \end{bmatrix} \end{bmatrix} (-1)^i \omega_i = J_p \begin{bmatrix} p \\ q \\ r \end{bmatrix} \times \begin{bmatrix} 0 \\ 0 \\ 1 \end{bmatrix} (-1)^i \omega_i$$

$$\tau_G = J_p \begin{bmatrix} q \\ p \\ 0 \end{bmatrix} \omega_r = J_p \begin{bmatrix} \dot{\theta} \\ \dot{\phi} \\ 0 \end{bmatrix} \omega_r \quad (3.21)$$

Where, $\omega_r = (-1)^i \omega_i = -\omega_1 + \omega_2 - \omega_3 + \omega_4 - \omega_5 + \omega_6$

3. Aerodynamic drag torque (τ_D): The torque produced by aerodynamic frictions is known as the aerodynamic torque/moment. Equation (3.22) expresses the equation for the aerodynamic torque.

$$F_D = \kappa_{\tau d} \dot{\xi} = I_{3 \times 3} \begin{bmatrix} \kappa_{\tau dx} & \kappa_{\tau dy} & \kappa_{\tau dz} \end{bmatrix}^T \begin{bmatrix} \dot{\phi} & \dot{\theta} & \dot{\psi} \end{bmatrix}^T \quad (3.22)$$

The vector of aerodynamics moment constant is $\kappa_{\tau d} = \text{diag}(\kappa_{\tau dx}, \kappa_{\tau dy}, \kappa_{\tau dz})$.

3.5.5 Hexacopter Dynamic Model

The dynamics of the hexacopter, including its translational (x, y, and z) and rotational (yaw, pitch, and roll) movements, are derived using the Newton-Euler formalism. This approach utilizes Newton's second law to calculate translational motion and the Euler equation to calculate rotational motion (Simon & Martinović, 2013).

Therefore, the following equations are obtained:

$$\begin{bmatrix} mI_{3 \times 3} & 0_{3 \times 3} \\ 0_{3 \times 3} & J \end{bmatrix} \begin{bmatrix} \dot{V}_b \\ \dot{\omega} \end{bmatrix} = \begin{bmatrix} \omega \wedge mV_b \\ \omega \wedge J\omega \end{bmatrix} = \begin{bmatrix} \sum F \\ \sum \tau \end{bmatrix} \quad (3.23)$$

$$\sum F = m\dot{V}_b + \omega \times mV_b \quad \text{or} \quad \dot{V}_b = -\omega \times V_b + \frac{1}{m} \sum F \quad (3.24)$$

$$\sum \tau = J_{cm} \dot{\omega} + \omega \times J_{cm} \omega \quad \text{or} \quad \dot{\omega} = J_{cm}^{-1} (-\omega \times J_{cm} \omega + \sum \tau) \quad (3.25)$$

Where: F is the body's force net, τ is resultant torque affecting body of the hexacopter, m is the body's mass, \dot{V}_b is acceleration of the body, V_b is body linear velocity, ω is angular velocity of the body, J_{cm} is inertia of the body in kgm^2 . Since a hexacopter is often

symmetric with respect to the x and y-axis, $J_{cm} = \text{diag}(J_{xx}, J_{yy}, J_{zz})$ can be used to define the inertia of the body about the center of mass.

$$J_{cm} = \begin{bmatrix} J_{xx} & 0 & 0 \\ 0 & J_{yy} & 0 \\ 0 & 0 & J_{zz} \end{bmatrix} \quad (3.26)$$

3.5.5.1 Translational Dynamics

According to Newton's second law in equation (3.27) and the earth's inertial frame, the hexacopters translational equation of motion is calculated.

$$ma = \sum F \quad (3.27)$$

The hexacopter's body frame provides the force acting on it, and the force needed to accelerate mass and generate centrifugal force is equal to the combined thrust of the rotors, aerodynamics drag force, and gravity, as shown in equation (3.28).

$$ma = m\dot{V}_b + \omega \times mV_b = \sum F = \mathfrak{R}_{bi}F_G + F_T - F_D \quad (3.28)$$

$$m\ddot{\chi} = \begin{bmatrix} 0 \\ 0 \\ -mg \end{bmatrix} + \mathfrak{R}_{ib}F_T - F_D$$

$$\begin{bmatrix} \ddot{x} \\ \ddot{y} \\ \ddot{z} \end{bmatrix} = \frac{F_T}{m} \begin{bmatrix} \cos \phi \cos \psi \sin \theta + \sin \phi \sin \psi \\ \cos \phi \sin \theta \sin \psi - \cos \psi \sin \phi \\ (\cos \theta \cos \phi) - g \end{bmatrix} - \frac{1}{m} \begin{bmatrix} \kappa_{fdx} \dot{x} \\ \kappa_{fdy} \dot{y} \\ \kappa_{fdz} \dot{z} \end{bmatrix}$$

$$\ddot{x} = \frac{F_T}{m} (\cos \phi \cos \psi \sin \theta + \sin \phi \sin \psi) - \frac{\kappa_{fdx}}{m} \dot{x} \quad (3.29)$$

$$\ddot{y} = \frac{F_T}{m} (\cos \phi \sin \theta \sin \psi - \cos \psi \sin \phi) - \frac{\kappa_{fdy}}{m} \dot{y} \quad (3.30)$$

$$\ddot{z} = \frac{F_T}{m} (\cos \theta \cos \phi) - g - \frac{\kappa_{fdz}}{m} \dot{z} \quad (3.31)$$

3.5.5.2 Rotational Dynamics of Hexacopter

Based on the general Euler inertial equation in equation (3.32), the hexacopters rotational equation of motion is calculated.

$$J \ddot{\xi} = \sum \tau \quad (3.32)$$

In the body frame, the external torque, $\tau_A = [\tau_\phi \quad \tau_\theta \quad \tau_\psi]^T$, is equal to the torques due to the centripetal forces ($\omega \times J \omega$), the gyroscopic forces (τ_G), aerodynamic drag torque (τ_D), and the angular acceleration of the inertia ($J \dot{\omega}$) as Equation (3.35).

$$J \dot{\omega} + \omega \times J \omega + \tau_G + \tau_D = \tau_A \quad (3.33)$$

$$\dot{\omega} = J^{-1}(-\omega \times J \omega - \tau_G + \tau_A - \tau_D)$$

$$\dot{\omega} = \begin{bmatrix} \dot{p} \\ \dot{q} \\ \dot{r} \end{bmatrix} = \begin{bmatrix} \frac{(J_{yy} - J_{zz})qr}{J_{xx}} \\ \frac{(J_{zz} - J_{xx})pr}{J_{yy}} \\ \frac{(J_{xx} - J_{yy})pq}{J_{zz}} \end{bmatrix} - \begin{bmatrix} \frac{J_p q}{J_{xx}} \\ -\frac{J_p p}{J_{yy}} \\ 0 \end{bmatrix} \omega_r + \begin{bmatrix} \tau_\phi / J_{xx} \\ \tau_\theta / J_{yy} \\ \tau_\psi / J_{zz} \end{bmatrix} - \begin{bmatrix} \frac{\kappa_{\tau dx} \dot{\phi}^2}{J_{xx}} \\ \frac{\kappa_{\tau dy} \dot{\theta}^2}{J_{yy}} \\ \frac{\kappa_{\tau dz} \dot{\psi}^2}{J_{zz}} \end{bmatrix} \quad (3.34)$$

$$\dot{p} = \frac{(J_{yy} - J_{zz})qr}{J_{xx}} - \frac{J_p q}{J_{xx}} \omega_r + \frac{\tau_\phi}{J_{xx}} - \frac{\kappa_{\tau dx} \dot{\phi}^2}{J_{xx}} \quad (3.35)$$

$$\dot{q} = \frac{(J_{zz} - J_{xx})pr}{J_{yy}} + \frac{J_p p}{J_{yy}} \omega_r + \frac{\tau_\theta}{J_{yy}} - \frac{\kappa_{\tau dy} \dot{\theta}^2}{J_{yy}} \quad (3.36)$$

$$\dot{r} = \frac{(J_{xx} - J_{yy})qp}{J_{zz}} + \frac{\tau_\psi}{J_{zz}} - \frac{\kappa_{\tau dz} \dot{\psi}^2}{J_{zz}} \quad (3.37)$$

Notice that from Equation (3.8), the matrix of transformations from $[p, q, r]$ to $[\dot{\phi}, \dot{\theta}, \dot{\psi}]$ is provided by:

$$\begin{bmatrix} \dot{\phi} \\ \dot{\theta} \\ \dot{\psi} \end{bmatrix} = \begin{bmatrix} 1 & \tan \theta \sin \phi & \tan \theta \cos \phi \\ 0 & \cos \phi & -\sin \phi \\ 0 & \sin \phi \sec \theta & \sec \theta \cos \phi \end{bmatrix} \begin{bmatrix} p \\ q \\ r \end{bmatrix} \quad (3.38)$$

The hexacopter always intentionally maintains small attitude angles during flight to

guarantee flight safety (Huang et al., 2019). That implies that $[\dot{\phi}, \dot{\theta}, \dot{\psi}] \approx [p, q, r]$.

Therefore, the rotational dynamics of the hexacopter are given below:

$$\ddot{\phi} = \frac{(J_{yy} - J_{zz})\dot{\theta}\dot{\psi}}{J_{xx}} - \frac{J_p\dot{\theta}}{J_{xx}}\omega_r - \frac{\kappa_{\tau dx}\dot{\phi}^2}{J_{xx}} + \frac{\tau_{\phi}}{J_{xx}} \quad (3.39)$$

$$\ddot{\theta} = \frac{(J_{zz} - J_{xx})\dot{\phi}\dot{\psi}}{J_{yy}} + \frac{J_p\dot{\phi}}{J_{yy}}\omega_r - \frac{\kappa_{\tau dy}\dot{\theta}^2}{J_{yy}} + \frac{\tau_{\theta}}{J_{yy}} \quad (3.40)$$

$$\ddot{\psi} = \frac{(J_{xx} - J_{yy})\dot{\phi}\dot{\theta}}{J_{zz}} - \frac{\kappa_{\tau dz}\dot{\psi}^2}{J_{zz}} + \frac{\tau_{\psi}}{J_{zz}} \quad (3.41)$$

3.5.6 Hexacopter Control Inputs and Rotor Speeds

The hexacopter system is underactuated, meaning that its input is less than its output. The system in our instance has four inputs and 6 DOFs. Thrust force, yaw torque, pitch torque, and roll torque are these inputs.

The following are the control inputs U for the hexacopter dynamics:

$$U_1 = F_T = \kappa(\omega_1^2 + \omega_2^2 + \omega_3^2 + \omega_4^2 + \omega_5^2 + \omega_6^2) \quad (3.42)$$

$$U_2 = \kappa l(-\omega_2^2 + \omega_5^2 + \frac{1}{2}(-\omega_1^2 - \omega_3^2 + \omega_4^2 + \omega_6^2)) \quad (3.43)$$

$$U_3 = \frac{\sqrt{3}}{2}\kappa l(\omega_1^2 - \omega_3^2 - \omega_4^2 + \omega_6^2) \quad (3.44)$$

$$U_4 = d(-\omega_1^2 + \omega_2^2 - \omega_3^2 + \omega_4^2 - \omega_5^2 + \omega_6^2) \quad (3.45)$$

Then the matrix of the control input is expressed as:

$$\begin{bmatrix} U_1 \\ U_2 \\ U_3 \\ U_4 \end{bmatrix} = \begin{bmatrix} \kappa & \kappa & \kappa & \kappa & \kappa & \kappa \\ \frac{-\kappa l}{2} & -\kappa l & \frac{-\kappa l}{2} & \frac{\kappa l}{2} & \kappa l & \frac{\kappa l}{2} \\ \frac{\sqrt{3}\kappa l}{2} & 0 & \frac{-\sqrt{3}\kappa l}{2} & \frac{-\sqrt{3}\kappa l}{2} & 0 & \frac{\sqrt{3}\kappa l}{2} \\ -d & d & -d & d & -d & d \end{bmatrix} \begin{bmatrix} \omega_1^2 \\ \omega_2^2 \\ \omega_3^2 \\ \omega_4^2 \\ \omega_5^2 \\ \omega_6^2 \end{bmatrix} \quad (3.46)$$

To calculate the rotor speed from the control inputs, it is essential to establish the inverse relationship between the rotor speeds and the inputs. This can be achieved by inverting the

matrix presented in Equation (3.47) using the pseudo-inverse method, which allows for the calculation of the rotor velocities because the matrix may not be square or may not have full rank. By applying this method, we can effectively derive the rotor speeds corresponding to the desired control inputs.

$$\begin{bmatrix} \omega_1^2 \\ \omega_2^2 \\ \omega_3^2 \\ \omega_4^2 \\ \omega_5^2 \\ \omega_6^2 \end{bmatrix} = \begin{bmatrix} \frac{1}{6\kappa} & \frac{1}{3\kappa l} & 0 & \frac{-1}{6d} \\ \frac{1}{6\kappa} & \frac{1}{6\kappa l} & \frac{-\sqrt{3}}{6\kappa l} & \frac{1}{6d} \\ \frac{1}{6\kappa} & \frac{-1}{6\kappa l} & \frac{-\sqrt{3}}{6\kappa l} & \frac{-1}{6d} \\ \frac{1}{6\kappa} & \frac{-1}{6\kappa l} & 0 & \frac{1}{6d} \\ \frac{1}{6\kappa} & \frac{1}{3\kappa l} & 0 & \frac{1}{6d} \\ \frac{1}{6\kappa} & \frac{-1}{6\kappa l} & \frac{\sqrt{3}}{6\kappa l} & \frac{-1}{6d} \\ \frac{1}{6\kappa} & \frac{1}{6\kappa l} & \frac{\sqrt{3}}{6\kappa l} & \frac{1}{6d} \end{bmatrix} \begin{bmatrix} U_1 \\ U_2 \\ U_3 \\ U_4 \end{bmatrix} \quad (3.47)$$

3.5.7 State Space Equation for Hexacopter Dynamics

A state-space form (Niguse, 2020) can be used to simplify the translational Equations (3.35)–(3.37) and rotational Equations (3.39)–(3.41) components that are discovered from the modelling. A hexacopters system has 12 states, and the state vector is expressed as follows:

$$X = [X_1 \ X_2 \ X_3 \ X_4 \ X_5 \ X_6 \ X_7 \ X_8 \ X_9 \ X_{10} \ X_{11} \ X_{12}]^T \quad (3.48)$$

The translational dynamics of the hexacopter is defined directly with altitude z , y , and x , while the rotational equations of motion use Euler angles and their rates. As a result, the states can be expressed as:

$$X = \left[\phi \ \dot{\phi} \ \theta \ \dot{\theta} \ \psi \ \dot{\psi} \ x \ \dot{x} \ y \ \dot{y} \ z \ \dot{z} \right]^T \quad (3.49)$$

Lastly, the hexacopter system's whole state space representation can be shown as follows:

$$\dot{x} = f(x, U) = \begin{cases} \dot{X}_1 = X_2 \\ \dot{X}_2 = c_1 X_4 X_6 + c_2 \omega_r X_4 + c_3 X_2^2 + d_1 U_2 + d_\phi \\ \dot{X}_3 = X_4 \\ \dot{X}_4 = c_4 X_2 X_6 + c_5 \omega_r X_2 + c_6 X_4^2 + d_2 U_3 + d_\theta \\ \dot{X}_5 = X_6 \\ \dot{X}_6 = c_7 X_2 X_4 + c_8 X_6^2 + d_3 U_4 + d_\psi \\ \dot{X}_7 = X_8 \\ \dot{X}_8 = d_4 U_1 U_x + d_5 X_8 + d_x \\ \dot{X}_9 = X_{10} \\ \dot{X}_{10} = d_4 U_1 U_y + d_6 X_{10} + d_y \\ \dot{X}_{11} = X_{12} \\ \dot{X}_{12} = -g + d_4 U_1 U_z + d_7 X_{12} + d_z \end{cases} \quad (3.50)$$

Where:

$$\begin{aligned} c_1 &= \frac{(J_{yy} - J_{zz})}{J_{xx}} & c_2 &= \frac{(-J_p)}{J_{xx}} & c_3 &= \frac{(-k_{\tau dx})}{J_{xx}} & d_1 &= \frac{1}{J_{xx}} \\ c_4 &= \frac{(J_{zz} - J_{xx})}{J_{yy}} & c_5 &= \frac{(J_p)}{J_{yy}} & c_6 &= \frac{(-k_{\tau dy})}{J_{yy}} & d_2 &= \frac{1}{J_{yy}} \\ c_7 &= \frac{(J_{xx} - J_{yy})}{J_{zz}} & c_8 &= \frac{(-k_{\tau dz})}{J_{zz}} & d_4 &= \frac{1}{m} & d_3 &= \frac{1}{J_{zz}} \\ d_5 &= \frac{(-\kappa_{fdx})}{m} & d_6 &= \frac{(-k_{fdy})}{m} & d_7 &= \frac{(-\kappa_{fdz})}{m} \end{aligned}$$

$$U_x = \cos X_1 \cos X_5 \sin X_3 + \sin X_1 \sin X_5$$

$$U_y = \cos X_1 \sin X_3 \sin X_5 - \cos X_5 \sin X_1$$

$$U_z = \cos x_3 \cos x_1 \quad \omega_r = (-1)^i \omega_i$$

$d_x, d_y, d_z, d_\phi, d_\theta, d_\psi$ shows the unknown disturbances such as aerodynamic torque and force, drag force and torque, and wind disturbance.

3.6 Open-Loop Analysis of the Hexacopter

A hexacopter is said to have six degrees of freedom and is driven by the speed of its propeller. The Newton Euler formalism is used to simulate the rotational and translational components of a hexacopter. To examine if the designed model satisfies the requirements for the hexacopter's operation and response to the supplied constant inputs, the MATLAB/Simulink model scheme is utilized.

The parameters of the simulation for proposed system are collected from at ASTU Space Technology Institute and other related paper, which are listed in Table 3.1

Table 3.1: The parameters value used in the simulation

| Symbol of parameters | Name of parameters | Numerical values and unit |
|---------------------------------|--------------------------------------|---------------------------|
| m | The body's mass | 2.5-12 kg |
| l | Arm length | 0.5 m |
| J_{xx} | x-axis body inertia | 0.01 kg m ² |
| J_{yy} | y-axis body inertia | 0.01 kg m ² |
| J_{zz} | z-axis body inertia | 0.01 kg m ² |
| g | Gravitational acceleration | 9.81 m/s ² |
| J_p | Inertia of motor | 0.025 kg m ² |
| K | Thrust constant | 4.1e-4 Nm/(rad/sec) |
| d | Drag constant | 0.5e-4 Nm/(rad/sec) |
| k_x | Aerodynamics translation coefficient | diag (2.5,2.1,2.9) |
| $k_{phi} = k_{theta} = k_{psi}$ | Aerodynamics rotation coefficient | diag (0.1,0.1,0.1) |
| ω_{max} | Maximum speed of the motor | 126 rad/sec (1200RPM) |

The hexacopter's planned open loop dynamic model's Simulink block diagram is shown in Figure 3.8. The six propellers of the rotors are displayed in the first section of the Simulink block. To determine the torques of the hexacopter's four control inputs, these speed constants are essential. For speed constants, a random value is selected below and above the rated

value. On the other hand, the rotational motion is driven by the torque input values that are converted from speed values in the second part of the block. The third section uses a MATLAB Simulink block to express the developed dynamic mathematical model of the hexacopter. which is the primary Simulink component. The state derivative of the system model's translational (x, y, z) and rotational (ϕ, θ, ψ) acceleration components are shown in the block's outputs. To find the state vector components $(\phi, \theta, \psi, x, y, z)$, the integral method is then applied to each component.

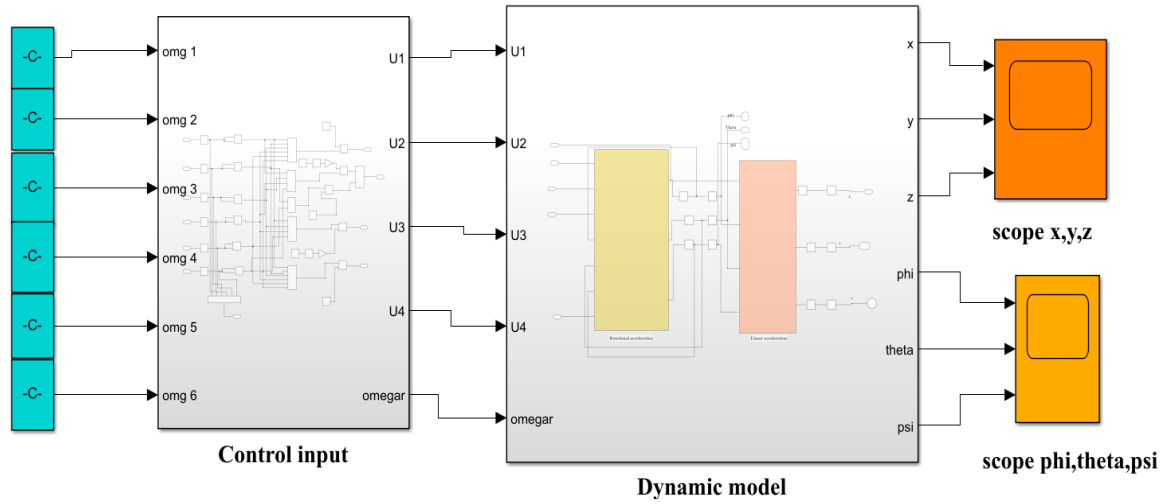
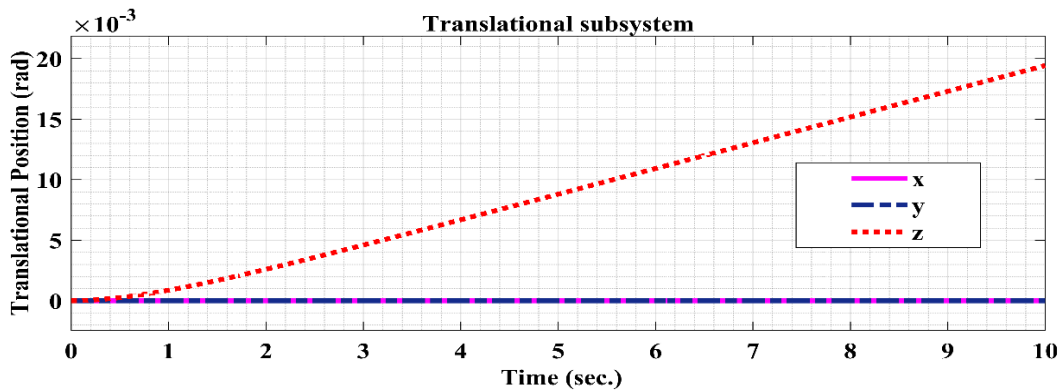


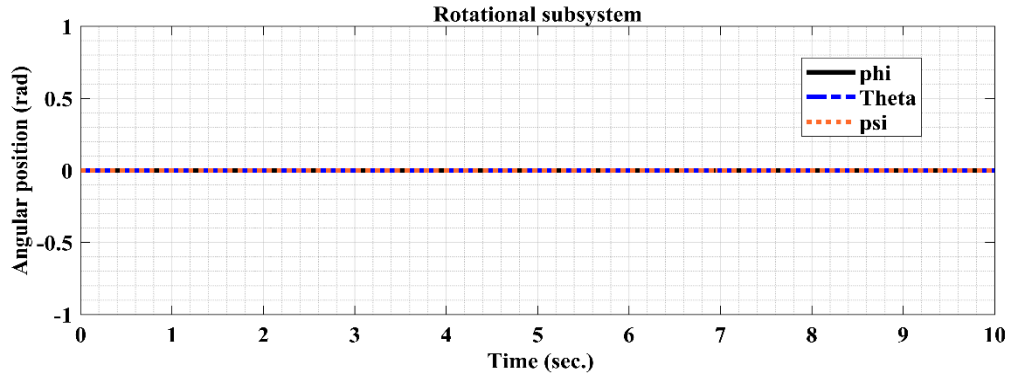
Figure 3.8: Open-loop block diagram for Simulink

The output of the open-loop system, as seen in the scope, is shown in the image below without a controller, when the parameters listed in Table 3.1 are applied. first find the rated speed at equilibrium or at all rotor speeds are equal.

$$\sum_{i=1}^6 T_i = mg, \quad 6k\omega_{rated}^2 = mg, \quad \omega_{rated} = \sqrt{\frac{mg}{6k}} \quad (3.51)$$



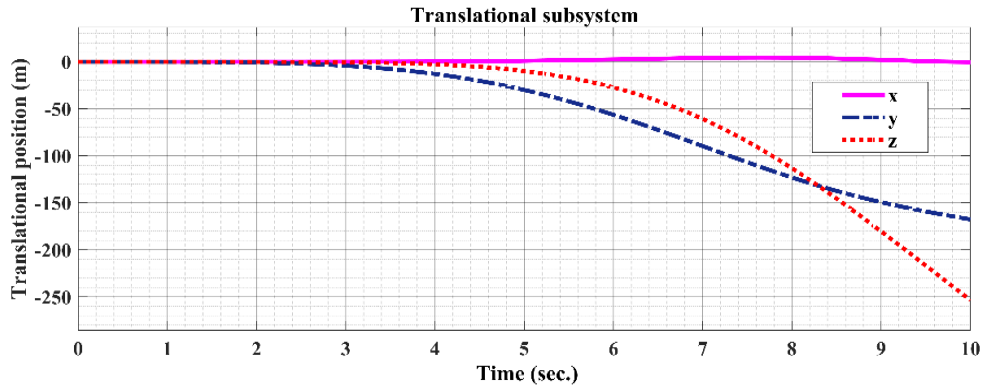
(a) Translational position



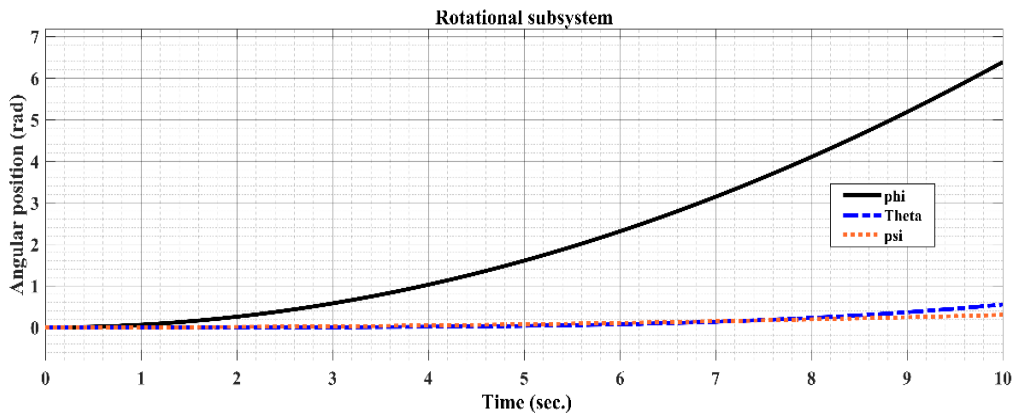
(b) Rotational position.

Figure 3.9: Simulation result at $\omega_1 = \omega_2 = \omega_3 = \omega_4 = \omega_5 = \omega_6 = 101.5 \text{ rad/sec}$

Figures 3.9 (a) and 3.9(b) show what happens when all six motors rotate at the same propeller speed. The hexacopter moves vertically along the Z-axis since the only inputs that affect the altitude state of the Z-dynamic are U1. So, there is no movement in the other direction.



(a) Translational position

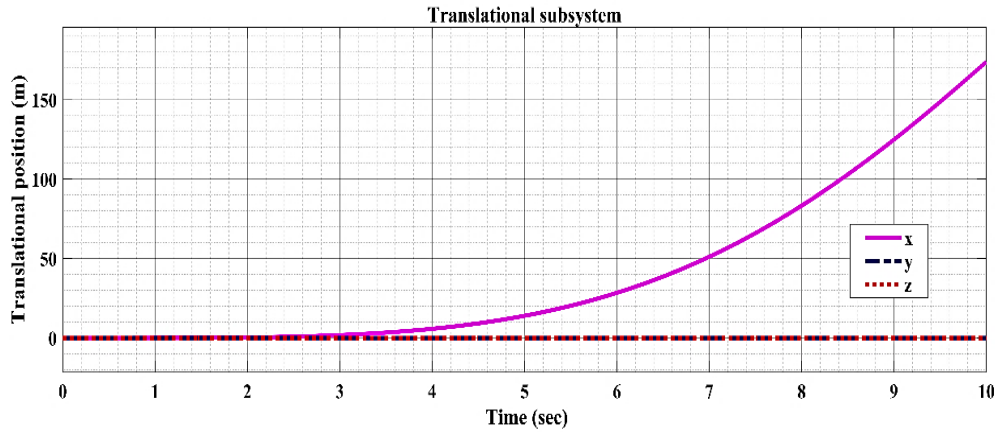


(b) Rotational position

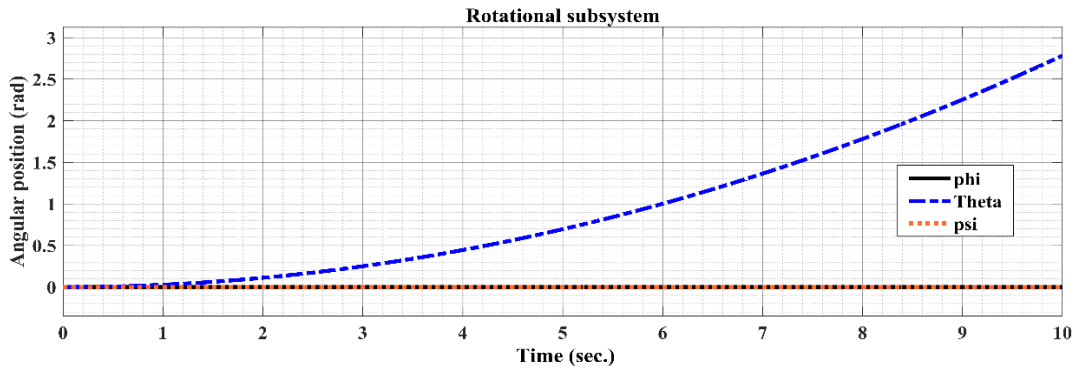
Figure 3.10: Simulation result at $\omega_1 = \omega_2 = \omega_3 = 101 \text{ rad/sec}$ and

$$\omega_4 = \omega_5 = \omega_6 = 102 \text{ rad/sec}$$

The rotor $\omega_1 - \omega_3$ speed decreased and rotor $\omega_4 - \omega_6$ speed increased are depicted in the two above Figures 3.10(a) and 3.10(b). Rotational dynamics (ϕ) shows an unstable reaction, yaw motion also change direction and the hexacopter goes downward along the negative y-axis and towards negative z-axis, while x-axis stays zero. Both control input U2 and control input U1 have an impact on the roll dynamics.



(a) Translational position



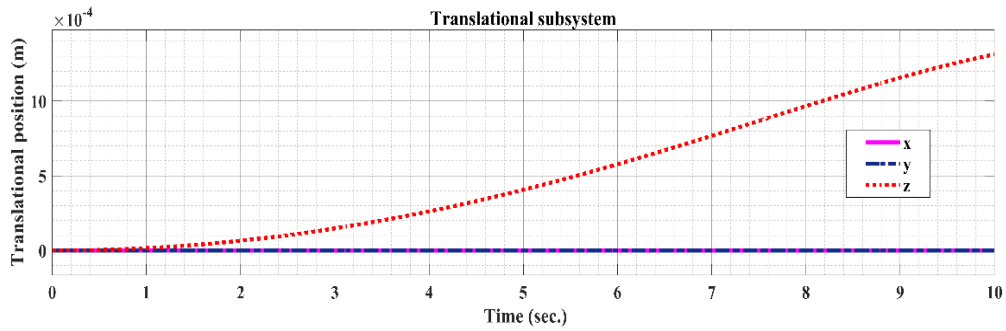
(b) Rotational position

Figure 3.11: Simulation result at $\omega_2 = \omega_5 = 101.5 \text{ rad/sec}$, $\omega_3 = \omega_4 = 101 \text{ rad/sec}$ and

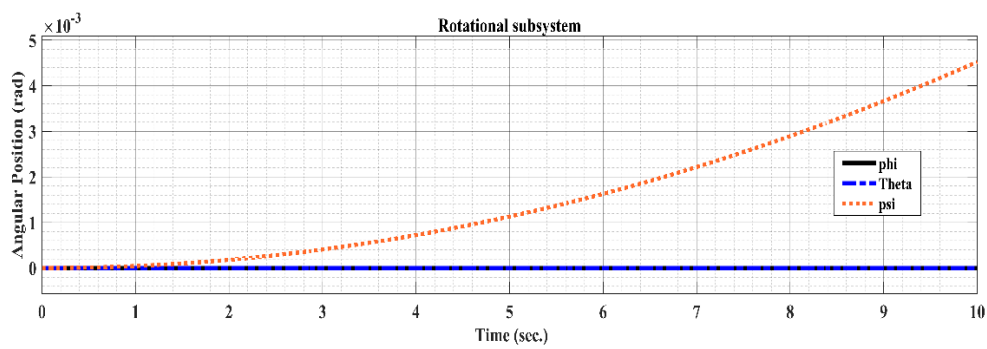
$$\omega_1 = \omega_6 = 102 \text{ rad/sec}$$

The rotor ω_3 and ω_4 speed decreased and rotor ω_1 and ω_6 speed increased at constant ω_2 and ω_5 speed, depicted in Figures 3.11(a) and 3.11(b). It affects both rotational

dynamics (theta) and translational dynamics (x). Control input U3 has an impact on the pitch dynamics.



(a) Translational position



(b) Rotational position

Figure 3.12: Simulation result at $\omega_1 = \omega_3 = \omega_5 = 101 \text{ rad} / \text{sec}$ and

$$\omega_2 = \omega_4 = \omega_6 = 102 \text{ rad} / \text{sec}$$

Figures 3.12(a) and 3.12(b) shows yaw input affects the z and psi dynamics. The input U4 affects the psi dynamics or yaw dynamics.

CHAPTER FOUR

4. CONTROLLER DESIGN

The hexacopter system is extremely unstable and nonlinear. To make it stable, an appropriate control system is also required. For this thesis, a sliding mode controller (SMC) based on model reference adaptive control (MRAC) is utilized to track a specified trajectory with a hexacopter.

4.1. Controlling System Block Diagram

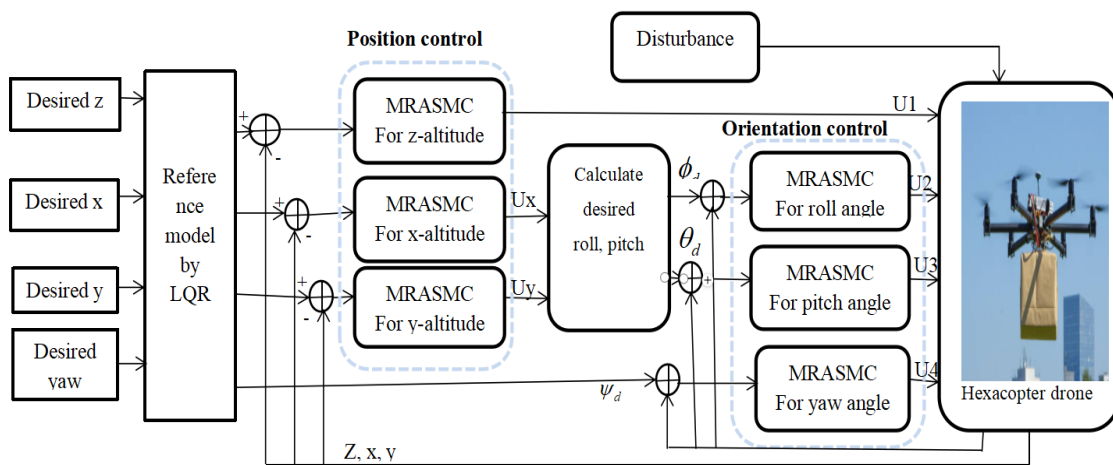


Figure 4.1: System block diagram

The block diagram in Figure 4.1 indicates the controlling system of the hexacopter drone. The control loop has an outer loop that controls two positions (X and Y) and an inner loop that controls movement along the X and Y directions (roll, pitch), heading or rotation around the vertical axis (yaw), and altitude (Z) of the hexacopter system. And also, external disturbances that can affect the hexacopters flight, such as air resistance or wind gusts. The desired angles (roll, pitch, and yaw) and desired position (X, Y) are fed into their respective control blocks. Each control block calculates the required adjustment and sends control signals (U_x , U_y , U_2 , U_3 , and U_4) to the hexacopter dynamics block. Then it considers these control signals and external disturbances to determine the actual motion of the hexacopter. Finally, the hexacopters motion likely feeds back into the control system through sensors. Because the system is underactuated, the X and Y states cannot be directly controlled like the other state variables can because they lack control inputs. Thus, it is necessary to develop

a mechanism for controlling this two-position state variable by indirectly controlling them in terms of θ_d , and ϕ_d .

From the translational component's dynamic model:

Let

$$\begin{aligned} u_x &= [\cos \phi_d \sin \theta_d \cos \psi_d + \sin \phi_d \sin \psi_d] \\ u_y &= [\cos \phi_d \sin \theta_d \sin \psi_d - \sin \phi_d \cos \psi_d] \end{aligned} \quad (4.1)$$

To get the desired value of roll and pitch angles, First, create a matrix that represents the above equation.

$$\begin{bmatrix} \sin \psi_d & -\cos \psi_d \\ \cos \psi_d & \sin \psi_d \end{bmatrix} \begin{bmatrix} \cos \phi_d \sin \theta_d \\ \sin \phi_d \end{bmatrix} = \begin{bmatrix} u_y \\ u_x \end{bmatrix} \quad (4.2)$$

After that, multiply it by the inverse matrix.

$$\begin{bmatrix} \cos \phi_d \sin \theta_d \\ \sin \phi_d \end{bmatrix} = \begin{bmatrix} \sin \psi_d u_y + \cos \psi_d u_x \\ -\cos \psi_d u_y + \sin \psi_d u_x \end{bmatrix} \quad (4.3)$$

Finally, the reference values of roll and pitch angles are:

$$\begin{bmatrix} \phi_d \\ \theta_d \end{bmatrix} = \begin{bmatrix} \sin^{-1} \left(\frac{-\cos \psi_d u_y + \sin \psi_d u_x}{\cos \phi_d} \right) \\ \sin^{-1} \left(\frac{\sin \psi_d u_y + \cos \psi_d u_x}{\cos \phi_d} \right) \end{bmatrix} \quad (4.4)$$

4.2. Generation of Trajectories by Using Minimum Jerk Trajectory

In control systems, trajectory generators are required for moving an object smoothly from one initial location to another. Many different methods are used to generate various kinds of trajectories. One method to generate a path to be followed is minimum jerk trajectory generation. Jerk, which is the acceleration's time derivative, is essential for both obtaining high accuracy and reducing vibration. It is possible to write it in Newton's dot notation as

$\ddot{\ddot{x}}$ (Sharkawy, 2021). The minimum jerk trajectory is an approach used in motion planning where the trajectory of a system is designed to minimize the "jerk" or the third derivative of position. The jerk is minimized by minimizing the sum of the squares of the jerk over the entire trajectory. Mathematically, the objective is to minimize:

$$MJT = \int_{t_0}^{t_f} \left\| \ddot{\mathcal{X}} \right\|^2 dt \quad (4.5)$$

In this research work, the minimum jerk trajectory is used to generate paths in the x, y, and z direction, enabling the hexacopter to transition smoothly from one position to another while minimizing vibrations during the hexacopter's motion. This approach is particularly beneficial for applications such as construction material transport and home/cargo delivery services, where stability and precision are essential for successful operation. By reducing vibrations, the hexacopter can maintain load integrity and enhance overall performance during its flight.

4.2.1. Trajectory Generation for Z Altitude

Let's now design a trajectory $z(t)$ such that it has an initial position $z(0) = a$ and its final position $z(T) = b$.

According to the Equation below, the functional is the integral of the jerk's square (Lidiya Girma, 2021).

$$\begin{aligned} z^*(t) &= \arg \min_{z(t)} \int_0^T L(\ddot{z}, \dot{z}, z, t) dt \quad \text{where } L = (\ddot{z})^2 \\ &= \arg \min_{z(t)} \int_0^T (\ddot{z})^2 dt \end{aligned} \quad (4.6)$$

To minimize this function, the best value for x must be determined. by applying the formula for Euler-Lagrange:

$$\frac{\partial L}{\partial z} - \frac{d}{dt} \left(\frac{\partial L}{\partial \dot{z}} \right) + \frac{d^2}{dt^2} \left(\frac{\partial L}{\partial \ddot{z}} \right) - \frac{d^3}{dt^3} \left(\frac{\partial L}{\partial \ddot{z}} \right) = 0 \quad (4.7)$$

$\frac{\partial L}{\partial z}, \frac{d}{dt} \left(\frac{\partial L}{\partial \dot{z}} \right), \frac{d^2}{dt^2} \left(\frac{\partial L}{\partial \ddot{z}} \right)$, are reduced to zero since they no longer directly depend on \ddot{z} .

Six order differential equations will be derived from what is left.

$$(\ddot{z})^6 = 0 \quad (4.8)$$

When you have a differential equation of the form $(\ddot{z})^6 = 0$, it implies that the function

$z(t)$ is a polynomial with a maximum degree of 5. The general solution to this equation will be:

$$z(t) = c_5 t^5 + c_4 t^4 + c_3 t^3 + c_2 t^2 + c_1 t^1 + c_0 \quad (4.9)$$

To determine the six coefficients of the fifth-order polynomial, it is necessary to solve the polynomial equation. This requires establishing additional boundary conditions to ensure a unique solution as shown in Table 4.1. These boundaries typically include initial and final positions, velocities, and possibly accelerations at the start and end of the trajectory. By defining these parameters, the polynomial can be accurately solved to yield the desired coefficients for the trajectory planning.

Table 4.1: Initial and final boundaries of position, velocity and acceleration

| Time | Position | Velocity | Acceleration |
|------|----------|----------|--------------|
| t=0 | a | 0 | 0 |
| t=T | b | 0 | 0 |

Based on the following assumptions: starting position $z(0) = a$, the final position $z(T) = b$, the initial velocity $\dot{z}(0) = 0$, the final velocity $\dot{z}(T) = 0$, the initial acceleration $\ddot{z}(0) = 0$ and the final acceleration $\ddot{z}(T) = 0$ let's express each of these boundary conditions in terms of six known boundaries and six unknown coefficients.

$$\begin{aligned}
z(t=0) &= c_5 t_0^5 + c_4 t_0^4 + c_3 t_0^3 + c_2 t_0^2 + c_1 t_0^1 + c_0 \\
z(t=T) &= c_5 T^5 + c_4 T^4 + c_3 T^3 + c_2 T^2 + c_1 T^1 + c_0 \\
\dot{z}(t=0) &= 5c_5 t_0^4 + 4c_4 t_0^3 + 3c_3 t_0^2 + 2c_2 t_0^1 + c_1 + 0 \\
\dot{z}(t=T) &= 5c_5 T^4 + 4c_4 T^3 + 3c_3 T^2 + 2c_2 T^1 + c_1 + 0 \\
\ddot{z}(t=0) &= 20c_5 t_0^3 + 12c_4 t_0^2 + 6c_3 t_0^1 + 2c_2 + 0 + 0 \\
\ddot{z}(t=T) &= 20c_5 T^3 + 12c_4 T^2 + 6c_3 T^1 + 2c_2 + 0 + 0
\end{aligned} \quad (4.10)$$

Then the matrix form is:

$$\begin{bmatrix} a \\ b \\ 0 \\ 0 \\ 0 \\ 0 \end{bmatrix} = \begin{bmatrix} 0 & 0 & 0 & 0 & 0 & 1 \\ T^5 & T^4 & T^3 & T^2 & T & 1 \\ 0 & 0 & 0 & 0 & 1 & 0 \\ 5T^4 & 4T^3 & 3T^2 & 2T & 1 & 0 \\ 0 & 0 & 0 & 2 & 0 & 0 \\ T^3 & 12T^2 & 6T & 2 & 0 & 0 \end{bmatrix} \begin{bmatrix} c_5 \\ c_4 \\ c_3 \\ c_2 \\ c_1 \\ c_0 \end{bmatrix} \quad (4.11)$$

$$\text{Let, } A = \begin{bmatrix} 0 & 0 & 0 & 0 & 0 & 1 \\ T^5 & T^4 & T^3 & T^2 & T & 1 \\ 0 & 0 & 0 & 0 & 1 & 0 \\ 5T^4 & 4T^3 & 3T^2 & 2T & 1 & 0 \\ 0 & 0 & 0 & 2 & 0 & 0 \\ T^3 & 12T^2 & 6T & 2 & 0 & 0 \end{bmatrix}, B = \begin{bmatrix} a \\ b \\ 0 \\ 0 \\ 0 \\ 0 \end{bmatrix}, C = \begin{bmatrix} c_5 \\ c_4 \\ c_3 \\ c_2 \\ c_1 \\ c_0 \end{bmatrix}$$

The following equation can be used to solve the coefficients:

$$C = A^{-1}B \quad (4.12)$$

To get a minimum jerk trajectory, the same steps are taken for the other state variables.

4.3. Design of PID Sliding Surface Based SMC for Hexacopter

In this work, six sliding mode controllers govern each of the six states of the Hexacopter dynamics. In conventional SMCs, the sliding surface design is linear. This can be troublesome for non-linear systems (like hexacopters) whose behaviour varies according on airspeed or payload weight. Under some operational conditions, a linear sliding surface might not accurately depict the desired behaviour. Furthermore, in traditional SMC, the system state is often driven by the reaching law in the direction of the sliding surface through the use of a signum function. This could lead to "chattering," or high-frequency control signal switching, which could be detrimental to actuator health and flight stability. By implementing a control for the PID sliding surface with a derivative, integral, and proportional error term into the sliding surface design, these drawbacks will be resolved. Increased adaptability and flexibility to non-linear system behaviour are made possible by this. Compared to typical SMC, the PID sliding surface offers a smoother and more continuous control action, which eliminates or significantly reduces chattering. (Nagarajan & Victoire, 2023); (Singh, 2014).

The PID sliding surface is expressed as:

$$S(t) = k_p e(t) + k_i \int_0^t e(\tau) d\tau + k_d \frac{d}{dt} e(t) \quad (4.13)$$

Where: $k_i, k_d, k_p \in \mathfrak{R}^+$ are a positive coefficient that enhance sliding surface design flexibility and $S(t) \in \mathfrak{R}$.

4.3.1. Roll Controller

The primary step is to create the PID sliding surface that will control the hexacopter's entire state. It depends on the error because it is trajectory tracking.

$$S(\phi) = k_p e(\phi) + k_i \int_0^\phi e(\tau) d\tau + k_d \frac{d}{dt} e(\phi) \quad (4.14)$$

The PID sliding surface's first order derivative is represented by:

$$\dot{S}(\phi) = k_p \dot{e}(\phi) + k_i e(\phi) + k_d \ddot{e}(\phi) \quad (4.15)$$

For roll movement, the error equation and the second derivative of the error is as follows:

$$e(\phi) = \phi_d - \phi \quad \dot{e}(\phi) = \dot{\phi}_d - \dot{\phi} \quad \ddot{e}(\phi) = \ddot{\phi}_d - \ddot{\phi} \quad (4.16)$$

When the error Equation (4.16) is added to the first order sliding surface equation (4.15), it yields:

$$\dot{S}(\phi) = k_i (\phi_d - \phi) + k_p (\dot{\phi}_d - \dot{\phi}) + k_d (\ddot{\phi}_d - \ddot{\phi}) \quad (4.17)$$

Substituting the Hexacopter's roll dynamics from Equation (3.39) in to the sliding surface derivative gives:

$$\dot{S}(\phi) = k_i (\phi_d - \phi) + k_p (\dot{\phi}_d - \dot{\phi}) + k_d \left(\ddot{\phi}_d - \left(\left(\frac{J_{yy} - J_{zz}}{J_{xx}} \right) \dot{\theta} \dot{\psi} - \frac{J_p}{J_{xx}} \dot{\theta} \omega_r - \frac{K_{\tau dx}}{J_{xx}} \dot{\phi}^2 + \frac{1}{J_{xx}} U_2 \right) \right) \quad (4.18)$$

The second step is sliding control law design for the roll of hexacopter that leads the paths to attract and remain stationary on the surface.

$$U_2(t) = U_{eq}(t) + U_{NI}(t) \quad (4.19)$$

Consider the linear controller $U_{eq}(t) = U_2$ because the system is in a sliding condition, the above Equation (4.18) becomes

$$\dot{S}(\phi) = k_i (\phi_d - \phi) + k_p (\dot{\phi}_d - \dot{\phi}) + k_d \left(\ddot{\phi}_d - \left(\left(\frac{J_{yy} - J_{zz}}{J_{xx}} \right) \dot{\theta} \dot{\psi} - \frac{J_p}{J_{xx}} \dot{\theta} \omega_r - \frac{K_{\tau dx}}{J_{xx}} \dot{\phi}^2 + \frac{1}{J_{xx}} U_{eq} \right) \right) \quad (4.20)$$

As $\dot{S}(\phi) = 0; U_{eq}(t)$ gives:

$$U_{eq}(t) = \frac{J_{xx}}{k_d} \left(k_i(\phi_d - \phi) + k_p(\dot{\phi}_d - \dot{\phi}) + k_d \left(\ddot{\phi}_d - \left(\frac{J_{yy} - J_{zz}}{J_{xx}} \right) \dot{\theta} \dot{\psi} + \frac{J_p}{J_{xx}} \dot{\theta} \omega_r + \frac{K_{\tau dx}}{J_{xx}} \dot{\phi}^2 \right) \right) \quad (4.21)$$

After that, a positive definite Lyapunov function V is created in order to design the nonlinear controller.

$$V = \frac{1}{2} S^2 \quad (4.22)$$

The derivative of the Lyapunov function V is $\dot{V} = S \dot{S} < 0$ must be negative definite to ensure system stability. To satisfy this condition for all $t > 0$ and $k_\phi > 0$, $U_{NI}(t)$ should be:

$$U_{NI}(t) = k_\phi \text{sgn}(S(\phi)) \quad (4.23)$$

Finally, the complete roll controller equation becomes:

$$U_2(t) = \frac{J_{xx}}{k_d} \left(k_i(\phi_d - \phi) + k_p(\dot{\phi}_d - \dot{\phi}) + k_d \left(\ddot{\phi}_d - \left(\frac{J_{yy} - J_{zz}}{J_{xx}} \right) \dot{\theta} \dot{\psi} + \frac{J_p}{J_{xx}} \dot{\theta} \omega_r + \frac{K_{\tau dx}}{J_{xx}} \dot{\phi}^2 \right) + k_\phi \text{sgn}(S(\phi)) \right) \quad (4.24)$$

4.3.2. Pitch Controller

The process for controlling a Pitch movement is also similar to that of other controls designed before. The sliding surface gives

$$S(\theta) = k_p e(\theta) + k_i \int_0^\theta e(\tau) d\tau + k_d \frac{d}{dt} e(\theta) \quad (4.25)$$

The PID sliding surface's first order derivative is represented by:

$$\dot{S}(\theta) = k_p \dot{e}(\theta) + k_i e(\theta) + k_d \ddot{e}(\theta) \quad (4.26)$$

For Pitch movement, the error equation and the second derivative of the error is as follows:

$$e(\theta) = \theta_d - \theta \quad \dot{e}(\theta) = \dot{\theta}_d - \dot{\theta} \quad \ddot{e}(\theta) = \ddot{\theta}_d - \ddot{\theta} \quad (4.27)$$

When the error Equation (4.27) is added to the first order sliding surface Equation (4.26) it yields:

$$\dot{S}(\theta) = k_i(\theta_d - \theta) + k_p(\dot{\theta}_d - \dot{\theta}) + k_d(\ddot{\theta}_d - \ddot{\theta}) \quad (4.28)$$

Substituting the Hexacopter's Pitch dynamics from Equation (3.40) in to the sliding surface derivative gives:

$$\dot{S}(\theta) = k_i(\theta_d - \theta) + k_p(\dot{\theta}_d - \dot{\theta}) + k_d \left(\ddot{\theta}_d - \left(\left(\frac{J_{zz} - J_{xx}}{J_{yy}} \right) \dot{\phi} \dot{\psi} + \frac{J_p}{J_{yy}} \dot{\phi} \dot{\omega}_r - \frac{\kappa_{\tau dy}}{J_{yy}} \dot{\theta}^2 + \frac{1}{J_{yy}} U_3 \right) \right) \quad (4.29)$$

As $\dot{S}(\theta) = 0; U_{eq}(t)$ gives:

$$U_{eq}(t) = \frac{J_{yy}}{k_d} \left(k_i(\theta_d - \theta) + k_p(\dot{\theta}_d - \dot{\theta}) + k_d \left(\ddot{\theta}_d - \left(\frac{J_{zz} - J_{xx}}{J_{yy}} \right) \dot{\phi} \dot{\psi} - \frac{J_p}{J_{yy}} \dot{\phi} \dot{\omega}_r + \frac{\kappa_{\tau dy}}{J_{yy}} \dot{\theta}^2 \right) \right) \quad (4.30)$$

The nonlinear part of the controller $U_{NI}(t)$ should be:

$$U_{NI}(t) = k_\theta \text{sgn}(S(\theta)) \quad (4.31)$$

Finally, the complete Pitch controller equation becomes:

$$U_3(t) = \frac{J_{yy}}{k_d} \left(k_i(\theta_d - \theta) + k_p(\dot{\theta}_d - \dot{\theta}) + k_d \left(\ddot{\theta}_d - \left(\frac{J_{zz} - J_{xx}}{J_{yy}} \right) \dot{\phi} \dot{\psi} - \frac{J_p}{J_{yy}} \dot{\phi} \dot{\omega}_r + \frac{\kappa_{\tau dy}}{J_{yy}} \dot{\theta}^2 \right) + k_\theta \text{sgn}(S(\theta)) \right) \quad (4.32)$$

4.3.3. Yaw Controller

The process for controlling a yaw movement is also similar to that of other controls designed before. The sliding surface gives

$$S(\psi) = k_p e(\psi) + k_i \int_0^\psi e(\tau) d\tau + k_d \frac{d}{dt} e(\psi) \quad (4.33)$$

The PID sliding surface's first order derivative is represented by:

$$\dot{S}(\psi) = k_p \dot{e}(\psi) + k_i e(\psi) + k_d \ddot{e}(\psi) \quad (4.34)$$

For yaw movement, the error equation and second order derivative are as follows:

$$e(\psi) = \psi_d - \psi \quad \dot{e}(\psi) = \dot{\psi}_d - \dot{\psi} \quad \ddot{e}(\psi) = \ddot{\psi}_d - \ddot{\psi} \quad (4.35)$$

When the error Equation (4.35) is added to the first order sliding surface Equation (4.34) it yields:

$$\dot{S}(\psi) = k_i(\psi_d - \psi) + k_p(\dot{\psi}_d - \dot{\psi}) + k_d(\ddot{\psi}_d - \ddot{\psi}) \quad (4.36)$$

Substituting the Hexacopter's yaw dynamics from Equation (3.41) in to the sliding surface derivative gives:

$$\dot{S}(\psi) = k_i(\psi_d - \psi) + k_p(\dot{\psi}_d - \dot{\psi}) + k_d \left(\ddot{\psi}_d - \left(\left(\frac{J_{xx} - J_{yy}}{J_{zz}} \right) \dot{\phi} \dot{\theta} - \frac{\kappa_{\tau dz}}{J_{zz}} \dot{\psi}^2 + \frac{1}{J_{zz}} U_4 \right) \right) \quad (4.37)$$

As $\dot{S}(\psi) = 0; U_{eq}(t)$ gives:

$$U_{eq}(t) = \frac{J_{zz}}{k_d} \left(k_i(\psi_d - \psi) + k_p(\dot{\psi}_d - \dot{\psi}) + k_d \left(\ddot{\psi}_d - \left(\frac{J_{xx} - J_{yy}}{J_{zz}} \right) \dot{\phi} \dot{\theta} + \frac{\kappa_{\tau dz}}{J_{zz}} \dot{\psi}^2 \right) \right) \quad (4.38)$$

The nonlinear part of the controller $U_{NI}(t)$ should be:

$$U_{NI}(t) = k_\psi \text{sgn}(S(\psi)) \quad (4.39)$$

Finally, the complete yaw controller equation becomes:

$$U_4(t) = \frac{J_{zz}}{k_d} \left(k_i(\psi_d - \psi) + k_p(\dot{\psi}_d - \dot{\psi}) + k_d \left(\ddot{\psi}_d - \left(\frac{J_{xx} - J_{yy}}{J_{zz}} \right) \dot{\phi} \dot{\theta} + \frac{\kappa_{\tau dz}}{J_{zz}} \dot{\psi}^2 \right) + k_\psi \text{sgn}(S(\psi)) \right) \quad (4.40)$$

4.3.4. Altitude Controller

The primary step is to create the PID sliding surface that will control the hexacopter's entire state. It depends on the error because it is trajectory tracking.

$$S(z) = k_p e(z) + k_i \int_0^z e(\tau) d\tau + k_d \frac{d}{dt} e(z) \quad (4.41)$$

The PID sliding surface's first order derivative is represented by:

$$\dot{S}(z) = k_p \dot{e}(z) + k_i e(z) + k_d \ddot{e}(z) \quad (4.42)$$

For altitude, the error equation and second order derivative are as follows:

$$e(z) = z_d - z \quad \dot{e}(z) = \dot{z}_d - \dot{z} \quad \ddot{e}(z) = \ddot{z}_d - \ddot{z} \quad (4.43)$$

When the error Equation (4.43) is added to the first order sliding surface equation (4.42) it yields:

$$\dot{S}(z) = k_i(z_d - z) + k_p(\dot{z}_d - \dot{z}) + k_d(\ddot{z}_d - \ddot{z}) \quad (4.44)$$

Substituting the Hexacopter's altitude dynamics from Equation (3.31) in to the sliding surface derivative gives:

$$\dot{S}(z) = k_i(z_d - z) + k_p(\dot{z}_d - \dot{z}) + k_d(\ddot{z}_d - \frac{1}{m}(\cos \theta \cos \phi)U_1 - g - \frac{\kappa_{fdz}}{m}\dot{z}) \quad (4.45)$$

As $\dot{S}(z) = 0$; $U_{eq}(t)$ gives:

$$U_{eq}(t) = \left(k_d \left(\ddot{z}_d + g + \frac{\kappa_{fdz}}{m}\dot{z} \right) + k_i(z_d - z) + k_p(\dot{z}_d - \dot{z}) \right) \frac{m}{k_d \cos \theta \cos \phi} \quad (4.46)$$

The nonlinear part of the controller $U_{NI}(t)$ should be:

$$U_{NI}(t) = k_z \text{sgn}(S(z)) \quad (4.47)$$

Finally, the complete altitude controller equation becomes:

$$U_1(t) = \left(k_d \left(\ddot{z}_d + g + \frac{\kappa_{fdz}}{m}\dot{z} \right) + k_i(z_d - z) + k_p(\dot{z}_d - \dot{z}) + k_z \text{sgn}(S(z)) \right) \frac{m}{k_d \cos \theta \cos \phi} \quad (4.48)$$

4.3.5. Position X Controller

The process for controlling the linear x motion is also similar to that of other controls designed before. The sliding surface gives

$$S(x) = k_p e(x) + k_i \int_0^x e(\tau) d\tau + k_d \frac{d}{dt} e(x) \quad (4.49)$$

The PID sliding surface's first order derivative is represented by:

$$\dot{S}(x) = k_p \dot{e}(x) + k_i e(x) + k_d \ddot{e}(x) \quad (4.50)$$

For linear x motion, the error equation and the second order derivative are as follows:

$$e(x) = x_d - x \quad \dot{e}(x) = \dot{x}_d - \dot{x} \quad \ddot{e}(x) = \ddot{x}_d - \ddot{x} \quad (4.51)$$

When the error Equation (4.51) is added to the first order sliding surface Equation (4.50), it yields:

$$\dot{S}(x) = k_i(x_d - x) + k_p(\dot{x}_d - \dot{x}) + k_d(\ddot{x}_d - \ddot{x}) \quad (4.52)$$

Substituting the Hexacopter's translational dynamics from Equation (3.29) in to the sliding surface derivative gives:

$$\dot{S}(x) = k_i(x_d - x) + k_p(\dot{x}_d - \dot{x}) + k_d \left(\ddot{x}_d - \frac{1}{m} u_x U_1 - \frac{\kappa_{fdx}}{m} \dot{x} \right) \quad (4.53)$$

As $\dot{S}(x) = 0; U_{eq}(t)$ gives:

$$U_{eq}(t) = \frac{m}{k_d U_1} \left(k_i(x_d - x) + k_p(\dot{x}_d - \dot{x}) + k_d \left(\ddot{x}_d + \frac{\kappa_{fdx}}{m} \dot{x} \right) \right) \quad (4.54)$$

The nonlinear part of controller $U_{NI}(t)$ should be:

$$U_{NI}(t) = k_x \text{sgn}(S(x)) \quad (4.55)$$

Finally, the complete position x controller equation becomes:

$$U_x(t) = \frac{m}{k_d U_1} \left(k_i(x_d - x) + k_p(\dot{x}_d - \dot{x}) + k_d \left(\ddot{x}_d + \frac{\kappa_{fdx}}{m} \dot{x} \right) + k_x \text{sgn}(S(x)) \right) \quad (4.56)$$

4.3.6. Position Y Controller

The process for controlling the linear y motion is also similar to that of other controls designed before. The sliding surface gives

$$S(y) = k_p e(y) + k_i \int_0^y e(\tau) d\tau + k_d \frac{d}{dt} e(y) \quad (4.57)$$

The PID sliding surface's first order derivative is represented by:

$$\dot{S}(y) = k_p \dot{e}(y) + k_i e(y) + k_d \ddot{e}(y) \quad (4.58)$$

For linear y motion, the error equation and its second order derivative are as follows:

$$e(y) = y_d - y \quad \dot{e}(y) = \dot{y}_d - \dot{y} \quad \ddot{e}(y) = \ddot{y}_d - \ddot{y} \quad (4.59)$$

When the error Equation (4.59) is added to the first order sliding surface equation (4.58) it yields:

$$\dot{S}(y) = k_i(y_d - y) + k_p(\dot{y}_d - \dot{y}) + k_d(\ddot{y}_d - \ddot{y}) \quad (4.60)$$

Substituting the Hexacopter's translational dynamics from Equation (3.30) in to the sliding surface derivative gives:

$$\dot{S}(y) = k_i(y_d - y) + k_p(\dot{y}_d - \dot{y}) + k_d \left(\ddot{y}_d - \frac{1}{m} u_x U_1 - \frac{\kappa_{fdy}}{m} \dot{y} \right) \quad (4.61)$$

As $\dot{S}(y) = 0; U_{eq}(t)$ gives:

$$U_{eq}(t) = \frac{m}{k_d U_1} \left(k_i (y_d - y) + k_p (\dot{y}_d - \dot{y}) + k_d \left(\ddot{y}_d + \frac{\kappa_{fdy}}{m} \dot{y} \right) \right) \quad (4.62)$$

The nonlinear part of the controller $U_{NI}(t)$ should be:

$$U_{NI}(t) = k_y \text{sgn}(S(y)) \quad (4.63)$$

Finally, the complete position y controller equation becomes:

$$u_y(t) = \frac{m}{k_d U_1} \left(k_i (y_d - y) + k_p (\dot{y}_d - \dot{y}) + k_d \left(\ddot{y}_d + \frac{\kappa_{fdy}}{m} \dot{y} \right) + k_y \text{sgn}(S(y)) \right) \quad (4.64)$$

4.4. Model Reference Adaptive Sliding Mode Controller for Hexacopter

Modern control systems must adapt to changing system dynamics and uncertainties, and one effective approach is the Model Reference Adaptive Controller (MRAC), which dynamically adjusts controller parameters to align a desired reference model. This thesis explains an MRAC scheme that integrates Sliding Mode Control (SMC) principles to enhance the system's robustness and tracking performance. In this framework, the reference model is specifically selected to generate the desired trajectory x_m that the plant output x_p has to follow, ensuring effective performance even in the presence of disturbances and variations in system behavior.

4.4.1. Reference Model Design

A reference model is crucial in specifying the desired response of an adaptive control system to command inputs, acting as a command shaping filter for effective command following. In adaptive control, the system adapts based on tracking error between the reference model and actual system output. For successful tracking, the reference model must be designed appropriately. This involves first linearizing the derived non-linear model. The linearized state-space model can be obtained using Taylor's series linearization method at the equilibrium point, which simplifies the complex dynamics of the system and facilitates the design of the reference model, ensuring that the adaptive controller can accurately follow the desired trajectory (Management et al., 2014).

$$\begin{aligned} \dot{x}_1 &= f_1(x_1, x_2) = 0 \\ \dot{x}_2 &= f_2(x_1, x_2) = 0 \end{aligned} \quad (4.65)$$

To determine the equilibrium points for $[x, y, z, \phi, \theta, \psi]$, By executing a Taylor series expansion and removing higher order terms on Equation (3.50), and using small angle approximations, a linear model is obtained:

$$\left\{ \begin{array}{l} \ddot{x} = -\frac{k_x}{m} \dot{x} + g\theta \\ \ddot{y} = -\frac{k_y}{m} \dot{y} - g\phi \\ \ddot{z} = -\frac{k_z}{m} \dot{z} + \frac{u_1}{m} \end{array} \right. \quad \left\{ \begin{array}{l} \ddot{\phi} = -\frac{J_p \omega_r}{J_x} \dot{\theta} + \frac{u_2}{J_x} \\ \ddot{\theta} = \frac{J_p \omega_r}{J_y} \dot{\phi} + \frac{u_3}{J_y} \\ \ddot{\psi} = \frac{u_4}{J_2} \end{array} \right. , \text{where, } \left\{ \begin{array}{l} \phi = \theta = \psi \approx 0 \\ \sin(\theta) \approx \theta \\ \cos(\theta) \approx 1 \\ \sin^2(\theta) \approx 0 \end{array} \right. \quad (4.66)$$

Finally, the linearized state space model for hexacopter become:

$$\left\{ \begin{array}{l} \dot{x} = Ax + Bu \\ y = Cx + Du \end{array} \right.$$

$$A = \begin{bmatrix} 0 & 1 & 0 & 0 & 0 & 0 & 0 & 0 & 0 & 0 & 0 & 0 \\ 0 & \frac{-k_x}{m} & 0 & 0 & 0 & 0 & 0 & 0 & g & 0 & 0 & 0 \\ 0 & 0 & 0 & 1 & 0 & 0 & 0 & 0 & 0 & 0 & 0 & 0 \\ 0 & 0 & 0 & \frac{-k_y}{m} & 0 & 0 & -g & 0 & 0 & 0 & 0 & 0 \\ 0 & 0 & 0 & 0 & 0 & 1 & 0 & 0 & 0 & 0 & 0 & 0 \\ 0 & 0 & 0 & 0 & 0 & \frac{-k_z}{m} & 0 & 0 & 0 & 0 & 0 & 0 \\ 0 & 0 & 0 & 0 & 0 & 0 & 0 & 1 & 0 & 0 & 0 & 0 \\ 0 & 0 & 0 & 0 & 0 & 0 & 0 & 0 & 0 & \frac{-J_r \omega_r}{J_x} & 0 & 0 \\ 0 & 0 & 0 & 0 & 0 & 0 & 0 & 0 & 0 & 1 & 0 & 0 \\ 0 & 0 & 0 & 0 & 0 & 0 & 0 & \frac{J_r \omega_r}{J_y} & 0 & 0 & 0 & 0 \\ 0 & 0 & 0 & 0 & 0 & 0 & 0 & 0 & 0 & 0 & 0 & 0 \\ 0 & 0 & 0 & 0 & 0 & 0 & 0 & 0 & 0 & 0 & 0 & 0 \end{bmatrix}, B = \begin{bmatrix} 0 & 0 & 0 & 0 \\ 0 & 0 & 0 & 0 \\ 0 & 0 & 0 & 0 \\ 0 & 0 & 0 & 0 \\ 0 & 0 & 0 & 0 \\ \frac{1}{m} & 0 & 0 & 0 \\ 0 & 0 & 0 & 0 \\ 0 & \frac{1}{J_x} & 0 & 0 \\ 0 & 0 & 0 & 0 \\ 0 & 0 & \frac{1}{J_y} & 0 \\ 0 & 0 & 0 & 0 \\ 0 & 0 & 0 & \frac{1}{J_z} \end{bmatrix} \quad (4.67)$$

$$C = \begin{bmatrix} 1 & 0 & 0 & 0 & 0 & 0 & 0 & 0 & 0 & 0 & 0 & 0 \\ 0 & 0 & 1 & 0 & 0 & 0 & 0 & 0 & 0 & 0 & 0 & 0 \\ 0 & 0 & 0 & 0 & 1 & 0 & 0 & 0 & 0 & 0 & 0 & 0 \\ 0 & 0 & 0 & 0 & 0 & 0 & 1 & 0 & 0 & 0 & 0 & 0 \\ 0 & 0 & 0 & 0 & 0 & 0 & 0 & 0 & 1 & 0 & 0 & 0 \\ 0 & 0 & 0 & 0 & 0 & 0 & 0 & 0 & 0 & 1 & 0 & 0 \end{bmatrix}, D = \begin{bmatrix} 0 & 0 & 0 & 0 \\ 0 & 0 & 0 & 0 \\ 0 & 0 & 0 & 0 \\ 0 & 0 & 0 & 0 \\ 0 & 0 & 0 & 0 \\ 0 & 0 & 0 & 0 \end{bmatrix} \quad (4.68)$$

The reference model specifies the desired response of the hexacopter to command inputs. It can be represented as:

$$\dot{\mathbf{x}}_{\text{ref}} = \mathbf{A}_{\text{ref}} \mathbf{x}_{\text{ref}} + \mathbf{B}_{\text{ref}} \mathbf{r} \quad (4.69)$$

Where: \mathbf{r} is the reference input. $\mathbf{A}_{\text{ref}}, \mathbf{B}_{\text{ref}}$ represents external bounded command vectors.

To ensure effective tracking, the matrices $\mathbf{A}_{\text{ref}}, \mathbf{B}_{\text{ref}}, \mathbf{C}_{\text{ref}}$, and \mathbf{D}_{ref} should be chosen based on the desired performance such as stability and response time.

The optimal LQR gain \mathbf{K}_{LQR} is used to obtain the reference model from linearized model of hexacopter. The matching condition is used to determine \mathbf{A}_{ref} .

$$\begin{aligned} \mathbf{A}_{\text{ref}} &= \mathbf{A} - \mathbf{B}\mathbf{K}_{\text{LQR}}^T \\ \mathbf{B}_{\text{ref}} &= \mathbf{B} \end{aligned} \quad (4.70)$$

The LQR controller aims to minimize the following quadratic cost function:

$$J = \int_0^{\infty} (\mathbf{x}^T \mathbf{Q} \mathbf{x} + \mathbf{u}^T \mathbf{R} \mathbf{u}) dt \quad (4.71)$$

Where: \mathbf{Q} is a positive semi-definite matrix that penalizes the state variables, and \mathbf{R} is a positive definite matrix that penalizes the control input.

To find the optimal gain (\mathbf{K}_{LQR}), solve the following Riccati equation:

$$\mathbf{A}^T \mathbf{P} + \mathbf{P} \mathbf{A} - \mathbf{P} \mathbf{B} \mathbf{R}^{-1} \mathbf{B}^T \mathbf{P} + \mathbf{Q} = 0 \quad (4.72)$$

Where: \mathbf{P} is the solution of the Riccati equation.

Then, we calculate the optimal LQR gain (\mathbf{K}_{LQR}) using:

$$\mathbf{K}_{\text{LQR}} = \mathbf{R}^{-1} \mathbf{B}^T \mathbf{P} \quad (4.73)$$

The control input can then be computed as:

$$\mathbf{u} = -\mathbf{K}_{\text{LQR}} \mathbf{x} \quad (4.74)$$

Finally, the designed reference model of a hexacopter by using the obtained LQR gain (\mathbf{K}_{LQR}) is as follows:

$$\dot{\mathbf{x}}_{\text{ref}} = (\mathbf{A} - \mathbf{B}\mathbf{K}_{\text{LQR}}) \mathbf{x}_{\text{ref}} + \mathbf{B}\mathbf{r}(t) \quad (4.75)$$

4.4.2. Model Reference Adaptive Sliding Mode Controller for the Translational

The primary step is defining the error and its derivative for position subsystem:

$$\begin{cases} e(x) = x_{ref} - x \\ e(y) = y_{ref} - y \\ e(z) = z_{ref} - z \end{cases} \quad \begin{cases} \dot{e}(x) = \dot{x}_{ref} - \dot{x} \\ \dot{e}(y) = \dot{y}_{ref} - \dot{y} \\ \dot{e}(z) = \dot{z}_{ref} - \dot{z} \end{cases} \quad (4.76)$$

The PID sliding surface that will control the hexacopter's entire state. It depends on the error because it is trajectory tracking.

$$\begin{aligned} S(x) &= k_p e(x) + k_i \int_0^x e(\tau) d\tau + k_d \frac{d}{dt} e(x) \\ S(y) &= k_p e(y) + k_i \int_0^y e(\tau) d\tau + k_d \frac{d}{dt} e(y) \\ S(z) &= k_p e(z) + k_i \int_0^z e(\tau) d\tau + k_d \frac{d}{dt} e(z) \end{aligned} \quad (4.77)$$

The PID sliding surface's first order derivative is represented by:

$$\begin{aligned} \dot{S}(x) &= k_p \dot{e}(x) + k_i e(x) + k_d \ddot{e}(x) \\ \dot{S}(y) &= k_p \dot{e}(y) + k_i e(y) + k_d \ddot{e}(y) \\ \dot{S}(z) &= k_p \dot{e}(z) + k_i e(z) + k_d \ddot{e}(z) \end{aligned} \quad (4.78)$$

Selecting the adaptive reaching laws for the hexacopter position is the second stage. We get:

$$\begin{aligned} \tilde{s}_{rx} &= \tilde{k}_x \text{sign}(x) \\ \tilde{s}_{ry} &= \tilde{k}_y \text{sign}(y) \\ \tilde{s}_{rz} &= \tilde{k}_z \text{sign}(z) \end{aligned} \quad (4.79)$$

Finally, the complete adaptive sliding mode controller for hexacopter position becomes:

$$\begin{aligned}
u_x(t) &= \frac{m}{k_d u_1} \left(k_i e(x) + k_p \dot{e}(x) + k_d \left(\ddot{x}_d + \frac{\kappa_{fdy}}{m} \dot{x} \right) + \tilde{k}_x \operatorname{sgn}(S(y)) \right) \\
u_y(t) &= \frac{m}{k_d u_1} \left(k_i e(y) + k_p \dot{e}(y) + k_d \left(\ddot{y}_d + \frac{\kappa_{fdy}}{m} \dot{y} \right) + \tilde{k}_y \operatorname{sgn}(S(y)) \right) \\
U_1(t) &= \left(k_d \left(\ddot{z}_d + g + \frac{\kappa_{fdz}}{m} \dot{z} \right) + k_i e(z) + k_p \dot{e}(z) + \tilde{k}_z \operatorname{sgn}(S(z)) \right) \frac{m}{k_d \cos \theta \cos \phi}
\end{aligned} \tag{4.80}$$

3.6.1.1 Model Reference Adaptive Sliding Mode Controller for the Rotational

The primary step is defining the error and its derivative for position subsystem:

$$\begin{cases} e(\phi) = \phi_{ref} - \phi \\ e(\theta) = \theta_{ref} - \theta \\ e(\psi) = \psi_{ref} - \psi \end{cases} \quad \begin{cases} \dot{e}(\phi) = \dot{\phi}_{ref} - \dot{\phi} \\ \dot{e}(\theta) = \dot{\theta}_{ref} - \dot{\theta} \\ \dot{e}(\psi) = \dot{\psi}_{ref} - \dot{\psi} \end{cases} \tag{4.81}$$

The PID sliding surface that will control the hexacopter's entire state. It depends on the error because it is trajectory tracking.

$$\begin{aligned}
S(\phi) &= k_p e(\phi) + k_i \int_0^\phi e(\tau) d\tau + k_d \frac{d}{dt} e(\phi) \\
S(\theta) &= k_p e(\theta) + k_i \int_0^\theta e(\tau) d\tau + k_d \frac{d}{dt} e(\theta) \\
S(\psi) &= k_p e(\psi) + k_i \int_0^\psi e(\tau) d\tau + k_d \frac{d}{dt} e(\psi)
\end{aligned} \tag{4.82}$$

The PID sliding surface's first order derivative is represented by:

$$\begin{aligned}
\dot{S}(\phi) &= k_p \dot{e}(\phi) + k_i e(\phi) + k_d \ddot{e}(\phi) \\
\dot{S}(\theta) &= k_p \dot{e}(\theta) + k_i e(\theta) + k_d \ddot{e}(\theta) \\
\dot{S}(\psi) &= k_p \dot{e}(\psi) + k_i e(\psi) + k_d \ddot{e}(\psi)
\end{aligned} \tag{4.83}$$

Selecting the adaptive reaching laws for the hexacopter position is the second stage. We get:

$$\begin{aligned}
\tilde{s}_{r\phi} &= \tilde{k}_\phi \operatorname{sign}(\phi) \\
\tilde{s}_{r\theta} &= \tilde{k}_\theta \operatorname{sign}(\theta) \\
\tilde{s}_{r\psi} &= \tilde{k}_\psi \operatorname{sign}(\psi)
\end{aligned} \tag{4.84}$$

Finally, the complete adaptive sliding mode controller for hexacopter position becomes:

$$\begin{aligned}
U_2(t) &= \frac{J_{xx}}{k_d} \left(k_i e(\phi) + k_p \dot{e}(\phi) + k_d \left(\ddot{\phi}_d - \left(\frac{J_{yy} - J_{zz}}{J_{xx}} \right) \dot{\theta} \dot{\psi} + \frac{J_p}{J_{xx}} \dot{\theta} \omega_r + \frac{K_{fd\phi}}{J_{xx}} \dot{\phi}^2 \right) + \tilde{k}_\phi \operatorname{sgn}(S(\phi)) \right) \\
U_3(t) &= \frac{J_{yy}}{k_d} \left(k_i e(\theta) + k_p \dot{e}(\theta) + k_d \left(\ddot{\theta}_d - \left(\frac{J_{zz} - J_{xx}}{J_{yy}} \right) \dot{\phi} \dot{\psi} - \frac{J_p}{J_{yy}} \dot{\phi} \omega_r + \frac{K_{fd\theta}}{m} \dot{\theta}^2 \right) + \tilde{k}_\theta \operatorname{sgn}(S(\theta)) \right) \\
U_4(t) &= \left(k_d \left(\ddot{\psi}_d - \left(\frac{J_{xx} - J_{yy}}{J_{zz}} \right) \dot{\phi} \dot{\theta} + \frac{K_{fd\psi}}{m} \dot{\psi}^2 \right) + k_i e(\psi) + k_p \dot{e}(\psi) + \tilde{k}_z \operatorname{sgn}(S(\psi)) \right) \frac{J_{zz}}{k_d}
\end{aligned} \tag{4.85}$$

CHAPTER FIVE

5. RESULTS AND DISCUSSIONS

In this chapter the following points are discussed, the stability and performance of the proposed Adaptive SMC for hexacopter dynamics, which are simulated using MATLAB/Simulink are discussed. The Simulink model of the UAV is developed both with and without disturbance. With the help of the suggested control system. The simulation's output is displayed graphically and discussed it using parameter performance index IAE. In order to achieve effective stabilization and trajectory tracking, a simulation study of employing the suggested controller for delivery application UAV is performed by minimizing the trajectory error and appearance of uncertainties. The hexacopter's tracking results can also be viewed in 2D and 3D.

5.1. Simulation Block Diagram for Tracking Problem

Figure 5.1 describes the overall proposed control system Simulink block diagram. The closed-loop block diagram is displayed in detail in Appendix. This block diagram is created using a number of MATLAB Simulink subsystem blocks. It includes altitude roll control, position X control, position Y control, attitude (Z-dynamics) control, heading yaw controller, and attitude pitch control Simulink blocks.

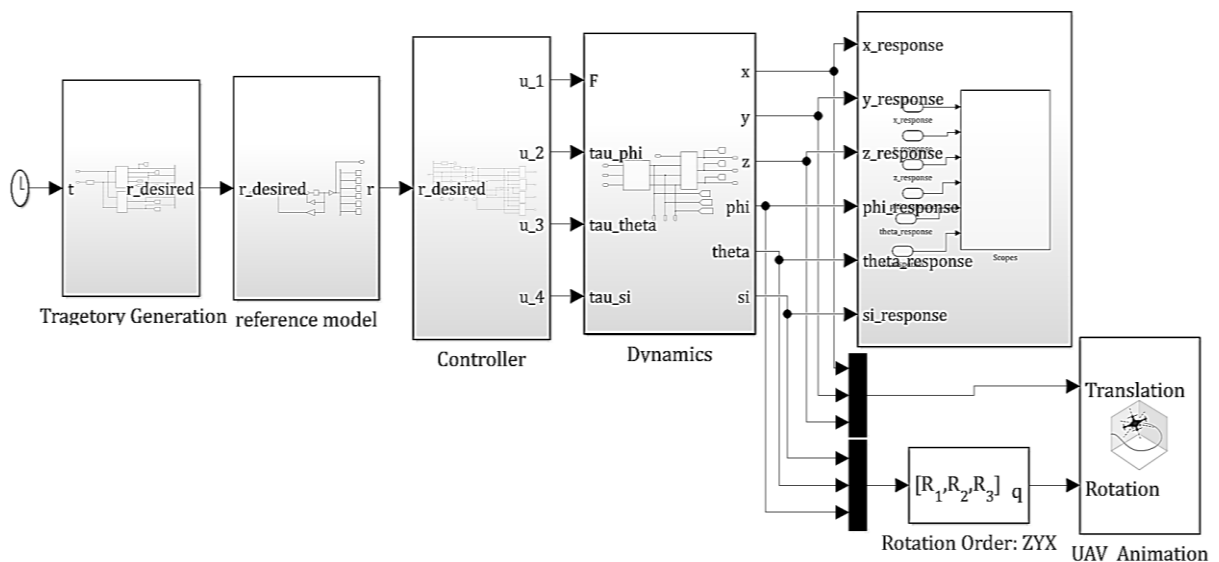


Figure 5.1: Simulink diagram of the proposed system

5.2. Parameters that are used in simulation purposes

To minimize the error and to achieve a recommended settling time, the modal reference adaptive control (MRAC) adjusts the controller parameters, such as the SMC constant rate (K and λ) and the PID sliding surface coefficient rates (k_i , k_p , and k_d), for all hexacopter dynamics in real-time. In the MRAC approach, the selection of proper initial values is essential, as it can significantly impact the controller's performance. The MRAC continuously updates the control surface based on the deviation by differentiate the actual response and the desired reference model, allowing modifications to the plant dynamics so that the controller can adjust. This adaptive nature makes MRAC a popular choice for systems with time-varying or uncertain parameters, such as flight control applications. Additionally, in order to satisfy the Lyapunov requirement in Equation 3.75, the K_i value needs to be higher than 0, and the k_i , k_p , and k_d values must be Hurwitz. The initial values of the controller values are listed below in Table 5.1:

Table 5.1: Initial parameters of controller

| Parameters | Values | parameters | values | Parameters | Values |
|--------------|---------|--------------|--------|-------------------|--------|
| k_{phi} | 0.05 | $k_p(y)$ | 500 | $k_d(psi)$ | 1 |
| k_{theta} | 2.5 | $k_p(z)$ | 350 | $k_d(x)$ | 0.01 |
| k_{psi} | 2.5 | $k_i(phi)$ | 100 | $k_d(y)$ | 0.01 |
| k_x | 0.00001 | $k_i(theta)$ | 100 | $k_d(z)$ | 200 |
| k_y | 0.00001 | $k_i(psi)$ | 10 | λ_{phi} | 0.001 |
| k_z | 4.75 | $k_i(x)$ | 0.5 | λ_{theta} | 0.0001 |
| $k_p(phi)$ | 3500 | $k_i(y)$ | 0.05 | λ_{psi} | 0.0001 |
| $k_p(theta)$ | 80 | $k_i(z)$ | 400 | λ_x | 0.001 |
| $k_p(psi)$ | 3.5 | $k_d(phi)$ | 0.2 | λ_y | 0.0001 |
| $k_p(x)$ | 1000 | $k_d(theta)$ | 2 | λ_z | 0.001 |

5.3. Simulation Result of MRA-SMC for Tracking Performance

As already discussed in chapter-3, in the case hexacopter model, aerodynamic effects and gyroscopic movements are integrated into the system's nonlinear model. The performance of the minimum jerk tracking in the proposed controller is evaluated by providing a desired trajectory to the system states. For the simulation, the reference trajectories listed below are utilized. It consists of 13 specific points, particularly suited for delivery applications.

$$\begin{cases} a_x = [0 \ 0 \ 10 \ 10 \ 10 \ 20 \ 20 \ 20 \ 20 \ 10 \ 10 \ 10 \ 0] \\ b_x = [0 \ 10 \ 10 \ 10 \ 20 \ 20 \ 20 \ 20 \ 10 \ 10 \ 10 \ 0 \ 0] \end{cases} \quad \begin{cases} a_{\phi} = [0 \ 0 \ 0 \ 0 \ 0 \ 0 \ 0 \ 0 \ 0 \ 0 \ 0 \ 0 \ 0] \\ b_{\phi} = [0 \ 0 \ 0 \ 0 \ 0 \ 0 \ 0 \ 0 \ 0 \ 0 \ 0 \ 0 \ 0] \end{cases}$$

$$\begin{cases} a_y = [0 \ 0 \ 0 \ -4 \ -4 \ -4 \ -4 \ -4 \ -4 \ -4 \ -4 \ 0 \ 0] \\ b_y = [0 \ 0 \ -4 \ -4 \ -4 \ -4 \ -4 \ -4 \ -4 \ -4 \ 0 \ 0 \ 0] \end{cases} \quad \begin{cases} a_{\theta} = [0 \ 0 \ 0 \ 0 \ 0 \ 0 \ 0 \ 0 \ 0 \ 0 \ 0 \ 0 \ 0] \\ b_{\theta} = [0 \ 0 \ 0 \ 0 \ 0 \ 0 \ 0 \ 0 \ 0 \ 0 \ 0 \ 0 \ 0] \end{cases}$$

$$\begin{cases} a_z = [0 \ 10 \ 10 \ 10 \ 6 \ 6 \ 2 \ 2 \ 6 \ 6 \ 10 \ 10 \ 10] \\ b_z = [10 \ 10 \ 10 \ 6 \ 6 \ 2 \ 2 \ 6 \ 6 \ 10 \ 10 \ 10 \ 0] \end{cases} \quad \begin{cases} a_{\psi} = [0 \ 0 \ 0 \ 0 \ 0 \ 0 \ 0 \ 0 \ 0 \ 0 \ 0 \ 0 \ 0] \\ b_{\psi} = [0 \ 0 \ 0 \ 0 \ 0 \ 0 \ 0 \ 0 \ 0 \ 0 \ 0 \ 0 \ 0] \end{cases}$$

Where: a and b are the initial and the final points, respectively. Figure 5.2 provides the 3D reference trajectories.

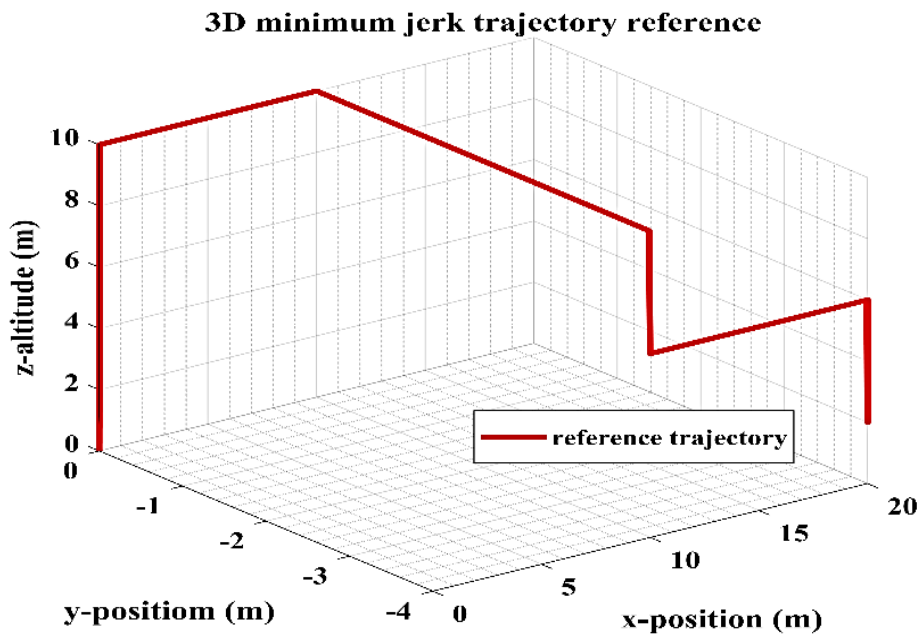


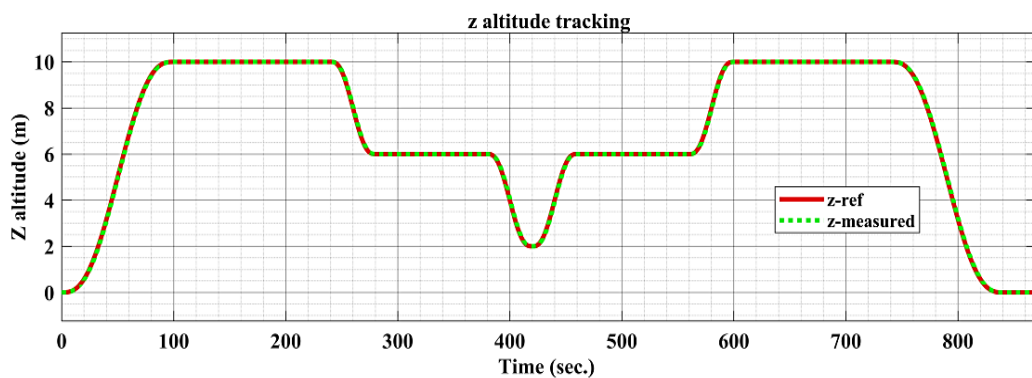
Figure 5.2: 3D minimum jerk trajectory reference

The performance analysis of the MRA-SMC controller for each state individually, using the same trajectory reference. A simulation analysis was performed to evaluate the performance of the controller, considering external uncertainties and varying masses (2.5 kg, 6 kg, and 12kg) for the minimum jerk reference trajectory.

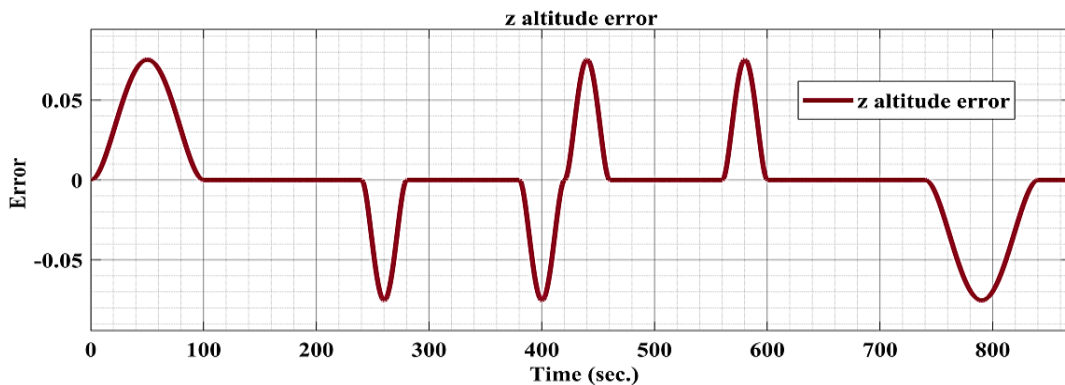
5.3.1. The ASMC System's Trajectory Tracking Performance

5.3.1.1. Tracking Performance of the Altitude Z Controller

Figure 5.3 shows the simulation results of the altitude tracking performance and the tracking error. Since the hexacopter always takes off or begins its journey from zero altitude ($Z=0$), height is always positive. The actual trajectory closely follows the desired trajectory from start to finish within a simulation time of 870 seconds. The error fluctuates within the range of ± 0.075 when the hexacopters changes direction, eventually stabilizing. This indicates that the hexacopter asymptotically follows the desired trajectory with an acceptable level of error.



(a)



(b)

Figure 5.3: Altitude Z (a) tracking performance and (b) tracking error response

5.3.1.2. Tracking Performance of the Position X Controller

Figure 5.4 shows the simulation results of the x-position tracking performance. The measured trajectory closely follows the reference trajectory from start to finish within a simulation time of 870 seconds. Additionally, it presents the tracking error of the controller between the measured trajectory and the reference trajectory. The error fluctuates within the range of ± 0.1 , indicating moments where the hexacopter deviates from the desired trajectory when the hexacopter changes direction, eventually stabilizing. This indicates that there is a minimum allowable error, and the hexacopter consistently follows the desired position trajectory.

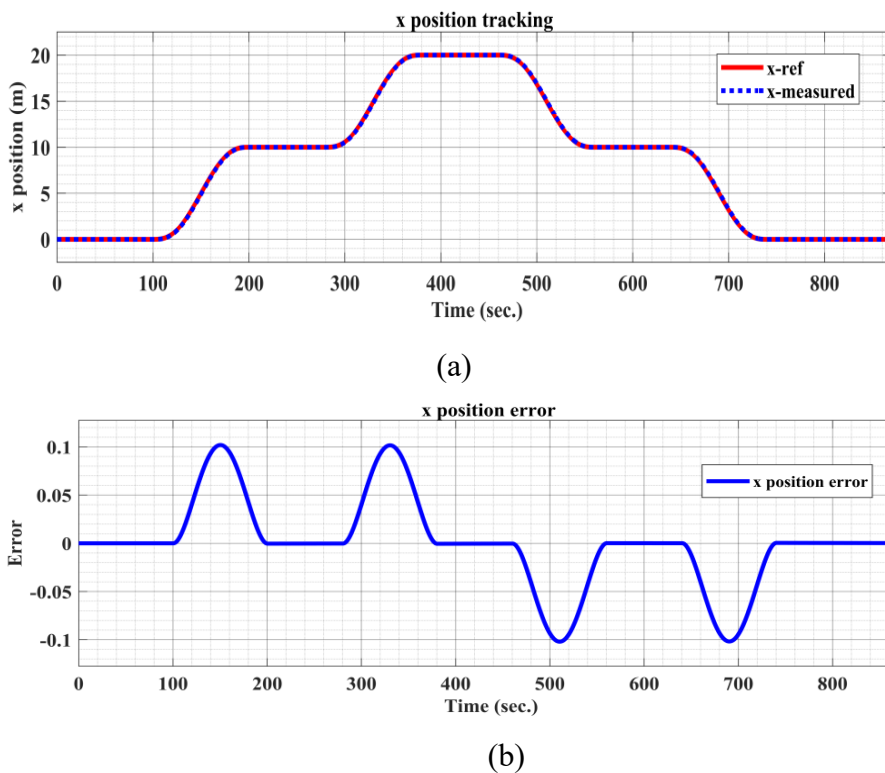
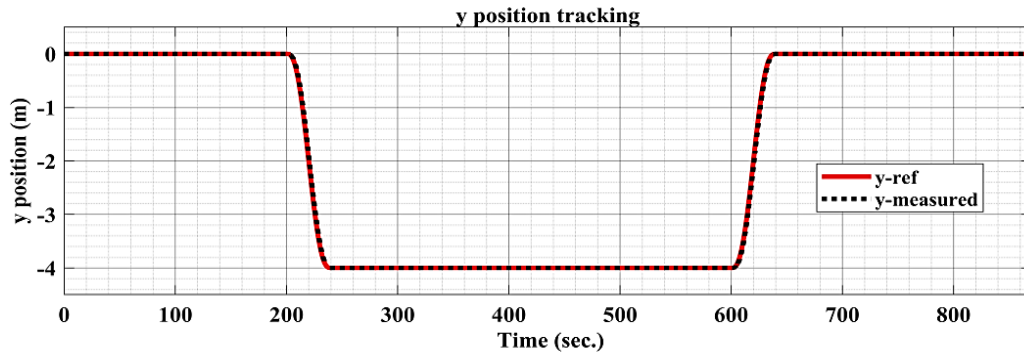


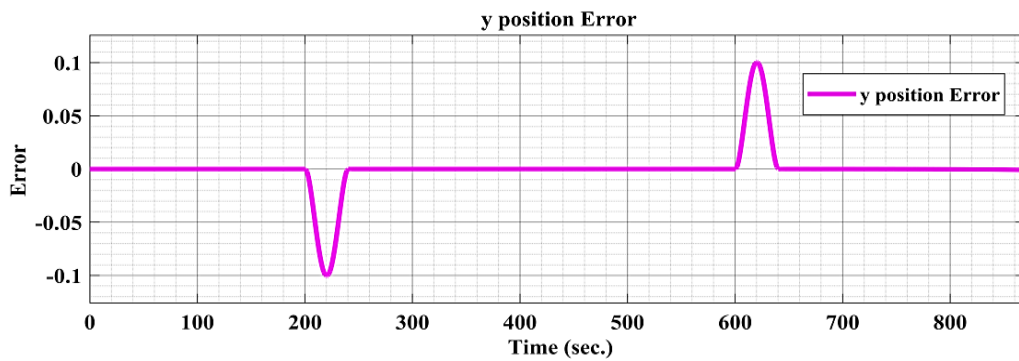
Figure 5.4: X position (a) tracking performance and (b) tracking error response

5.3.1.3. Position Y tracking Performance

Figure 5.5 shows the simulation results of the y-position tracking performance. The measured trajectory closely follows the reference trajectory from start to finish within a simulation time of 870 seconds. Additionally, it presents the tracking error of the controller between the measured trajectory and the reference trajectory. Initially, the error is zero, indicating that the desired trajectory is accurately tracked. However, as time progresses, the error fluctuates within the range of ± 0.1 , indicating moments where the hexacopter deviates from the desired trajectory. This indicates that there is a minimum allowable error, and the hexacopter consistently follows the desired position trajectory.



(a)

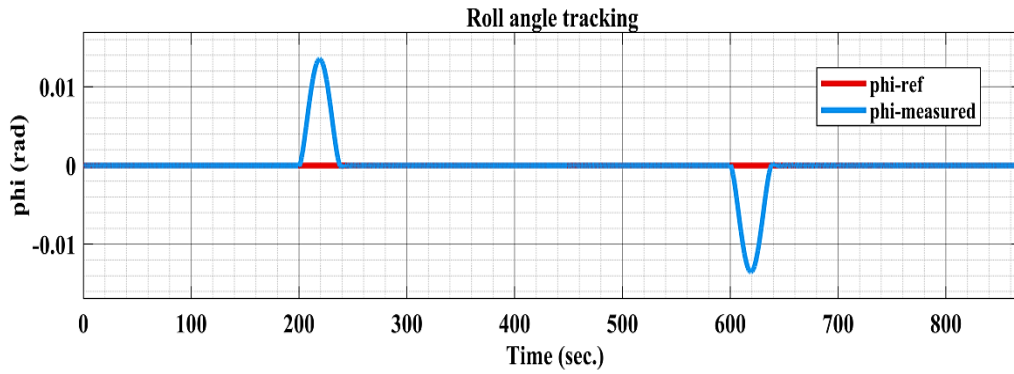


(b)

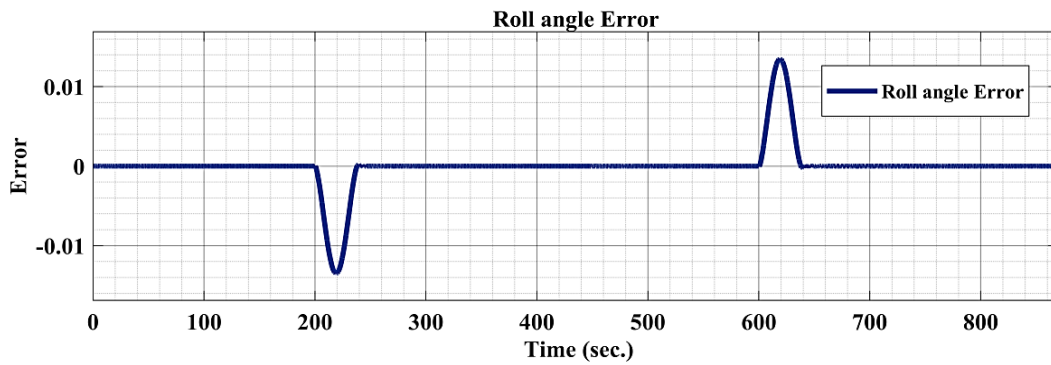
Figure 5.5: Y position (a) tracking performance and (b) tracking error response

5.3.1.4. Roll angle (Phi) tracking Performance

The rotational component phi's simulation response and corresponding tracking errors are displayed in Figure 5.6 when it comes to following a given trajectory. The response, as illustrated in the figure, the actual trajectory closely follows the desired trajectory from start to finish within a simulation time of 850 seconds. But there is some small deviations or errors between zero inputs and actual trajectories. This is because of the system is underactuated or interrelation between roll and y positions. However, the error fluctuates within the range of $\pm 0.015\text{m}$, indicates that there is a minimum allowable error, and the hexacopter consistently follows the desired attitude trajectory.



(a)

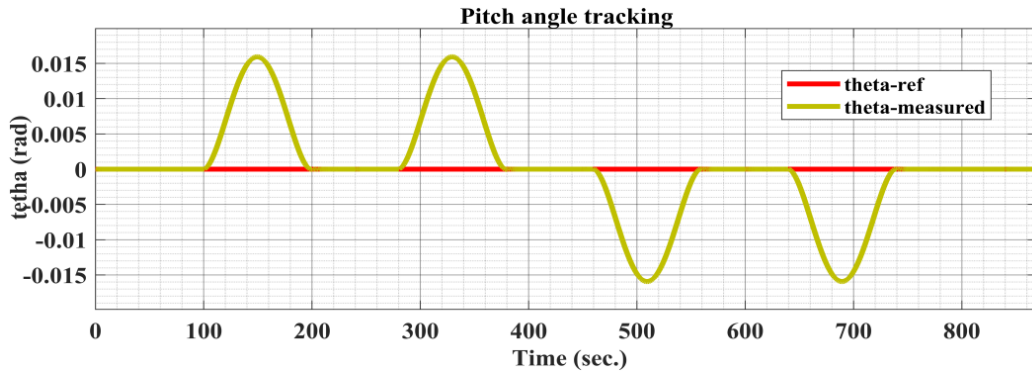


(b)

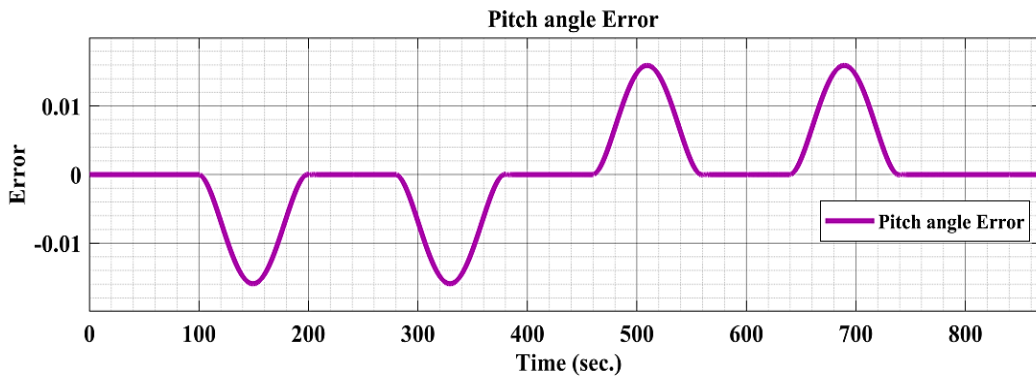
Figure 5.6: Phi (a) tracking performance and (b) tracking error response

5.3.1.5. Pitch angle (Theta) tracking Performance

The rotational component pitch angle simulation response and corresponding tracking errors are displayed in when it comes to following a given trajectory. The response, as can be seen in the Figure 5.7, the measured trajectory closely follows the desired trajectory from start to finish. But there is some small deviations or errors between zero inputs and actual trajectories. This is because of the system is underactuated or interrelation between pitch and x positions. However, the error fluctuates within the range of $\pm 0.017m$, indicates that there is a minimum allowable error, and the hexacopter consistently follows the desired attitude trajectory.



(a)

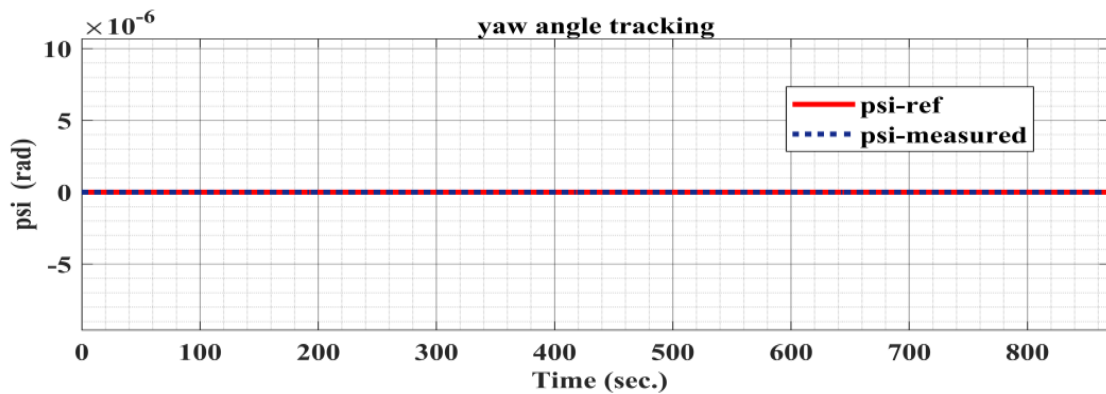


(b)

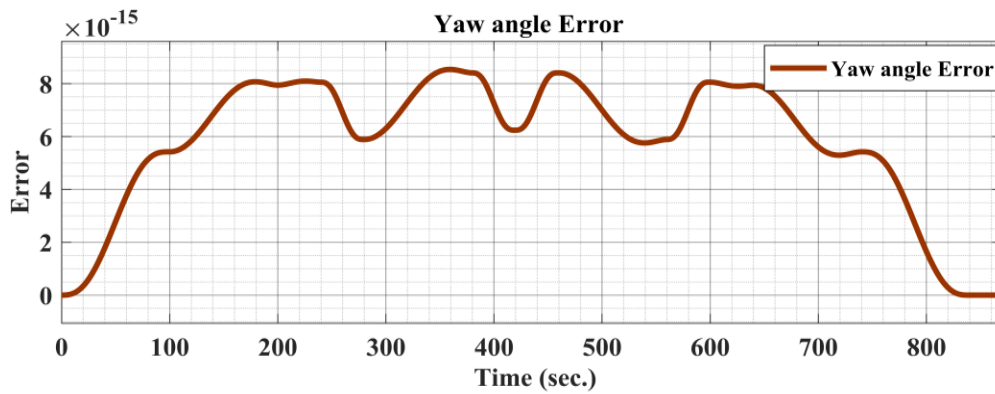
Figure 5.7: Theta (a) tracking performance and (b) tracking error response

5.3.1.6. Yaw angle (Psi) tracking Performance

Figure 5.8 shows the outcomes of the simulation yaw angle tracking performance and its corresponding tracking errors. The actual trajectory tracks the desired trajectory perfectly because the tracking error of the controller between the actual trajectory and the reference trajectory is $0.84e-14$, which means almost zero. This indicates that the hexacopter consistently follows the desired position trajectory.



(a)



(b)

Figure 5.8: Output of psi (a) tracking performance and (b) tracking error response

5.3.1.7. 3D Trajectory Tracking

Figure 5.9 shows the 3D reference trajectory tracking of a hexacopter system using the Adaptive Sliding Mode Controller (ASMC). By combining the Z altitude, X and Y positions, Roll, Theta, and Yaw orientations, the hexacopter's flight is briefly illustrated as it tracks the specified generated minimum jerk trajectory from the ground throughout its flight. The hexacopter takes off from the ground position according to the provided reference trajectory, moves to the necessary locations to complete its tasks by following the reference trajectory to the control system, and returns to the starting place.

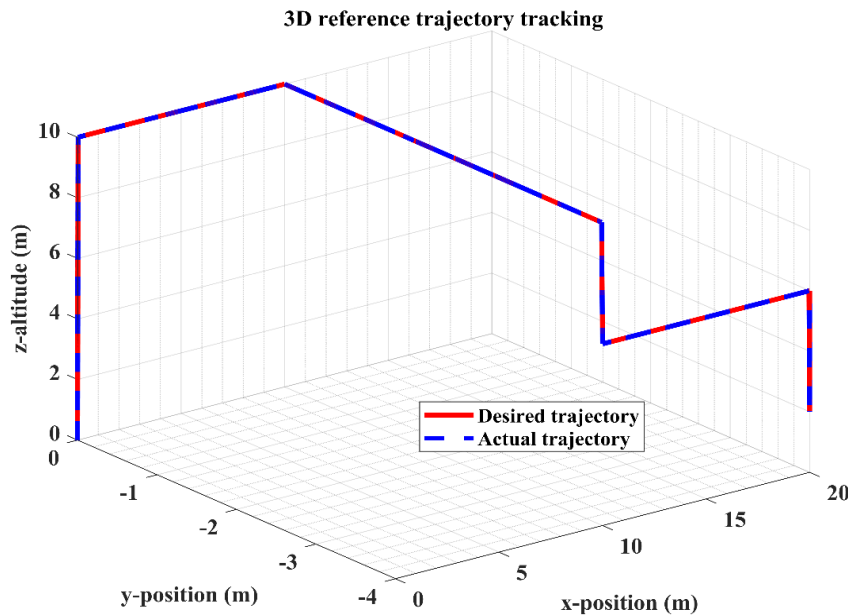


Figure 5.9: Performance of the 3D reference trajectory tracking controller using ASMC

5.3.2. Control Signal of ASMC system for Tracking

In Figure 5.10 up to Figure 5.13 describes the four-control input signal that are required to produce the appropriate trajectory. Control input U1 and U2 exhibits noticeable chattering effect indicating rapid fluctuations that can enhance responsiveness but may lead to instability if not carefully managed. This responsiveness is advantageous for tasks requiring quick adjustments, such as navigating variable environments, while control input U3 and U4 shows minimal effect, with U3 maintaining stability and U4 demonstrating controlled oscillations. This balance allows the hexacopter to achieve both stability during hover and agility during maneuvers.

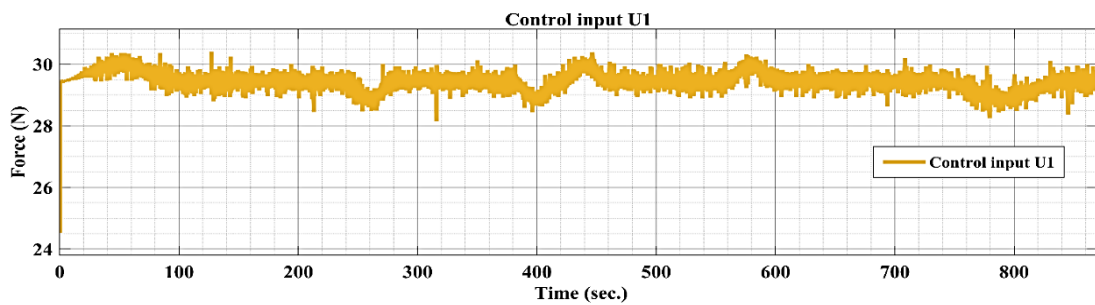


Figure 5.10: Control input U1

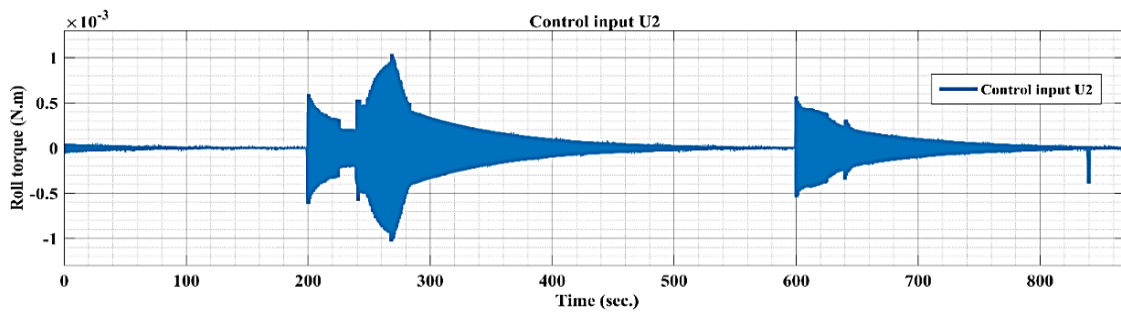


Figure 5.11: Control input U2

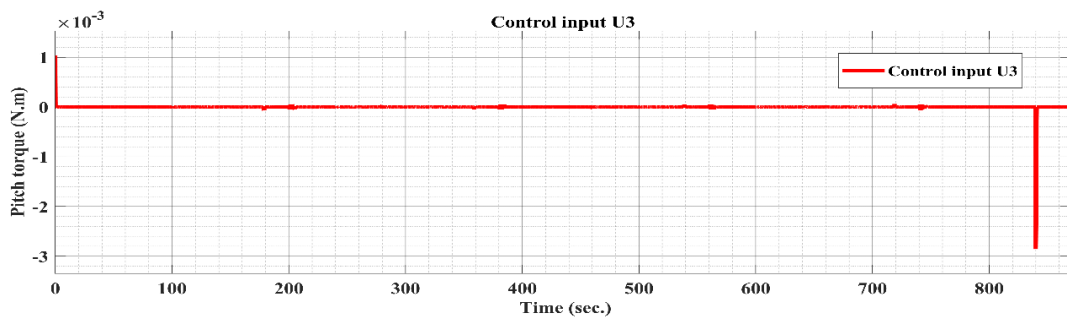


Figure 5.12: Control input U3

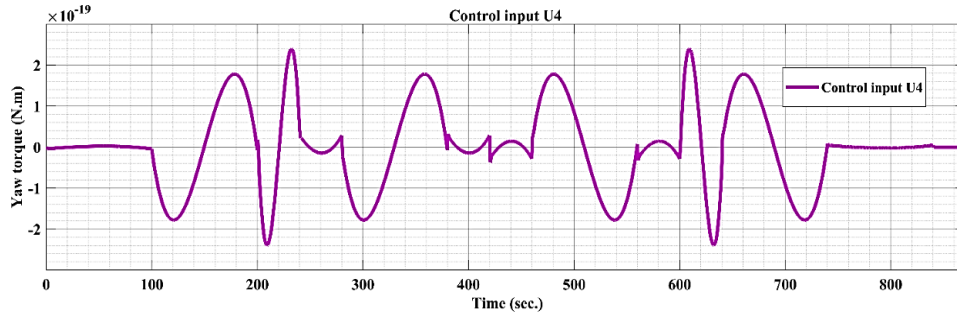


Figure 5.13: Control input U4

5.4. Simulation Results when the Hexacopter is Subjected to Uncertain Parameters and External Disturbances

This section evaluates and analyzes the controller's robustness and ability to track the provided minimum jerk reference trajectory in the face of external disturbances and uncertain parameters by using MATLAB/Simulink.

The following are the external disturbance and parametric uncertainties that are applied to the system:

- A mass variation of 2.5kg-12kg represents the parameter uncertainty.
- The plant is capable of facing a variety of disturbances, including wind disturbances. Assuming that a constant wind value is applied to the hexacopter system is from -0.01 to 0.01 applied in X, from -0.5 to 0.5 applied in Z direction, and from -0.01 to 0.01 in Y direction.

5.4.1. Trajectory Tracking Performance of ASMC for Mass Varies from 2.5kg-12kg

The parametric uncertainty of the hexacopter system is mass variation and it is varied when the hexacopters changes direction not at initially and during normal flight time. This means the mass of the hexacopter is changed when changes direction and all the signals are arranged for the changed mass of the hexacopter. The controller is designed once and applied to the system. The hexacopter does not change its mass at initially and during normal flights, the mass is changed only during change direction. And this proposed controller is used for different masses (2.5kg-12kg) of the hexacopter.

5.4.1.1. Tracking Performance of the Position X Controller

The results presented in Figure 5.14 and Figure 5.15 shows the effectiveness of the modal reference adaptive sliding mode controller in maintaining trajectory tracking for a hexacopter across varying mass conditions (2.5 kg, 6 kg, and 12 kg). In Figure 5.14, the hexacopter closely follows the reference trajectory with minimal deviations, indicating robust control performance despite the increased mass. Figure 5.15 highlights the tracking error, showing that the system effectively corrects deviations, with errors oscillating around zero and peaking at approximately 0.05 m for the 12 kg configuration. Although the error is slightly larger for greater mass, the controller successfully stabilizes the position over time, demonstrating quick convergence to the desired trajectory and confirming the controller's resilience to changes in system dynamics.

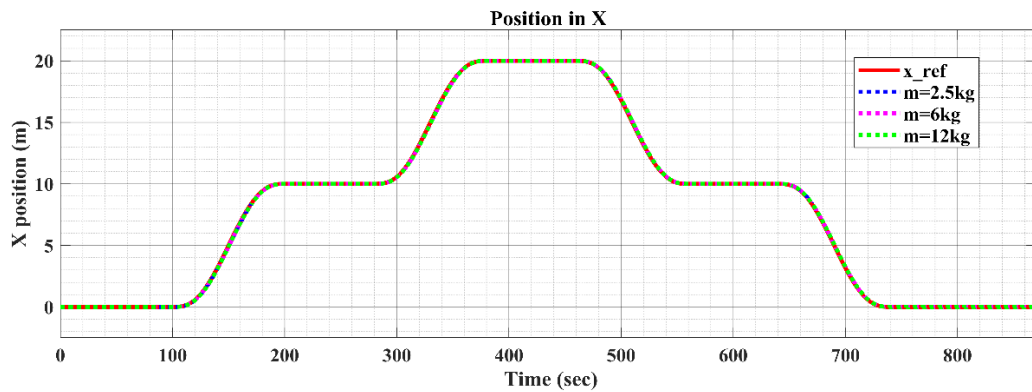


Figure 5.14: X position trajectory tracking controller for different mass

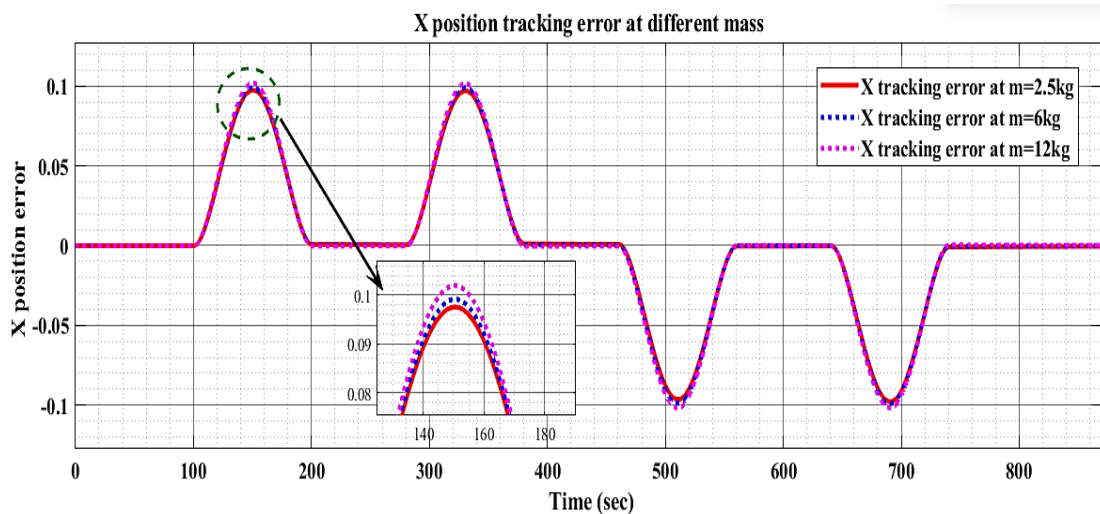


Figure 5.15: X position trajectory tracking error for different mass

5.4.1.2. Tracking Performance of the Position Y Controller:

Figure 5.16 and Figure 5.17 present the performance of the Y position trajectory tracking controller for a hexacopter across different mass configurations. In Figure 5.16, the hexacopter closely follows the reference trajectory, indicating that the controller effectively manages position tracking regardless of the mass. The response remains stable, with minimal deviations from the desired path, demonstrating the controller's robustness. Figure 5.17 indicates the tracking error, where the Y position error peaks around 0.1 m but quickly converges back to near zero, suggesting that the controller efficiently corrects deviations caused by mass changes. The tracking errors for different masses show slight variations, but the overall performance remains consistent, reflecting the controller's adaptability to different payloads.

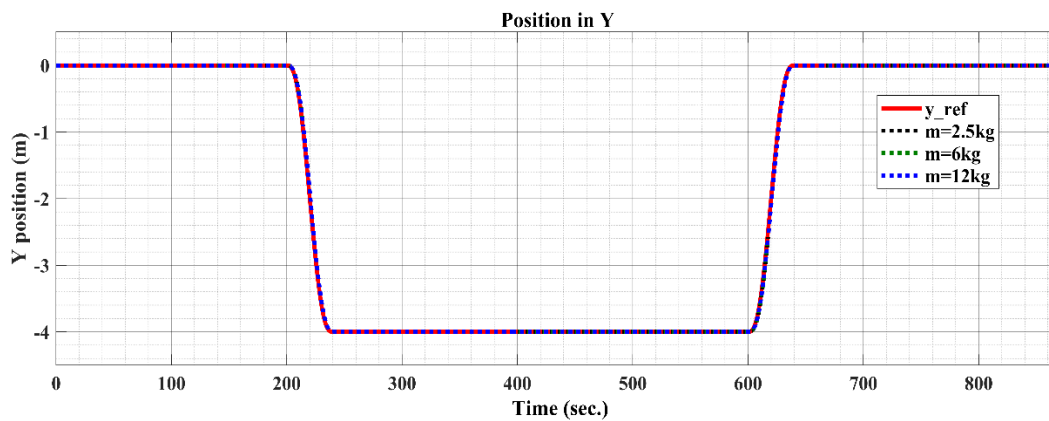


Figure 5.16: Y position trajectory tracking controller for different mass

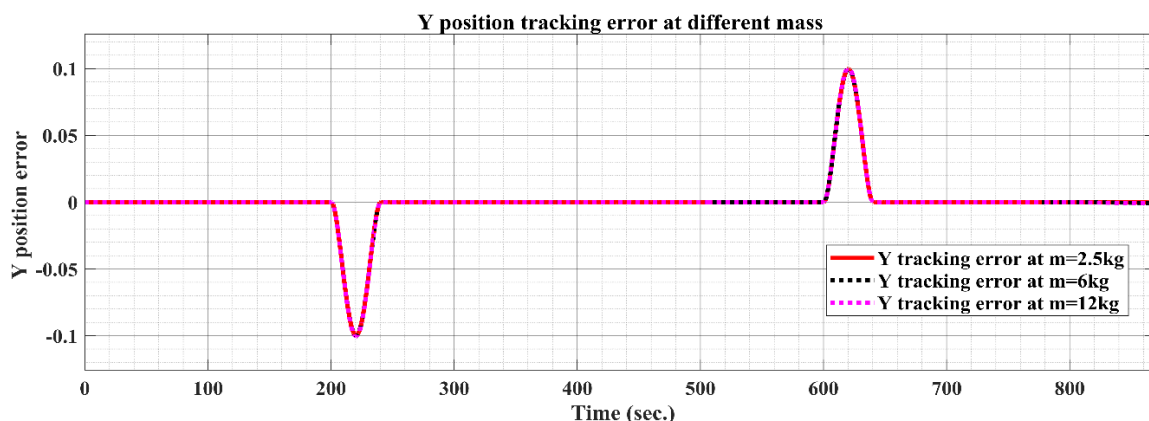


Figure 5.17: Y position trajectory tracking error for different mass

5.4.1.3. Tracking Performance of the Altitude Z Controller

Figure 5.18 and Figure 5.19 shows the performance of the altitude trajectory tracking controller for a hexacopter across various mass configurations, highlighting both the altitude response and tracking error. In Figure 5.18, the desired altitude is effectively followed by the system, with the subsystems exhibiting consistent behavior despite the mass variations. The various subsystems demonstrate minor deviations from the desired path, indicating good control performance. Figure 5.19 focuses on the tracking error, revealing that the altitude error remains within a small range, with peaks of about 0.06 m for the different masses tested (2.5 kg, 6 kg, and 12 kg). The controller shows resilience, effectively correcting deviations and maintaining altitude stability over time.

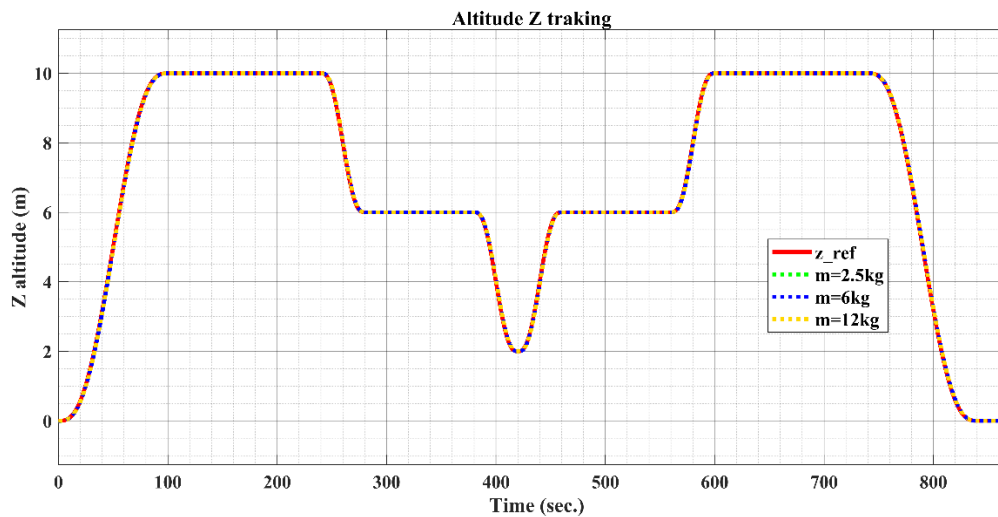


Figure 5.18: Z altitude trajectory tracking controller for different mass

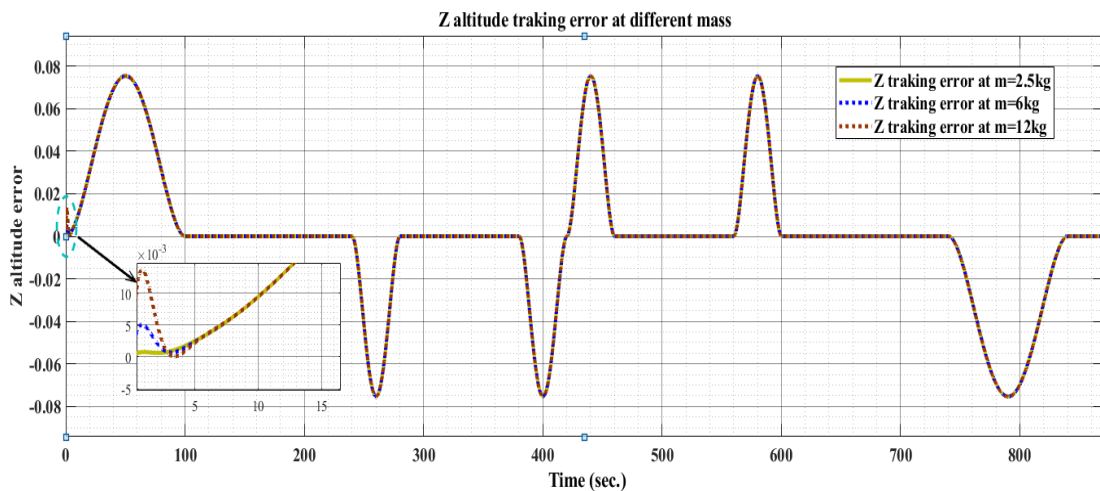


Figure 5.19: Z altitude trajectory tracking error for different mass

5.4.2. Trajectory Tracking Performance of ASMC for Mass Varies from 2.5kg-12kg with External Disturbances

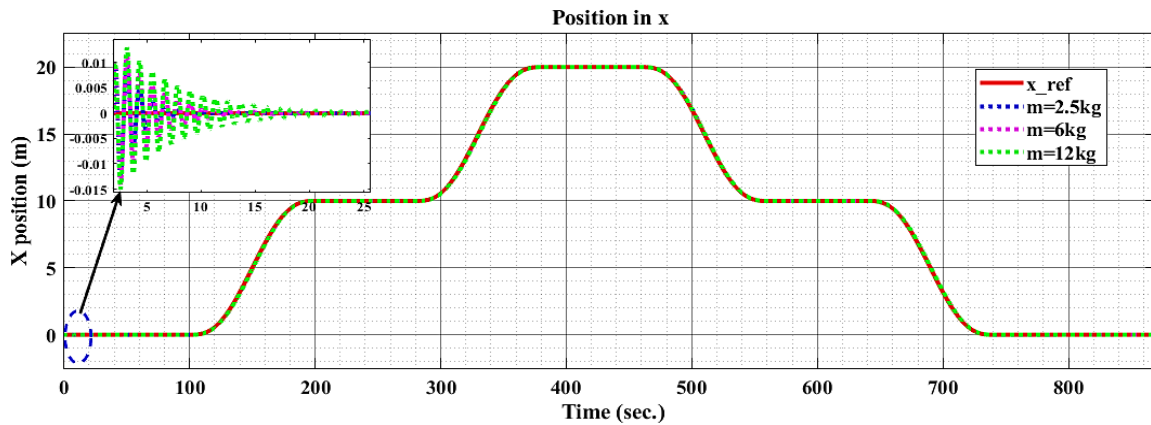


Figure 5.20: X position trajectory tracking with external disturbance.

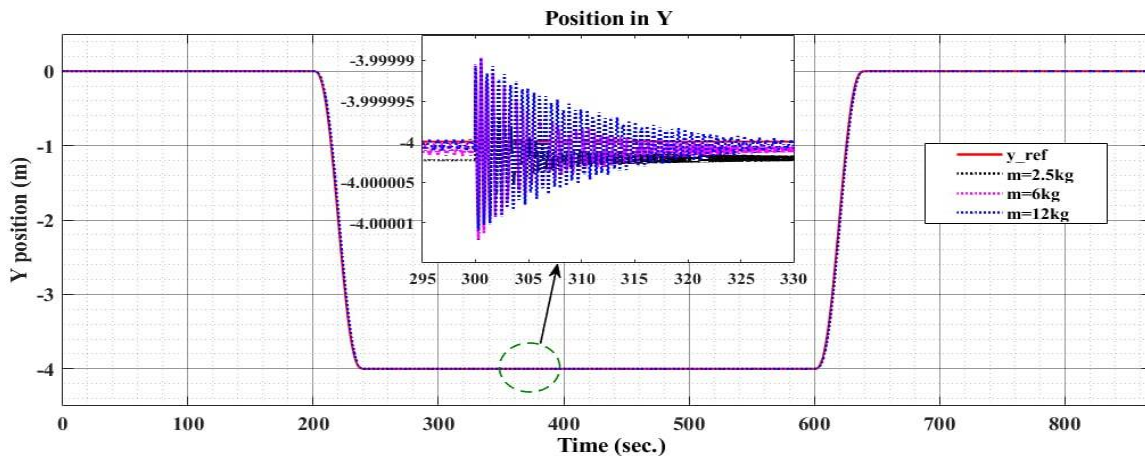


Figure 5.21: Y position trajectory tracking with external disturbance

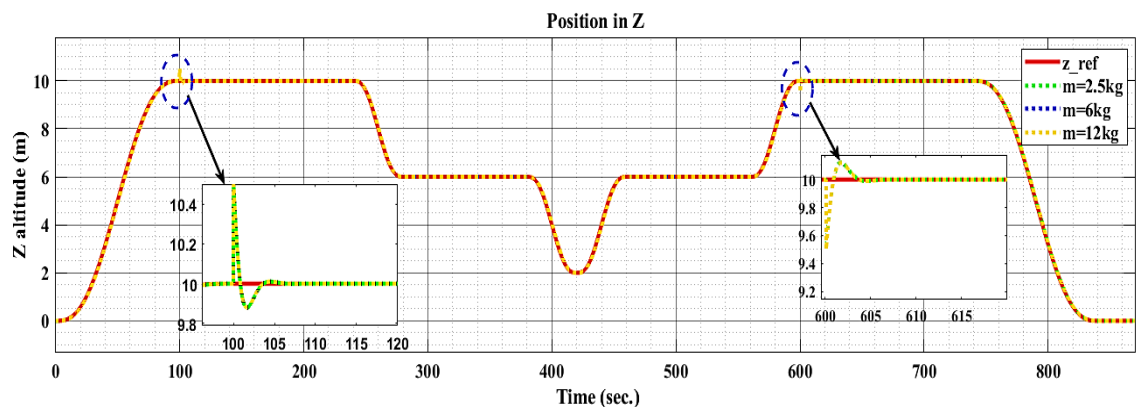


Figure 5.22: Z - altitude trajectory tracking with in external disturbance

The test results for the altitude response, as shown in Figure 5.20, indicate that the hexacopter UAV performs well in the presence of external disturbances. Specifically, when

the mass is increased to 12 kg, a minor increase in error of approximately 0.015 m is observed. This deviation is relatively small compared to the nominal values, suggesting that the controller effectively manages the impact of disturbances. As time progresses, the error diminishes, ultimately stabilizing the system. The figures also illustrate the Y and Z positions (Figure 5.21 and Figure 5.22), demonstrating that the controller successfully compensates for disturbances. The UAV maintains stability by returning all positions to their desired trajectory values.

5.5. Performance Index Analysis

Performance index values for Modal Reference Adaptive Sliding Mode Control (MRA-SMC) applied to hexacopter drone indicates varying levels of effectiveness across different parameters. In this thesis, the Integral of Absolute Error (IAE) performance index is utilized to assess the systems robustness, as shown in Table 5.2.

Table 5.2: Performance index values for MRA-SMC

| Performance index | X position | Y position | Z position | Roll | Pitch | Yaw |
|-------------------|------------|------------|------------|-----------|--------|--------|
| IAE | 21.5656 | 4.3508 | 14.6922 | 2.488e-11 | 3.3982 | 0.5760 |

The overall IAE performance index value is calculated to be 44.58 over a time frame of 870 seconds. It indicates that the proposed controller demonstrates improved performance. The table shows the specific IAE values for each parameter: 21.5656 for X position, 4.3508 for Y position, 14.6922 for Z position, an exceptionally low value of 2.488e-11 for Roll, 3.3982 for Pitch, and 0.5760 for Yaw. These results underscore the effectiveness of the MRA-SMC in managing the hexacopter's dynamics.

CHAPTER SIX

6. CONCLUSION AND RECOMMENDATION

6.1. Conclusion

This research investigates the applications of Model reference adaptive sliding mode controller (MRAC) technique to solve stabilization problems of hexacopter UAV, especially for achieving minimum jerk trajectory. The nonlinear dynamic model of the hexacopter UAV is developed by using Newton-Euler method by incorporating aerodynamic effects. Following the formulation of the system dynamics, a minimum jerk trajectory is generated as a reference path. Model reference adaptive sliding mode controller controllers are designed for the model.

The efficiency and performance of the designed controller is tested for minimum jerk trajectory in MATLAB software environment by considering external disturbance (i.e., wind disturbance) and parametric uncertainties (mass variation).

Finally, the results of the simulation show that the proposed Model reference adaptive sliding mode controller (MRAC) tracks the specified trajectory with minimal tracking error of 0.01. It handles mass variation from 2.5kg to 12kg efficiently without external disturbance and also with external disturbance

According to the simulation results, The Modal Reference Adaptive Control with SMC stabilizes the hexacopter's altitude, position, attitude, and heading, achieving nearly zero tracking error without external disturbance and also with external disturbance. Overall, the controller exhibits significant stability, robustness, and reduced chattering effects, making it a promising solution for precise UAV control in dynamic environments.

6.2. Recommendation

For future researchers, this study suggests the following actions:

- Model and control the hexacopter system by considering obstacle dictation sensor model especially for delivery applications.
- Take the hexacopter's motor dynamics into account while modelling and controlling it.
- Consider the hexacopter model's hardware implementation.

REFERENCE

- Alaimo, A., Artale, V., Milazzo, C. L. R., & Ricciardello, A. (2014). PID controller applied to hexacopter flight. *Journal of Intelligent and Robotic Systems: Theory and Applications*, 73(1–4), 261–270. <https://doi.org/10.1007/s10846-013-9947-y>
- Alghamdi, Y., Munir, A., & La, H. M. (2021). Architecture, Classification, and Applications of Contemporary Unmanned Aerial Vehicles. *IEEE Consumer Electronics Magazine*, 10(6), 9–20. <https://doi.org/10.1109/MCE.2021.3063945>
- Alias, J. M., Anandhan, A. R., & Menon, A. M. (2018). Design of Different Controllers in Quadcopter. *IOSR Journal of Engineering*, 2018, 61–72.
- Bisgaard, M., la Cour-Harbo, A., Johnson, E. N., Bendtsen, J. D., Sorensen, K., Singhose, W., Dickerson, S., Theoretical, J. O. F., Mechanics, A., Bisgaard, M., la Cour-Harbo, A., Dimon Bendtsen, J., Group, S. R., Blackburn, D., Singhose, W., Kitchen, J., Patrangenu, V., Lawrence, J., Kamoi, T., ... Cruz, P. (2010). Modeling and Simulation of a Helicopter Slung Load Stabilization Device. *International Journal of Applied Information Systems*, 33(6), 348–353.
- Busarakum, S., & Srichatrapimuk, V. (2014). The design of sliding mode control of a hexarotor. *Proceedings - 2014 IEEE Conference on System, Process and Control, ICSPC 2014, December*, 47–52. <https://doi.org/10.1109/SPC.2014.7086228>
- Dewangan, R. K., Shukla, A., & Godfrey, W. W. (2019). Three-dimensional path planning using Grey wolf optimizer for UAVs. *Applied Intelligence*, 49(6), 2201–2217. <https://doi.org/10.1007/s10489-018-1384-y>
- Everaerts, J. (2014). The use of unmanned aerial vehicles (UAVs) for remote sensing and mapping. *The International Archives of the Photogrammetry, Remote Sensing and Spatial Information Sciences*, 37(Inter-Commission WG I/V), 1187–1191.
- Le, D.-K., & Nam, T.-K. (2015). A study on the modeling of a hexacopter. *Journal of the Korean Society of Marine Engineering*, 39(10), 1023–1030.
- Mallick, R. K., & Nahak, N. (2016). *Grey Wolves-Based Optimization Technique for*. 1458–1463.
- Mirjalili, S., Mirjalili, S. M., & Lewis, A. (2014). Grey Wolf Optimizer. *Advances in Engineering Software*, 69, 46–61. <https://doi.org/10.1016/j.advengsoft.2013.12.007>
- Nagarajan, A., & Victoire, A. A. (2023). Optimization Reinforced PID-Sliding Mode Controller for Rotary Inverted Pendulum. *IEEE Access*, 11(February), 24420–24430.

<https://doi.org/10.1109/ACCESS.2023.3254591>

- Niguse, B. (2020). *Control of Hexacopter Unmanned Aerial Vehicle By Using Non-Linear Integral Sliding Mode Controller*. July. Control of Hexacopter UAV by using Non-Linear Instegraal Sliding Model Controller
- Niit, E. (2017). *Design and Implementation of an Adaptive Controller for a Quadcopter*. December.
- Optimum, G. W. O., & Microgrids, G. (2018). *Grey Wolf Optimization-Based Optimum Energy-Management and Battery-Sizing Method for Grid-Connected Microgrids*. 1–27. <https://doi.org/10.3390/en11040847>
- Pati, A., Singh, S., & Negi, R. (2014). *Sliding Mode Controller Design Using PID Sliding Surface for Half Car Suspension System*. 1–6.
- Poudel, R., Maskey, R. K., & Shrestha, P. L. (2015). *Design and Development of Hexacopter for Environmental Research Design and Development of Hexa-copter for Environmental Research*. April.
- Rao, K. V., & Mathew, A. T. (2018). Dynamic modeling and control of a hexacopter using PID and back stepping controllers. *EPSCICON 2018 - 4th International Conference on Power, Signals, Control and Computation, 1*, 1–7.
- Rathod, P. D., & Shinde, G. U. (2023). Autonomous Aerial System (UAV) for Sustainable Agriculture: A Review. *International Journal of Environment and Climate Change*, 13(8). <https://doi.org/10.9734/ijecc/2023/v13i82080>
- Romdlony, M. Z., Rosa, M. R., Syamsudin, E. M. P., Trilaksono, B. R., & Wibowo, A. S. (2022a). Design and application of models reference adaptive control (MRAC) on ball and beam. *Journal of Mechatronics, Electrical Power, and Vehicular Technology*, 13(1). <https://doi.org/10.14203/j.mev.2022.v13.15-23>
- Romdlony, M. Z., Rosa, M. R., Syamsudin, E. M. P., Trilaksono, B. R., & Wibowo, A. S. (2022b). Design and application of models reference adaptive control (MRAC) on ball and beam. *Journal of Mechatronics, Electrical Power, and Vehicular Technology*, 13(1), 15–23. <https://doi.org/10.14203/j.mev.2022.v13.15-23>
- Simon, J., & Martinović, G. (2013). *Navigation of Mobile Robots Using WSN' s RSSI Parameter and Potential Field Method*. 10(4), 107–118.
- Singh, K. (2014). *Design of Sliding Mode PID Controller with Improved reaching laws for Nonlinear Systems*.
- SINGH, K. (2018). *Modelling and Controls of a Hexacopter*. December, 16.
- Stamate, M. A., Pupăză, C., Nicolescu, F. A., & Moldoveanu, C. E. (2023). Improvement

- of Hexacopter UAVs Attitude Parameters Employing Control and Decision Support Systems. *Sensors*, 23(3). <https://doi.org/10.3390/s23031446>
- Sun, C., Agha, S. A., Mohamed, Z., & Shaheed, M. H. (2022). Optimised Sliding Mode Control of a Hexacopter: Simulation and Experiments. *Electronics (Switzerland)*, 11(16). <https://doi.org/10.3390/electronics11162519>
- Tin, C., Tun, Z. M., Tun, H. M., Naing, Z. M., & Moe, W. K. (2015). Development Of Arduino Based Hexacopter. *International Journal of Scientific & Technology Research*, 4(8), 141–146.
- Vinjavarapu, S., Dandu, M., & Babu, S. J. (2019). *FABRICATION OF A PROTOTYPE FOR*. 6(6), 718–727.
- Walle, S. M. (2019). *Dynamic Modeling and Trajectory Tracking Control of Hexacopter Using Sliding Mode Controller a Master'S Thesis*. January.
- Yilmaz, E. (2019). *Modeling and Nonlinear Adaptive Control of an Aerial Manipulation System by Emre Yilmaz*.
- Zhang, J., Gu, D., Deng, C., & Wen, B. (2019). Robust and Adaptive Backstepping Control for Hexacopter UAVs. *IEEE Access*, 7. <https://doi.org/10.1109/ACCESS.2019.2951282>
- Zhang, S., Dan, Z., Qian, Q., Guo, Y., & Zhang, J. (2020). Nonlinear PID Pressure Control Based on Extremum Seeking. *Chinese Control Conference, CCC, 2020-July*. <https://doi.org/10.23919/CCC50068.2020.9189051>

REFERENCE LINKS

[L1]<https://images.app.goo.gl/MZoFHrZWnNKdV5zr9>

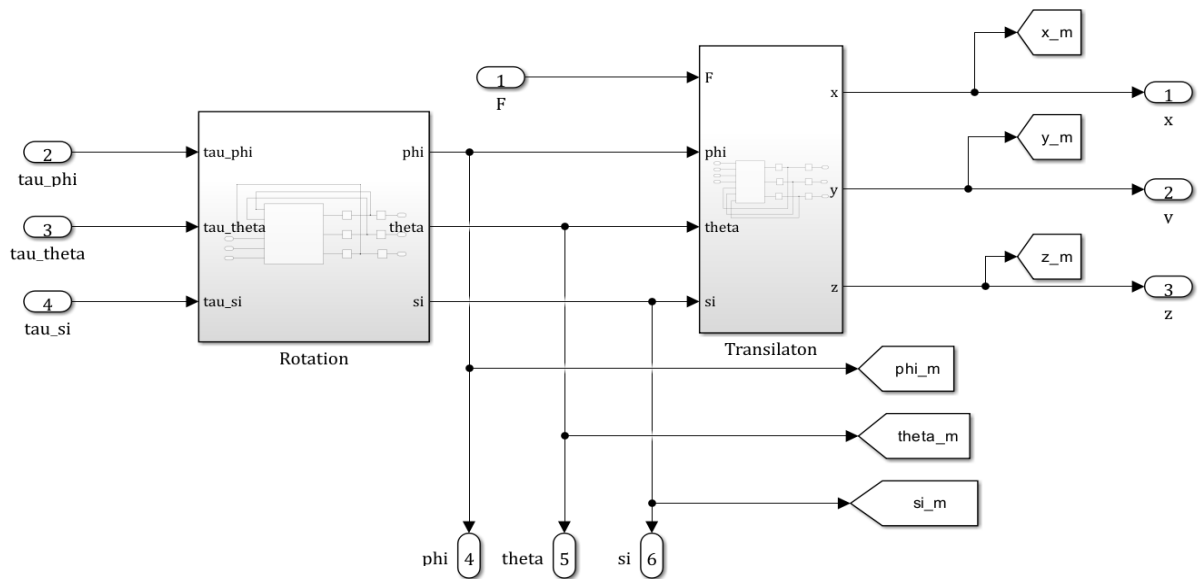
[L2]https://www.researchgate.net/figure/Lawrence-and-Elmer-Sperry-Photo-5-1916_fig1_334701913?_tp=eyJjb250ZXh0Ijp7ImZpcnN0UGFnZSI6Il9kaXJlY3QiLCJwYWdlIj

[L3]https://www.google.com/url?sa=i&url=https%3A%2F%2Fardupilot.org%2Fcopter%2Fdocs%2Fconnect-escs-and-0CBQQjRxqFwoTCNCEXl6_nYgDFQAAAAAdAAAAABAE

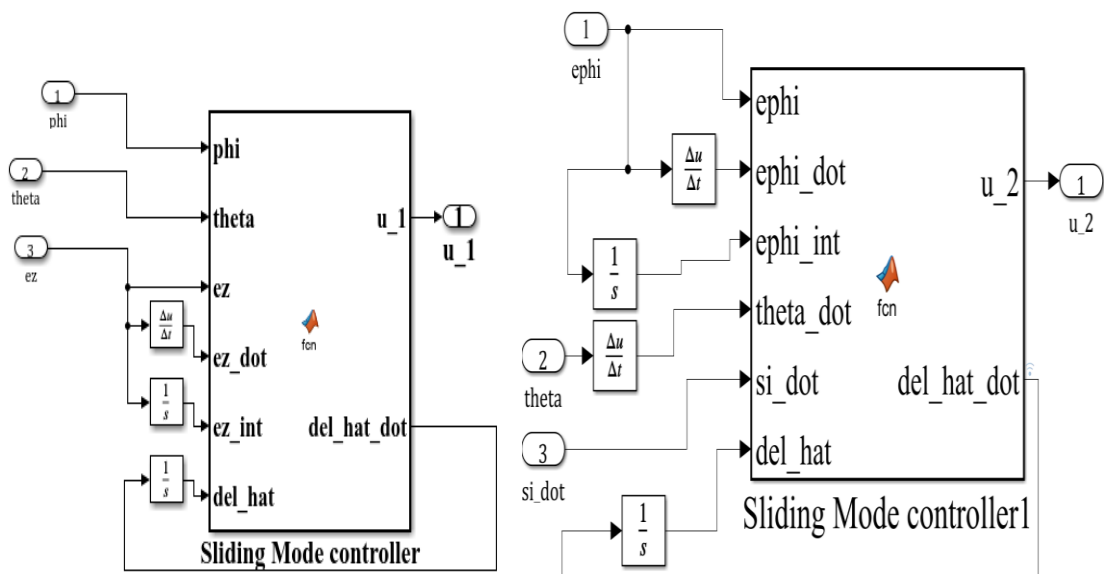
[L4]<https://www.google.com/url?sa=i&url=https%3A%2F%2Fwww.semanticscholar.org%2Fpaper%2FDynamic-Modeling-and-Control-of-a-HexaRotor-using-Moussid->

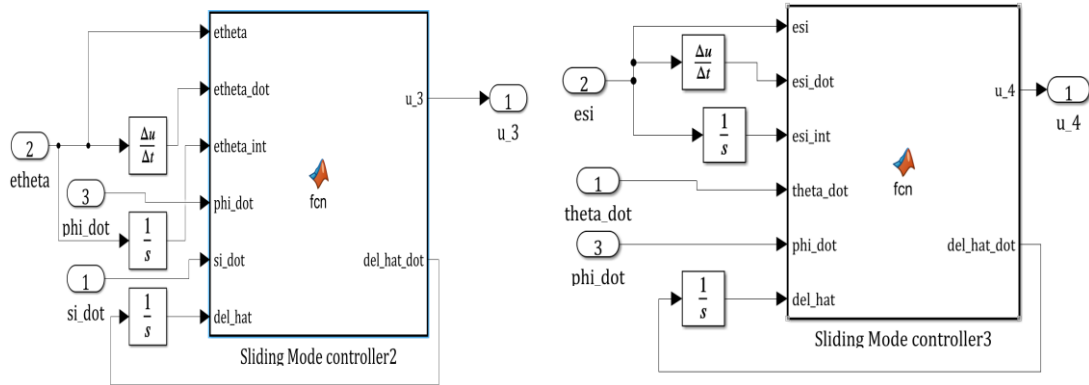
APPENDICES

APPENDIX A: Dynamic Modeling Block Diagram

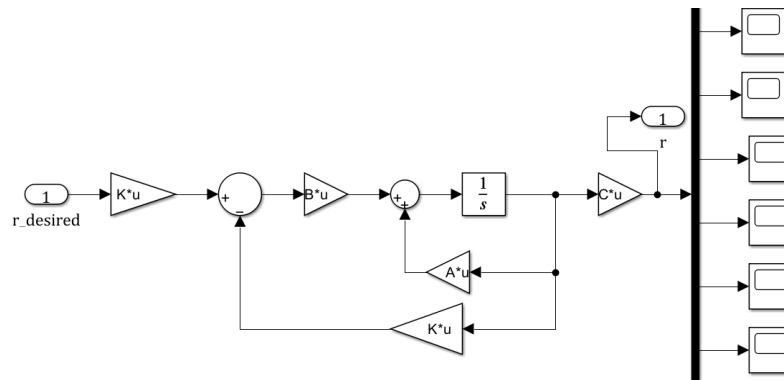


APPENDIX B: Proposed Controller Simulink diagram





APPENDIX C: LQR Based Reference Model Simulink



APPENDIX D: MATLAB Code for Reference Model of the System

```

g=9.81;
m=2.5;
[Jx,Jy,Jz]=deal(0.1);
kx=1.5;
ky=0.1;
kz=1.9;
Jr=6e-5;
omega_r=0.025;
s=Jr*omega_r;
A=[0 1 0 0 0 0 0 0 0 0;
  0 -kx/m 0 0 0 0 0 0 g 0 0 0;
  0 0 0 1 0 0 0 0 0 0 0;
  0 0 0 -ky/m 0 0 -g 0 0 0 0 0;
  0 0 0 0 0 1 0 0 0 0 0 0;
  0 0 0 0 0 -kz/m 0 0 0 0 0 0 0;
  0 0 0 0 0 0 0 1 0 0 0 0;
  0 0 0 0 0 0 0 0 0 -s/Jx 0 0;
  0 0 0 0 0 0 0 0 0 1 0 0;
  0 0 0 0 0 0 0 0 0 s/Jy 0 0 0];

```

```

0 0 0 0 0 0 0 0 0 1;
0 0 0 0 0 0 0 0 0 0];
B=[ 0 0 0 0;
0 0 0 0;
0 0 0 0;
0 0 0 0;
0 0 0 0;
1/m 0 0 0;
0 0 0 0;
0 1/Jx 0 0;
0 0 0 0;
0 0 1/Jy 0;
0 0 0 0;
0 0 0 1/Jz];
C=[1 0 0 0 0 0 0 0 0 0;
0 0 1 0 0 0 0 0 0 0;
0 0 0 1 0 0 0 0 0 0;
0 0 0 0 1 0 0 0 0 0;
0 0 0 0 0 1 0 0 0 0;
0 0 0 0 0 0 1 0 0 0;
0 0 0 0 0 0 0 1 0 0];
[rowb,colb]=size(B);
[rowc,colc]=size(C);
D=zeros(rowc,colb);
Co=rank(ctrb(A,B));
Ov=rank(observ(A,C));
% Q=1000*eye(12);
Q=1000*C'*C;
R=1;
k_lqr=lqr(A,B,Q,R);

```

Document ID: 66eae1980205d05849cfe373


Document Name: Final_thesis, Senayt Setarge,,

Document Pages: 95

Document Status: ● Completed

Document Completion Date: September 18, 2024, 14:21 UTC

Signer: almaz (almaztekle24@gmail.com)

| Signer | Signature | Timestamps |
|---|---|--|
| <p>almaz almaztekle24@gmail.com Using IP: 196.189.127.157 IP Location: Ethiopia, Addis Ababa</p> <p>Authentication method: Email</p> |  | <p>Viewed: September 18, 2024, 14:21 UTC Signed: September 18, 2024, 14:21 UTC</p> |